

Argonne National Laboratory

EXPERIMENTS WITH
CENTRAL SUPERHEATER CORE CSH-1,
BORAX-V

by

BORAX-V Project Staff

Property of
ANL-W Technical Library

LEGAL NOTICE

This report was prepared as an account of Government sponsored work. Neither the United States, nor the Commission, nor any person acting on behalf of the Commission:

A. Makes any warranty or representation, expressed or implied, with respect to the accuracy, completeness, or usefulness of the information contained in this report, or that the use of any information, apparatus, method, or process disclosed in this report may not infringe privately owned rights; or

B. Assumes any liabilities with respect to the use of, or for damages resulting from the use of any information, apparatus, method, or process disclosed in this report.

As used in the above, "person acting on behalf of the Commission" includes any employee or contractor of the Commission, or employee of such contractor, to the extent that such employee or contractor of the Commission, or employee of such contractor prepares, disseminates, or provides access to, any information pursuant to his employment or contract with the Commission, or his employment with such contractor.

ARGONNE NATIONAL LABORATORY
9700 South Cass Avenue
Argonne, Illinois 60440

EXPERIMENTS WITH
CENTRAL SUPERHEATER CORE CSH-1,
BORAX-V

by

BORAX-V Project Staff
Idaho Division

Contributors:

| | |
|---------------------|----------------------|
| R. E. Rice (Editor) | J. I. Hagen |
| E. J. Brooks | R. J. Jiacoletti** |
| D. H. Brown | C. C. Miles |
| J. D. Cerchione | D. Mohr [†] |
| R. A. Cushman | R. W. Thiel |
| D. C. Cutforth | W. R. Wallin |
| W. B. Doe* | |

*Remote Control Division

**University of Wyoming

[†]Allis-Chalmers Mfg. Company

January 1965

Operated by The University of Chicago
under
Contract W-31-109-eng-38
with the
U. S. Atomic Energy Commission

TABLE OF CONTENTS

| | <u>Page</u> |
|--|-------------|
| I. INTRODUCTION | 13 |
| II. REACTOR DESCRIPTION | 14 |
| III. REACTIVITY MEASUREMENTS | 22 |
| A. Zero-power Reactivity Measurements | 22 |
| 1. Loading | 22 |
| 2. Adjustment of Fuel-to-water Ratio | 23 |
| 3. Control Rod Calibration. | 28 |
| 4. Available Excess Reactivity. | 35 |
| 5. Temperature Reactivity Effects | 38 |
| 6. Boric Acid Effects | 38 |
| 7. Superheater Flooding Measurements | 41 |
| a. Static Reactivity Measurements | 42 |
| (1) Flooding from Below. | 43 |
| (2) Flooding from Above. | 45 |
| b. Flooding Time Measurements. | 47 |
| c. Reactivity Addition Rates from Superheater Flooding. | 48 |
| 8. Reactivity Worth of Fueled Oscillator | 49 |
| 9. Additional Fuel-to-water Ratio Experiments. | 49 |
| 10. Experimental Techniques and Error | 51 |
| B. High-power Reactivity Measurements | 53 |
| IV. NEUTRON FLUX MAPPING. | 55 |
| A. Coarse Neutron Flux Distributions | 55 |
| 1. Measurement Techniques. | 55 |
| 2. Radial Neutron Flux Distributions. | 58 |
| 3. Axial Flux Distributions | 61 |
| 4. Cadmium Ratio Measurements | 65 |
| a. Reference Core | 66 |
| b. Core with 12 Flow Rods Dispersed | 66 |
| B. Fine-power-distribution Measurements | 66 |
| 1. Measurement Techniques. | 66 |
| 2. Normalization | 72 |
| a. Measurements in Boiling Fuel Rod Locations | 72 |
| b. Measurements Adjacent to Superheater Coolant Channels. | 72 |
| c. Average Activation in Boiling Fuel Assemblies | 77 |
| 3. Results. | 81 |
| 4. Analysis. | 82 |
| 5. Flux Distribution in 12-flow-rod Boiling Fuel Assembly | 87 |

TABLE OF CONTENTS

| | <u>Page</u> |
|--|-------------|
| V. IN-REACTOR-VESSEL INSTRUMENTATION MEASUREMENTS AND DEVELOPMENT | 88 |
| A. Reactor Data | 88 |
| 1. Boiling Fuel Rod Temperatures | 88 |
| 2. Superheater Fuel Plate and Steam Temperatures | 88 |
| 3. Reactor Water Subcooling | 94 |
| 4. Core Inlet Water Velocity | 95 |
| 5. Core Exit Void Fraction | 97 |
| 6. Downcomer Void Fraction | 97 |
| 7. Calibration and Use of the Downcomer Stauscheibe Tube | 99 |
| 8. Measurement of Reactor-water Level | 99 |
| B. Acoustic Water-level Probe | 100 |
| VI. WATER CHEMISTRY MEASUREMENTS AND CATALYTIC RECOMBINATION EXPERIMENT | 104 |
| A. Water Chemistry Measurements | 104 |
| B. Steam Dome Tests | 105 |
| C. Radiolytic Gas Recombination Experiment | 107 |
| VII. PLANT PERFORMANCE | 110 |
| A. General | 110 |
| B. Special Operating Experiences | 115 |
| 1. Power Oscillations with a Partially Flooded Superheater | 115 |
| a. Observations | 115 |
| b. Analysis | 116 |
| 2. Short-period Scram | 121 |
| 3. Effects of Moisture on High-impedance Thermo- couple Extension Leads | 122 |
| a. Description | 122 |
| b. Experience | 124 |
| c. Tests | 125 |
| d. Conclusions | 127 |
| C. Reactor Vessel | 127 |
| 1. Radiation Effects | 127 |
| 2. Temperature Distribution in Reactor Vessel Wall | 128 |
| 3. Reactor Vessel Water-level Measurement | 128 |
| 4. Belleville Spring | 128 |

TABLE OF CONTENTS

| | <u>Page</u> |
|--|-------------|
| D. Water and Steam Systems | 129 |
| 1. Steam Systems. | 129 |
| 2. Boron Addition and Batch Feed Systems | 129 |
| 3. Turbogenerator System. | 129 |
| 4. Feedwater System | 130 |
| 5. Auxiliary Water System. | 130 |
| 6. Superheater Flood-and-drain System. | 130 |
| 7. Superheater Steam Outlet Manifolds and Couplings | 130 |
| E. Reactor Control, Electrical | 131 |
| F. Control Rods | 131 |
| G. Fuel. | 134 |
| 1. Boiling Fuel Rods. | 134 |
| 2. Boiling Fuel Assembly Boxes. | 134 |
| 3. Fuel Handling and Storage | 135 |
| 4. Superheater Fuel Seals | 135 |
| VIII. SUPERHEATER FUEL EXPERIENCE | 137 |
| A. Superheater Fuel Assembly Leak Repairs. | 137 |
| B. Fission Product Experiments | 139 |
| C. Examination of Defective Superheater Fuel. | 140 |
| 1. On-site Superheater Fuel Inspection | 140 |
| 2. Examination of Superheater Fuel Assembly C-3. | 142 |
| a. Disassembly | 142 |
| b. Crack in Lower-nozzle Weld | 143 |
| c. Examination of Individual Elements. | 143 |
| (1) Element 12 | 144 |
| (2) Element 13 | 145 |
| (3) Element 14 | 146 |
| (4) Element 15 | 146 |
| (5) Element 16 | 147 |
| d. Source of Fission Products | 148 |
| e. Deposits in the Insulating Gap. | 149 |
| 3. Conclusions. | 150 |
| ACKNOWLEDGMENTS | 151 |
| REFERENCES. | 152 |

LIST OF FIGURES

| <u>No.</u> | <u>Title</u> | <u>Page</u> |
|------------|---|-------------|
| 1. | Reactor with Central Superheater | 16 |
| 2. | Boiling Fuel Rod | 17 |
| 3. | Fuel Rod and Cutaway Section of Boiling Fuel Assembly | 18 |
| 4. | Boron-stainless-steel Poison Rod | 19 |
| 5. | Cross Section, Central Superheater Fuel Assembly | 20 |
| 6. | Central Superheater Fuel Assembly | 20 |
| 7. | Flow Diagram | 21 |
| 8. | Final Loading, Boiling Core B-2. | 22 |
| 9. | Flow Rod | 27 |
| 10. | Loading Diagram, Core CSH-1 | 30 |
| 11. | Zero-power, Room-temperature Loading, Core CSH-1 | 31 |
| 12. | Zero-power, Operating-temperature Loading, Core CSH-1A. | 31 |
| 13. | Differential Reactivity Worth vs Nine-control-rod-bank Position, Cores CSH-1 and CSH-1A | 33 |
| 14. | Differential Reactivity Worth of Control Rods No. 1, 2, and Outer Bank at 487-490°F, Core CSH-1A | 34 |
| 15. | Differential Reactivity Worth of Control Rods No. 1, 2, and Outer Bank at 73-83°F, Core CSH-1 | 35 |
| 16. | Critical Position and Differential Reactivity Worth of Control Rod No. 1 with Respect to Eight-control-rod Bank, Core CSH-1 | 36 |
| 17. | Nine-control-rod-bank Position vs Reactivity, Cores CSH-1 and CSH-1A | 37 |
| 18. | Nine-control-rod-bank Position vs Temperature, Core CSH-1A | 39 |
| 19. | Temperature vs Reactivity, Core CSH-1A. | 40 |
| 20. | Nine-control-rod-bank Position vs Boric Acid Concentration, Cores CSH-1 and CSH-1A | 40 |
| 21. | Reactivity vs Boric Acid Concentration, Cores CSH-1 and CSH-1A. | 41 |
| 22. | Reactivity vs Superheater Water Level, Nine-control-rod Bank, Core CSH-1 | 44 |

LIST OF FIGURES

| <u>No.</u> | <u>Title</u> | <u>Page</u> |
|------------|--|-------------|
| 23. | Reactivity vs Superheater Water Level, Eight-control-rod Bank, Bottom Flooding, Core CSH-1 | 45 |
| 24. | Reactivity vs Superheater Water Level, Eight-control-rod Bank, Top Flooding, Core CSH-1. | 46 |
| 25. | Reactivity vs Time, Flooding Central Superheater from Top, Core CSH-1. | 47 |
| 26. | Relationship between Reactivity (ρ), Soluble Poison Concentration (C_B), and Control Rod Height (h) | 53 |
| 27. | Power vs Nine-control-rod-bank Position, Core CSH-1. | 54 |
| 28. | Flux-wire Holder in Boiling Fuel Assembly | 56 |
| 29. | Flux-wire Holders in Superheater Fuel Assembly | 57 |
| 30. | Block Diagram of Flux-wire Counting System | 57 |
| 31. | Diagonal Radial Neutron Flux Distributions, Core CSH-1. | 58 |
| 32. | Transverse Radial Neutron Flux Distributions, Core CSH-1 | 59 |
| 33. | Influence of Control Rod Position on Radial Neutron Flux Distribution, Core CSH-1. | 60 |
| 34. | Axial Neutron Flux Distributions, Core Position 54, Core CSH-1. | 61 |
| 35. | Axial Neutron Flux Distributions, Core Position 63, Core CSH-1. | 62 |
| 36. | Axial Neutron Flux Distributions in Thimbles, Core CSH-1A | 63 |
| 37. | Point-to-average Axial Neutron Flux Distributions in Thimbles, Core CSH-1A | 64 |
| 38. | Axial Neutron Flux Distributions in Thimbles, Core CSH-1 | 65 |
| 39. | Cadmium Ratios, Core CSH-1. | 67 |
| 40. | Axial Cadmium Ratios in Thimbles, Core CSH-1 | 68 |
| 41. | Cadmium Ratios in Core Positions 42 and 57 (12 Dispersed Flow Rods), Core CSH-1C | 69 |
| 42. | Radial Cadmium Ratio Distribution, Core CSH-1 | 70 |
| 43. | Modified Boiling Fuel Assembly for Fine-flux Mapping. | 71 |
| 44. | Preliminary Normalized Fine-flux Data, Irradiation No. 1, Core CSH-1. | 73 |

LIST OF FIGURES

| <u>No.</u> | <u>Title</u> | <u>Page</u> |
|------------|---|-------------|
| 45. | Preliminary Normalized Fine-flux Data, Irradiation No. 2, Core CSH-1. | 74 |
| 46. | Preliminary Normalized Fine-flux Data, Irradiation No. 3, Core CSH-1. | 75 |
| 47. | Preliminary Normalized Fine-flux Data, Irradiation No. 4, Core CSH-1. | 76 |
| 48. | Foil Activity Depression through Insulating Box, Central Superheater Fuel Element | 78 |
| 49. | Final Normalized Fine-power Map, Core CSH-1 | 81 |
| 50. | Relative Flux-wire Activities and Average for a Fuel Rod (Circled), Core Position 52, Core CSH-1 | 82 |
| 51. | Average Fission Rates Parallel to Fuel Plates in Central Superheater Fuel Assemblies, Core CSH-1 | 83 |
| 52. | Local-to-average Ratio of Power Produced in Individual Fuel Assemblies, Core CSH-1 | 86 |
| 53. | Fine-power Distribution in Core Position 57 (12 Dispersed Flow Rods), Core CSH-1C | 87 |
| 54. | Indicated UO_2 Temperature vs Reactor Thermal Power, Boiling Fuel Rods Nos. ZA-17, -18, -19, and -20, Core CSH-1B. | 89 |
| 55. | Indicated UO_2 Temperature vs Reactor Thermal Power, Boiling Fuel Rod No. YA-15, Core CSH-1B. | 90 |
| 56. | Indicated UO_2 Temperature vs Reactor Thermal Power, Boiling Fuel Rods Nos. VA-1 and VA-2, Core CSH-1B | 91 |
| 57. | Instrumented Superheater Fuel Element. | 92 |
| 58. | Numbered Thermocouple Locations in Instrumented Superheater Fuel Assemblies. | 92 |
| 59. | Downcomer Void Fraction and Core Inlet Subcooling vs Reactor Power, Core CSH-1B. | 95 |
| 60. | Inlet Velocity and Flow vs Reactor Power, Instrumented Boiling Fuel Assembly I-1, Core CSH-1B. | 96 |
| 61. | Exit Void Ratio vs Reactor Power, Instrumented Boiling Fuel Assembly I-1, Core CSH-1B | 98 |
| 62. | Schematic Diagram of Acoustic Water-level Probe. | 101 |
| 63. | Details of Acoustic Water-level Probe. | 102 |

LIST OF FIGURES

| <u>No.</u> | <u>Title</u> | <u>Page</u> |
|------------|---|-------------|
| 64. | Movable Steam Probe, Core CSH-1B | 105 |
| 65. | Measurements on Condensed Static Steam from Steam Dome, Core CSH-1B. | 106 |
| 66. | Abridged Schematic Diagram, Radiolytic Gas Recombination Test Apparatus | 108 |
| 67. | Loading Diagram, Core CSH-1B | 111 |
| 68. | Bottom View of Internal Steam Separator, Core CSH-1 | 112 |
| 69. | Power Loading, Core CSH-1B. | 112 |
| 70. | Oscillations with Partially Flooded Superheater, Core CSH-1B. | 116 |
| 71. | Calculated Gain of Zero-power Transfer Function | 118 |
| 72. | Terminal Box for Instrumented Superheater Fuel Assembly. | 123 |
| 73. | Thermocouple Measuring Circuit Schematic Diagram for Superheater Fuel and Steam Temperatures | 123 |
| 74. | Reactor Head and Pit Installation, Core CSH-1B | 124 |
| 75. | Control Rod Inspection Tools | 132 |
| 76. | Control Rod Follower Repair Tools | 133 |
| 77. | Superheater Seal-removal Jig. | 136 |
| 78. | Repair Welding Machine for Superheater Fuel Assemblies (Shielding Removed) | 138 |
| 79. | Southeast Side of Superheater Fuel Assembly C-3, Core CSH-1 | 141 |
| 80. | Northeast Side of Superheater Fuel Assembly C-3, Core CSH-1 | 141 |
| 81. | Upper End of Superheater Fuel Assembly C-3, Core CSH-1. | 142 |
| 82. | Lower End of Superheater Fuel Assembly C-3, Core CSH-1. | 143 |
| 83. | Cracked Weld below Element 15, Superheater Fuel Assembly C-3, Core CSH-1 | 144 |
| 84. | Sections through Element 12, Superheater Fuel Assembly C-3, Core CSH-1 | 145 |
| 85. | Section 3/8 in. above Bottom of Fuel Plates, Superheater Fuel Assembly C-3, Core CSH-1. | 146 |

LIST OF FIGURES

| <u>No.</u> | <u>Title</u> | <u>Page</u> |
|------------|--|-------------|
| 86. | Buckling in Element 15, Superheater Fuel Assembly C-3, Core CSH-1. | 147 |
| 87. | Buckling in Element 15, Longitudinal Section, Superheater Fuel Assembly C-3, Core CSH-1. | 147 |
| 88. | Longitudinal Section of Element 16, Superheater Fuel Assembly C-3, Core CSH-1 | 148 |
| 89. | Metallographic Section of Torn Lower End of Fuel Plate from Element 14, Superheater Fuel Assembly C-3, Core CSH-1. | 149 |
| 90. | Deposits on Fuel Plate and Inside of Insulating Tube, Element 16, Superheater Fuel Assembly C-3, Core CSH-1. . . | 149 |

LIST OF TABLES

| <u>No.</u> | <u>Title</u> | <u>Page</u> |
|------------|--|-------------|
| I. | Design Parameters, BORAX-V Central Superheater Core at 20 MWt | 14 |
| II. | Loading Sequence, Core CSH-1 | 24-26 |
| III. | Experiments with Varied Fuel-to-water Ratio. | 29 |
| IV. | Reactivity Effects of Flooding Superheater, Core CSH-1 | 43 |
| V. | Additional Fuel-to-water Ratio Experiments, Core CSH-1B . . | 50 |
| VI. | Boiling Fuel Assembly Average Flux-wire Activation, Core CSH-1. | 77 |
| VII. | Final Normalization Factors, Core CSH-1 | 80 |
| VIII. | Local-to-average Fuel Assembly Power Production, Core CSH-1. | 85 |
| IX. | Superheater Fuel and Steam Temperatures, Core CSH-1B . . | 93 |
| X. | Reactor Water-level Measurements, Core CSH-1B. | 100 |
| XI. | Water Chemistry Measurements, Core CSH-1B. | 104 |
| XII. | Boric Acid Concentration in Steam Dome, Core CSH-1B . . . | 107 |
| XIII. | Data from Superheated-steam Fission-product Monitor, Core CSH-1B. | 113 |
| XIV. | Power Operation, Core CSH-1B | 114 |
| XV. | Oscillations with Partially Flooded Superheater, Core CSH-1A. | 119 |
| XVI. | Electrochemical Cell Potential for Chromel-P vs Alumel as a Function of Conductor Spacing, Load, and Electrolyte pH. | 126 |
| XVII. | Fission-product Experiment, Core CSH-1B. | 139 |

| | |
|-----|--|
| 1 | Introduction |
| 2 | Objectives |
| 3 | Methodology |
| 4 | Results |
| 5 | Discussion |
| 6 | Conclusion |
| 7 | References |
| 8 | Appendix |
| 9 | Index |
| 10 | Summary |
| 11 | Abstract |
| 12 | Keywords |
| 13 | 1. Introduction |
| 14 | 2. Objectives |
| 15 | 3. Methodology |
| 16 | 4. Results |
| 17 | 5. Discussion |
| 18 | 6. Conclusion |
| 19 | 7. References |
| 20 | 8. Appendix |
| 21 | 9. Index |
| 22 | 10. Summary |
| 23 | 11. Abstract |
| 24 | 12. Keywords |
| 25 | 13. 1. Introduction |
| 26 | 14. 2. Objectives |
| 27 | 15. 3. Methodology |
| 28 | 16. 4. Results |
| 29 | 17. 5. Discussion |
| 30 | 18. 6. Conclusion |
| 31 | 19. 7. References |
| 32 | 20. 8. Appendix |
| 33 | 21. 9. Index |
| 34 | 22. 10. Summary |
| 35 | 23. 11. Abstract |
| 36 | 24. 12. Keywords |
| 37 | 25. 13. 1. Introduction |
| 38 | 26. 14. 2. Objectives |
| 39 | 27. 15. 3. Methodology |
| 40 | 28. 16. 4. Results |
| 41 | 29. 17. 5. Discussion |
| 42 | 30. 18. 6. Conclusion |
| 43 | 31. 19. 7. References |
| 44 | 32. 20. 8. Appendix |
| 45 | 33. 21. 9. Index |
| 46 | 34. 22. 10. Summary |
| 47 | 35. 23. 11. Abstract |
| 48 | 36. 24. 12. Keywords |
| 49 | 37. 25. 13. 1. Introduction |
| 50 | 38. 26. 14. 2. Objectives |
| 51 | 39. 27. 15. 3. Methodology |
| 52 | 40. 28. 16. 4. Results |
| 53 | 41. 29. 17. 5. Discussion |
| 54 | 42. 30. 18. 6. Conclusion |
| 55 | 43. 31. 19. 7. References |
| 56 | 44. 32. 20. 8. Appendix |
| 57 | 45. 33. 21. 9. Index |
| 58 | 46. 34. 22. 10. Summary |
| 59 | 47. 35. 23. 11. Abstract |
| 60 | 48. 36. 24. 12. Keywords |
| 61 | 49. 37. 25. 13. 1. Introduction |
| 62 | 50. 38. 26. 14. 2. Objectives |
| 63 | 51. 39. 27. 15. 3. Methodology |
| 64 | 52. 40. 28. 16. 4. Results |
| 65 | 53. 41. 29. 17. 5. Discussion |
| 66 | 54. 42. 30. 18. 6. Conclusion |
| 67 | 55. 43. 31. 19. 7. References |
| 68 | 56. 44. 32. 20. 8. Appendix |
| 69 | 57. 45. 33. 21. 9. Index |
| 70 | 58. 46. 34. 22. 10. Summary |
| 71 | 59. 47. 35. 23. 11. Abstract |
| 72 | 60. 48. 36. 24. 12. Keywords |
| 73 | 61. 49. 37. 25. 13. 1. Introduction |
| 74 | 62. 50. 38. 26. 14. 2. Objectives |
| 75 | 63. 51. 39. 27. 15. 3. Methodology |
| 76 | 64. 52. 40. 28. 16. 4. Results |
| 77 | 65. 53. 41. 29. 17. 5. Discussion |
| 78 | 66. 54. 42. 30. 18. 6. Conclusion |
| 79 | 67. 55. 43. 31. 19. 7. References |
| 80 | 68. 56. 44. 32. 20. 8. Appendix |
| 81 | 69. 57. 45. 33. 21. 9. Index |
| 82 | 70. 58. 46. 34. 22. 10. Summary |
| 83 | 71. 59. 47. 35. 23. 11. Abstract |
| 84 | 72. 60. 48. 36. 24. 12. Keywords |
| 85 | 73. 61. 49. 37. 25. 13. 1. Introduction |
| 86 | 74. 62. 50. 38. 26. 14. 2. Objectives |
| 87 | 75. 63. 51. 39. 27. 15. 3. Methodology |
| 88 | 76. 64. 52. 40. 28. 16. 4. Results |
| 89 | 77. 65. 53. 41. 29. 17. 5. Discussion |
| 90 | 78. 66. 54. 42. 30. 18. 6. Conclusion |
| 91 | 79. 67. 55. 43. 31. 19. 7. References |
| 92 | 80. 68. 56. 44. 32. 20. 8. Appendix |
| 93 | 81. 69. 57. 45. 33. 21. 9. Index |
| 94 | 82. 70. 58. 46. 34. 22. 10. Summary |
| 95 | 83. 71. 59. 47. 35. 23. 11. Abstract |
| 96 | 84. 72. 60. 48. 36. 24. 12. Keywords |
| 97 | 85. 73. 61. 49. 37. 25. 13. 1. Introduction |
| 98 | 86. 74. 62. 50. 38. 26. 14. 2. Objectives |
| 99 | 87. 75. 63. 51. 39. 27. 15. 3. Methodology |
| 100 | 88. 76. 64. 52. 40. 28. 16. 4. Results |
| 101 | 89. 77. 65. 53. 41. 29. 17. 5. Discussion |
| 102 | 90. 78. 66. 54. 42. 30. 18. 6. Conclusion |
| 103 | 91. 79. 67. 55. 43. 31. 19. 7. References |
| 104 | 92. 80. 68. 56. 44. 32. 20. 8. Appendix |
| 105 | 93. 81. 69. 57. 45. 33. 21. 9. Index |
| 106 | 94. 82. 70. 58. 46. 34. 22. 10. Summary |
| 107 | 95. 83. 71. 59. 47. 35. 23. 11. Abstract |
| 108 | 96. 84. 72. 60. 48. 36. 24. 12. Keywords |
| 109 | 97. 85. 73. 61. 49. 37. 25. 13. 1. Introduction |
| 110 | 98. 86. 74. 62. 50. 38. 26. 14. 2. Objectives |
| 111 | 99. 87. 75. 63. 51. 39. 27. 15. 3. Methodology |
| 112 | 100. 88. 76. 64. 52. 40. 28. 16. 4. Results |
| 113 | 101. 89. 77. 65. 53. 41. 29. 17. 5. Discussion |
| 114 | 102. 90. 78. 66. 54. 42. 30. 18. 6. Conclusion |
| 115 | 103. 91. 79. 67. 55. 43. 31. 19. 7. References |
| 116 | 104. 92. 80. 68. 56. 44. 32. 20. 8. Appendix |
| 117 | 105. 93. 81. 69. 57. 45. 33. 21. 9. Index |
| 118 | 106. 94. 82. 70. 58. 46. 34. 22. 10. Summary |
| 119 | 107. 95. 83. 71. 59. 47. 35. 23. 11. Abstract |
| 120 | 108. 96. 84. 72. 60. 48. 36. 24. 12. Keywords |
| 121 | 109. 97. 85. 73. 61. 49. 37. 25. 13. 1. Introduction |
| 122 | 110. 98. 86. 74. 62. 50. 38. 26. 14. 2. Objectives |
| 123 | 111. 99. 87. 75. 63. 51. 39. 27. 15. 3. Methodology |
| 124 | 112. 100. 88. 76. 64. 52. 40. 28. 16. 4. Results |
| 125 | 113. 101. 89. 77. 65. 53. 41. 29. 17. 5. Discussion |
| 126 | 114. 102. 90. 78. 66. 54. 42. 30. 18. 6. Conclusion |
| 127 | 115. 103. 91. 79. 67. 55. 43. 31. 19. 7. References |
| 128 | 116. 104. 92. 80. 68. 56. 44. 32. 20. 8. Appendix |
| 129 | 117. 105. 93. 81. 69. 57. 45. 33. 21. 9. Index |
| 130 | 118. 106. 94. 82. 70. 58. 46. 34. 22. 10. Summary |
| 131 | 119. 107. 95. 83. 71. 59. 47. 35. 23. 11. Abstract |
| 132 | 120. 108. 96. 84. 72. 60. 48. 36. 24. 12. Keywords |
| 133 | 121. 109. 97. 85. 73. 61. 49. 37. 25. 13. 1. Introduction |
| 134 | 122. 110. 98. 86. 74. 62. 50. 38. 26. 14. 2. Objectives |
| 135 | 123. 111. 99. 87. 75. 63. 51. 39. 27. 15. 3. Methodology |
| 136 | 124. 112. 100. 88. 76. 64. 52. 40. 28. 16. 4. Results |
| 137 | 125. 113. 101. 89. 77. 65. 53. 41. 29. 17. 5. Discussion |
| 138 | 126. 114. 102. 90. 78. 66. 54. 42. 30. 18. 6. Conclusion |
| 139 | 127. 115. 103. 91. 79. 67. 55. 43. 31. 19. 7. References |
| 140 | 128. 116. 104. 92. 80. 68. 56. 44. 32. 20. 8. Appendix |
| 141 | 129. 117. 105. 93. 81. 69. 57. 45. 33. 21. 9. Index |
| 142 | 130. 118. 106. 94. 82. 70. 58. 46. 34. 22. 10. Summary |
| 143 | 131. 119. 107. 95. 83. 71. 59. 47. 35. 23. 11. Abstract |
| 144 | 132. 120. 108. 96. 84. 72. 60. 48. 36. 24. 12. Keywords |
| 145 | 133. 121. 109. 97. 85. 73. 61. 49. 37. 25. 13. 1. Introduction |
| 146 | 134. 122. 110. 98. 86. 74. 62. 50. 38. 26. 14. 2. Objectives |
| 147 | 135. 123. 111. 99. 87. 75. 63. 51. 39. 27. 15. 3. Methodology |
| 148 | 136. 124. 112. 100. 88. 76. 64. 52. 40. 28. 16. 4. Results |
| 149 | 137. 125. 113. 101. 89. 77. 65. 53. 41. 29. 17. 5. Discussion |
| 150 | 138. 126. 114. 102. 90. 78. 66. 54. 42. 30. 18. 6. Conclusion |
| 151 | 139. 127. 115. 103. 91. 79. 67. 55. 43. 31. 19. 7. References |
| 152 | 140. 128. 116. 104. 92. 80. 68. 56. 44. 32. 20. 8. Appendix |
| 153 | 141. 129. 117. 105. 93. 81. 69. 57. 45. 33. 21. 9. Index |
| 154 | 142. 130. 118. 106. 94. 82. 70. 58. 46. 34. 22. 10. Summary |
| 155 | 143. 131. 119. 107. 95. 83. 71. 59. 47. 35. 23. 11. Abstract |
| 156 | 144. 132. 120. 108. 96. 84. 72. 60. 48. 36. 24. 12. Keywords |
| 157 | 145. 133. 121. 109. 97. 85. 73. 61. 49. 37. 25. 13. 1. Introduction |
| 158 | 146. 134. 122. 110. 98. 86. 74. 62. 50. 38. 26. 14. 2. Objectives |
| 159 | 147. 135. 123. 111. 99. 87. 75. 63. 51. 39. 27. 15. 3. Methodology |
| 160 | 148. 136. 124. 112. 100. 88. 76. 64. 52. 40. 28. 16. 4. Results |
| 161 | 149. 137. 125. 113. 101. 89. 77. 65. 53. 41. 29. 17. 5. Discussion |
| 162 | 150. 138. 126. 114. 102. 90. 78. 66. 54. 42. 30. 18. 6. Conclusion |
| 163 | 151. 139. 127. 115. 103. 91. 79. 67. 55. 43. 31. 19. 7. References |
| 164 | 152. 140. 128. 116. 104. 92. 80. 68. 56. 44. 32. 20. 8. Appendix |
| 165 | 153. 141. 129. 117. 105. 93. 81. 69. 57. 45. 33. 21. 9. Index |
| 166 | 154. 142. 130. 118. 106. 94. 82. 70. 58. 46. 34. 22. 10. Summary |
| 167 | 155. 143. 131. 119. 107. 95. 83. 71. 59. 47. 35. 23. 11. Abstract |
| 168 | 156. 144. 132. 120. 108. 96. 84. 72. 60. 48. 36. 24. 12. Keywords |
| 169 | 157. 145. 133. 121. 109. 97. 85. 73. 61. 49. 37. 25. 13. 1. Introduction |
| 170 | 158. 146. 134. 122. 110. 98. 86. 74. 62. 50. 38. 26. 14. 2. Objectives |
| 171 | 159. 147. 135. 123. 111. 99. 87. 75. 63. 51. 39. 27. 15. 3. Methodology |
| 172 | 160. 148. 136. 124. 112. 100. 88. 76. 64. 52. 40. 28. 16. 4. Results |
| 173 | 161. 149. 137. 125. 113. 101. 89. 77. 65. 53. 41. 29. 17. 5. Discussion |
| 174 | 162. 150. 138. 126. 114. 102. 90. 78. 66. 54. 42. 30. 18. 6. Conclusion |
| 175 | 163. 151. 139. 127. 115. 103. 91. 79. 67. 55. 43. 31. 19. 7. References |
| 176 | 164. 152. 140. 128. 116. 104. 92. 80. 68. 56. 44. 32. 20. 8. Appendix |
| 177 | 165. 153. 141. 129. 117. 105. 93. 81. 69. 57. 45. 33. 21. 9. Index |
| 178 | 166. 154. 142. 130. 118. 106. 94. 82. 70. 58. 46. 34. 22. 10. Summary |
| 179 | 167. 155. 143. 131. 119. 107. 95. 83. 71. 59. 47. 35. 23. 11. Abstract |
| 180 | 168. 156. 144. 132. 120. 108. 96. 84. 72. 60. 48. 36. 24. 12. Keywords |
| 181 | 169. 157. 145. 133. 121. 109. 97. 85. 73. 61. 49. 37. 25. 13. 1. Introduction |
| 182 | 170. 158. 146. 134. 122. 110. 98. 86. 74. 62. 50. 38. 26. 14. 2. Objectives |
| 183 | 171. 159. 147. 135. 123. 111. 99. 87. 75. 63. 51. 39. 27. 15. 3. Methodology |
| 184 | 172. 160. 148. 136. 124. 112. 100. 88. 76. 64. 52. 40. 28. 16. 4. Results |
| 185 | 173. 161. 149. 137. 125. 113. 101. 89. 77. 65. 53. 41. 29. 17. 5. Discussion |
| 186 | 174. 162. 150. 138. 126. 114. 102. 90. 78. 66. 54. 42. 30. 18. 6. Conclusion |
| 187 | 175. 163. 151. 139. 127. 115. 103. 91. 79. 67. 55. 43. 31. 19. 7. References |
| 188 | 176. 164. 152. 140. 128. 116. 104. 92. 80. 68. 56. 44. 32. 20. 8. Appendix |
| 189 | 177. 165. 153. 141. 129. 117. 105. 93. 81. 69. 57. 45. 33. 21. 9. Index |
| 190 | 178. 166. 154. 142. 130. 118. 106. 94. 82. 70. 58. 46. 34. 22. 10. Summary |
| 191 | 179. 167. 155. 143. 131. 119. 107. 95. 83. 71. 59. 47. 35. 23. 11. Abstract |
| 192 | 180. 168. 156. 144. 132. 120. 108. 96. 84. 72. 60. 48. 36. 24. 12. Keywords |
| 193 | 181. 169. 157. 145. 133. 121. 109. 97. 85. 73. 61. 49. 37. 25. 13. 1. Introduction |
| 194 | 182. 170. 158. 146. 134. 122. 110. 98. 86. 74. 62. 50. 38. 26. 14. 2. Objectives |
| 195 | 183. 171. 159. 147. 135. 123. 111. 99. 87. 75. 63. 51. 39. 27. 15. 3. Methodology |
| 196 | 184. 172. 160. 148. 136. 124. 112. 100. 88. 76. 64. 52. 40. 28. 16. 4. Results |
| 197 | 185. 173. 161. 149. 137. 125. 113. 101. 89. 77. 65. 53. 41. 29. 17. 5. Discussion |
| 198 | 186. 174. 162. 150. 138. 126. 114. 102. 90. 78. 66. 54. 42. 30. 18. 6. Conclusion |
| 199 | 187. 175. 163. 151. 139. 127. 115. 103. 91. 79. 67. 55. 43. 31. 19. 7. References |
| 200 | 188. 176. 164. 152. 140. 128. 116. 104. 92. 80. 68. 56. 44. 32. 20. 8. Appendix |
| 201 | 189. 177. 165. 153. 141. 129. 117. 105. 93. 81. 69. 57. 45. 33. 21. 9. Index |
| 202 | 190. 178. 166. 154. 142. 130. 118. 106. 94. 82. 70. 58. 46. 34. 22. 10. Summary |
| 203 | 191. 179. 167. 155. 143. 131. 119. 107. 95. 83. 71. 59. 47. 35. 23. 11. Abstract |
| 204 | 192. 180. 168. 156. 144. 132. 120. 108. 96. 84. 72. 60. 48. 36. 24. 12. Keywords |
| 205 | 193. 181. 169. 157. 145. 133. 121. 109. 97. 85. 73. 61. 49. 37. 25. 13. 1. Introduction |
| 206 | 194. 182. 170. 158. 146. 134. 122. 110. 98. 86. 74. 62. 50. 38. 26. 14. 2. Objectives |
| 207 | 195. 183. 171. 159. 147. 135. 123. 111. 99. 87. 75. 63. 51. 39. 27. 15. 3. Methodology |
| 208 | 196. 184. 172. 160. 148. 136. 124. 112. 100. 88. 76. 64. 52. 40. 28. 16. 4. Results |
| 209 | 197. 185. 173. 161. 149. 137. 125. 113. 101. 89. 77. 65. 53. 41. 29. 17. 5. Discussion |
| 210 | 198. 186. 174. 162. 150. 138. 126. 114. 102. 90. 78. 66. 54. 42. 30. 18. 6. Conclusion |
| 211 | 199. 187. 175. 163. 151. 139. 127. 115. 103. 91. 79. 67. 55. 43. 31. 19. 7. References |
| 212 | 200. 188. 176. 164. 152. 140. 128. 116. 104. 92. 80. 68. 56. 44. 32. 20. 8. Appendix |
| 213 | 201. 189. 177. 165. 153. 141. 129. 117. 105. 93. 81. 69. 57. 45. 33. 21. 9. Index |
| 214 | 202. 190. 178. 166. 154. 142. 130. 118. 106. 94. 82. 70. 58. 46. 34. 22. 10. Summary |
| 215 | 203. 191. 179. 167. 155. 143. 131. 119. 107. 95. 83. 71. 59. 47. 35. 23. 11. Abstract |
| 216 | 204. 192. 180. 168. 156. 144. 132. 120. 108. 96. 84. 72. 60. 48. 36. 24. 12. Keywords |
| 217 | 205. 193. 181. 169. 157. 145. 133. 121. 109. 97. 85. 73. 61. 49. 37. 25. 13. 1. Introduction |
| 218 | 206. 194. 182. 170. 158. 146. 134. 122. 110. 98. 86. 74. 62. 50. 38. 26. 14. 2. Objectives |
| 219 | 207. 195. 183. 171. 159. 147. 135. 123. 111. 99. 87. 75. 63. 51. 39. 27. 15. 3. Methodology |
| 220 | 208. 196. 184. 172. 160. 148. 136. 124. 112. 100. 88. 76. 64. 52. 40. 28. 16. 4. Results |
| 221 | 209. 197. 185. 173. 161. 149. 137. 125. 113. 101. 89. 77. 65. 53. 41. 29. 17. 5. Discussion |
| 222 | 210. 198. 186. 174. 162. 150. 138. 126. 114. 102. 90. 78. 66. 54. 42. 30. 18. 6. Conclusion |
| 223 | 211. 199. 187. 175. 163. 151. 139. 127. 115. 103. 91. 79. 67. 55. 43. 31. 19. 7. References |
| 224 | 212. 200. 188. 176. 164. 152. 140. 128. 116. 104. 92. 80. 68. 56. 44. 32. 20. 8. Appendix |
| 225 | 213. 201. 189. 177. 165. 153. 141. 129. 117. 105. 93. 81. 69. 57. 45. 33. 21. 9. Index |
| 226 | 214. 202. 190. 178. 166. 154. 142. 130. 118. 106. 94. 82. 70. 58. 46. 34. 22. 10. Summary |
| 227 | 215. 203. 1 |

EXPERIMENTS WITH CENTRAL SUPERHEATER CORE CSH-1, BORAX-V

by

BORAX-V Project Staff

I. INTRODUCTION

BORAX-V was the first integral boiling-water-nuclear superheating reactor to be operated in the United States. It first produced superheated steam on October 10, 1963.

Following a considerable time during which low-power experiments were performed, and after a few days of operation at power up to 10.2 MWt, a sizeable leak of moderator water into the superheater was measured and a low level of fission product radioactivity was discovered in the superheated steam. Power operation was discontinued on October 16, 1963. Investigation revealed that the water leak was caused by a weld crack in one superheater fuel assembly and that the fission products were coming from a few tears in the bottom of superheater plates that were distorted by restraints caused by improperly performed leak-repair welds on the assemblies.

The feasibility of continuing operation with this core was analyzed by the reactor staff, and it was concluded that although the superheater fuel was distorted and a low level of fission products would be present continuously in the steam, operation could be performed with reasonable safety by the adoption of special operating procedures. However, since repair welds had also been made to other superheater fuel assemblies and there was no assurance that additional similar failures would not occur, a management decision was made to discontinue operation of central superheater core CSH-1 and to proceed directly to the program involving the peripheral superheater core. The fuel for that core was reworked to correct the weld defects and was not subject to the problems involving the central superheater fuel.

In spite of the brief operating period, much valuable information was obtained and is reported in this document. However, a major part of the planned power experimental program on this core could not be accomplished completely. This included the attainment of full power; power split, power distribution, and core and plant power performance experiments; reactor stability measurements, water chemistry experiments, defective fuel experiments, etc. This program was deferred and subsequently accomplished in considerable detail with the peripheral superheater core.⁽¹⁾

II. REACTOR DESCRIPTION⁽²⁾

The BORAX-V reactor and power plant are located in two buildings one-half mile from the control building at the National Reactor Testing Station in Idaho.

Three core structure configurations have been tested in this flexible experimental facility: a pure boiling-water core, a boiling core with a centrally located superheater, and a boiling-water core with a peripherally located superheater. In all cases, it was possible to operate with either forced or natural circulation of water through the boiler zone of the core, but only natural circulation was used. Water served as moderator and reflector in both the boiling and superheating regions of the core.

The principal design parameters of BORAX-V at the rated power are shown in Table I.

Table I
DESIGN PARAMETERS, BORAX-V CENTRAL SUPERHEATER CORE
AT 20 MWt

| | | |
|---|---------------|--------------------|
| Pressure, psig | 600 | |
| Temperatures, °F | | |
| Saturated steam | 489 | |
| Superheated steam | 850 | |
| Boiling fuel rod (center maximum) | 2,300 | |
| Superheater fuel plates (center maximum) | 1,130 | |
| Maximum heat flux, Btu/hr-ft ² | | |
| Boiling rod | 310,000 | |
| Superheater plates | 100,000 | |
| Power density, average, kW/liter of core volume | | |
| Boiling zone | 42.5 | |
| Superheat zone | 40.5 | |
| | <u>Boiler</u> | <u>Superheater</u> |
| Number of fuel assemblies | 48 | 12 |

Figure 1 is a cutaway view of the BORAX-V reactor vessel containing the core with central superheater. All cores had an equivalent diameter of 39 in. and a height of 24 in., with the bottom of the active core positioned 3 ft above the bottom of the reactor vessel. The poison section of the nine control rods was made of Boral canned in stainless steel, and the follower section was made of X-8001 aluminum alloy. The central and four intermediate control rods were cruciform, and the four outer rods were T-shaped.

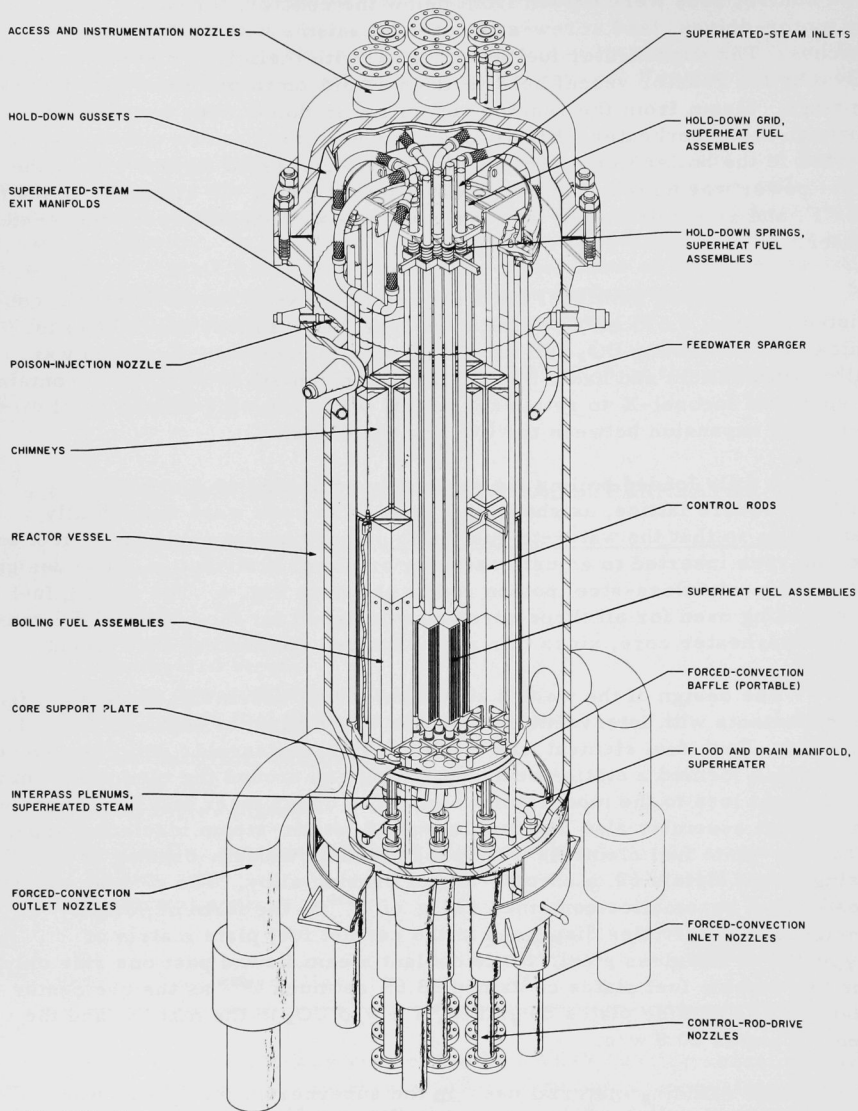
The control rods were driven from below the reactor, through a linear seal, by motor-driven, lead screw-and-nut mechanisms with solenoid scram latches. The superheater fuel assemblies, with their long risers, were held down by the reactor vessel head through a hold-down plate and individual coil springs. Steam from the reactor vessel steam dome made two passes through the superheater. Eighty-one percent of the reactor power was required in the boiler to convert feedwater into saturated steam; 17% of the total power was used in the superheater to superheat the steam from 489 to 850°F, and an additional 2% was lost from the superheater to the moderator water.

The boiling zone fuel elements for BORAX-V, shown in Fig. 2, consisted of rods, 0.375 in. OD, clad with Type 304 stainless steel 0.015 in. thick, and containing UO_2 pellets of 4.95 w/o enrichment. Each rod was filled with helium and had a fission gas expansion space which also contained a spring of Inconel-X to retain the pellets while allowing for the axial differential expansion between the UO_2 and the cladding.

A fully loaded boiling fuel assembly contained 49 fuel rods in a 1/2-in.-square lattice, as shown in Fig. 3. The rods were individually latched in so that the water-to-fuel ratio or enrichment could be varied, or poison rods inserted to adjust reactivity or power distribution. The design of a boron-stainless-steel poison rod is shown in Fig. 4. The boiling fuel rod loading used for all three cores was designed for the boiler of the central superheater core, since this zone required the highest enrichment.

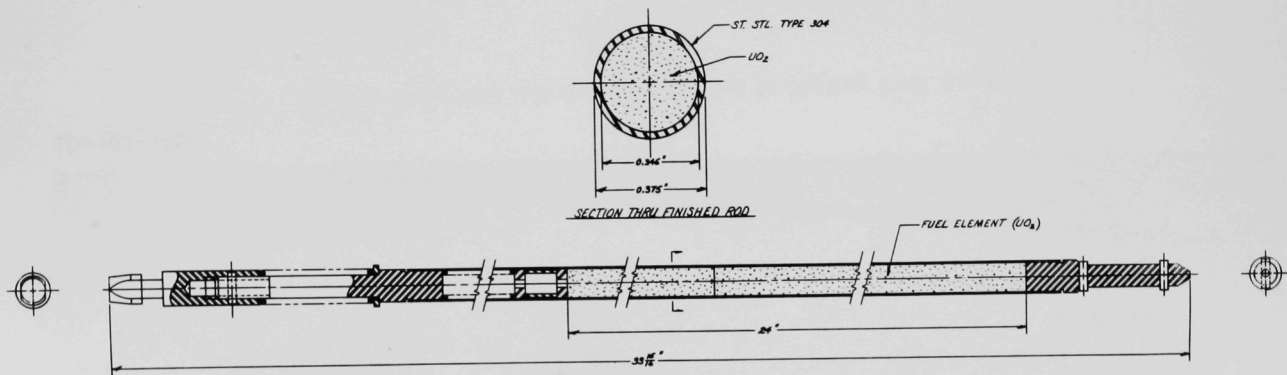
The design of the welded superheater fuel assembly, made up of five fuel elements with intervening moderator water gaps, is shown in Figs. 1, 5, and 6. Each fuel element was contained in a rectangular stainless-steel tube which formed a static-steam insulating gap around the element to minimize heat loss to the moderator water. The upper riser and lower nozzle in the fuel assembly also had double-walled, static-steam insulating gaps. The four-plate fuel elements were assembled by vacuum-brazing at 2150°F, using Coast Metals 60, a chrome-nickel brazing alloy. The central superheater fuel assemblies contained 430 g of U^{235} in the form of 93 w/o-enriched UO_2 particles dispersed in the cermet fuel plate matrix of Type 304-B stainless steel. Since coolant steam flowed past one side only, the two outside fuel plates contained 53.6% as much U^{235} as the two center plates. The outside plates contained 11.4 w/o UO_2 in the matrix, and the central plates 20.8 w/o.

The cladding material used on the superheater fuel plates was Type 304-L stainless steel, which is susceptible to chloride stress corrosion. Chloride stress corrosion was inhibited by the maintenance of less than 0.04 ppm of Cl^- in the reactor water and steam by means of the makeup water, reactor water, and condensate demineralizer systems and continuous chloride monitoring.



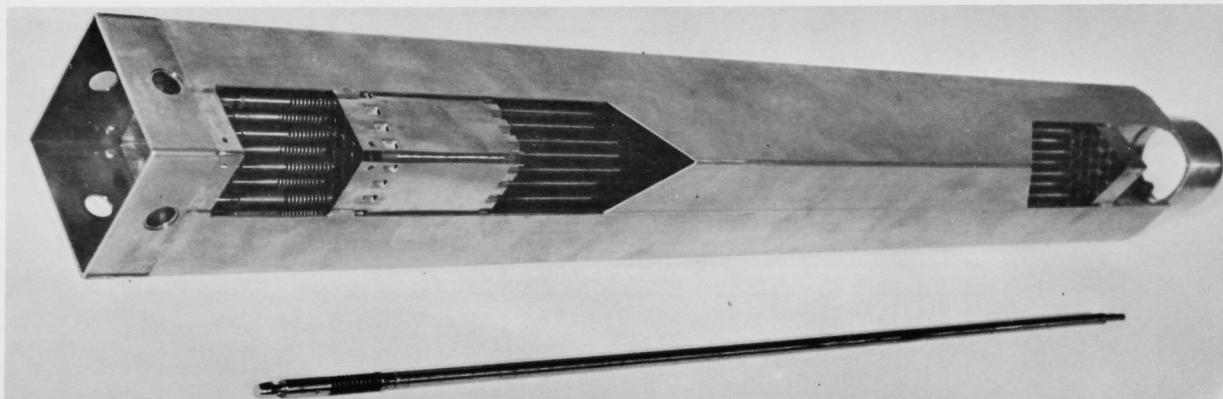
103-371-B

Fig. 1. Reactor with Central Superheater



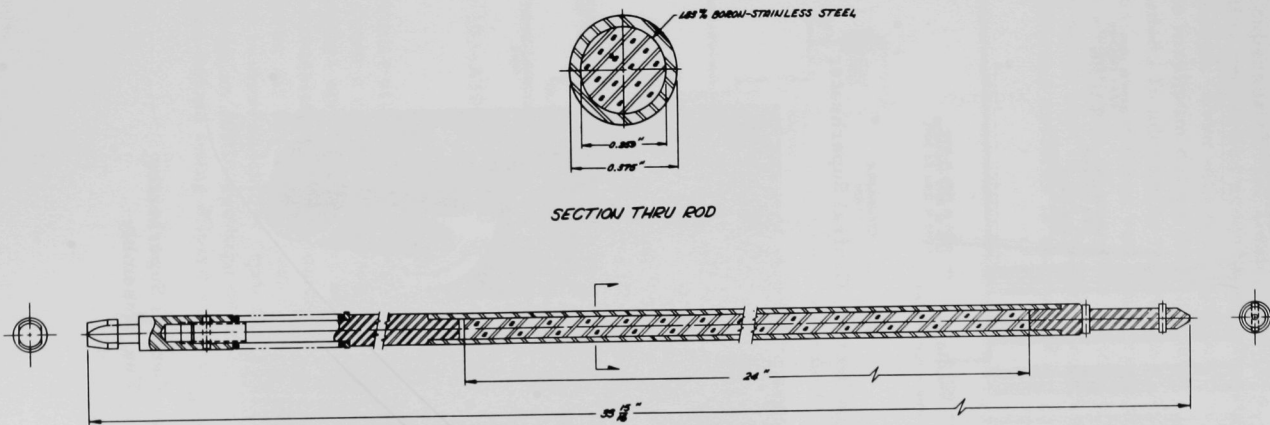
ID-103-A3322

Fig. 2. Boiling Fuel Rod



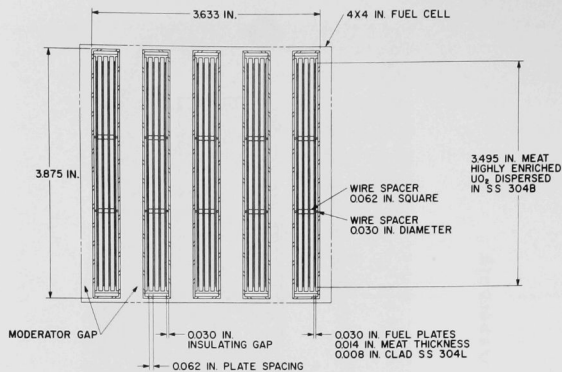
ID-103-3466

Fig. 3. Fuel Rod and Cutaway Section of Boiling Fuel Assembly



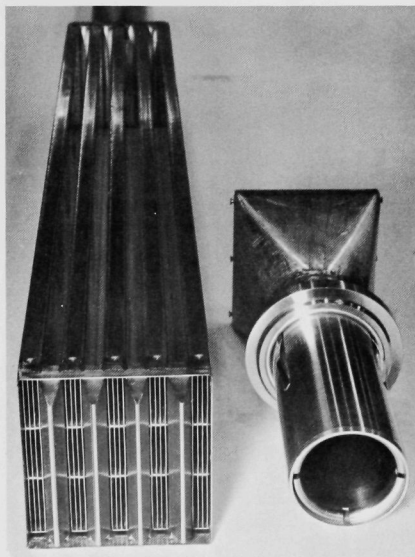
ID-103-A3323

Fig. 4. Boron-stainless-steel Poison Rod



ID-103-A3234

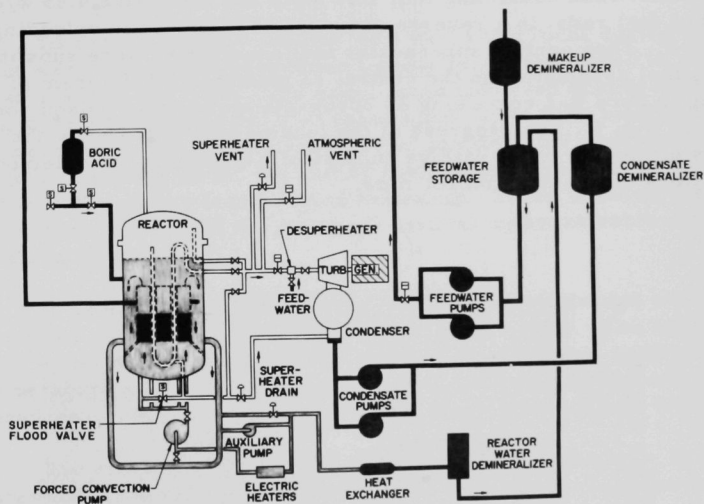
Fig. 5. Cross Section, Central Superheater Fuel Assembly



ID-103-3776

Fig. 6. Central Superheater Fuel Assembly

The superheater fuel element had good shutdown radiation and conductive cooling properties across the static-steam insulating gap to the moderator water. Even with no steam flow and a total reactor power of 0.8 MWt, the maximum design fuel surface temperature of 1200°F could not be exceeded. In addition to the design of the superheater fuel element, BORAX-V had a superheater vent valve system that opened automatically on any normal shutdown or scram to assure continued flow of cooling steam produced by decay heat in the boiling zone. A schematic diagram of the BORAX-V process systems is shown in Fig. 7.



ID-103-A3015

Fig. 7. Flow Diagram

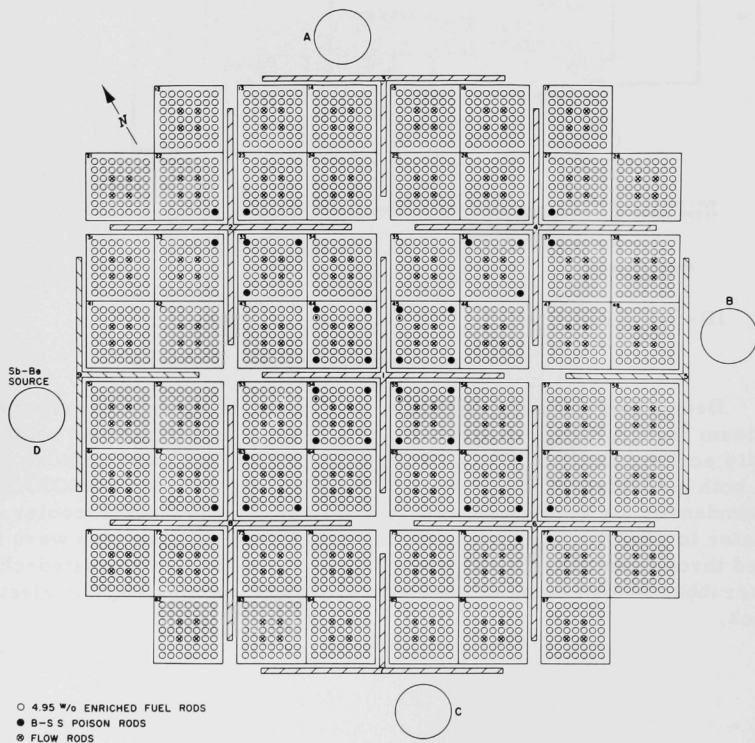
Because of the postulated high rate of fission product carryover in the steam from a ruptured superheater fuel element, steam line radioactivity scrams and alarms, plus sensitive fission product monitors sampling both saturated and superheated steam, were provided on BORAX-V. The condenser air ejector exhaust system had a special after-cooler and demister to remove moisture from the gas. The exhaust gases were then passed through an AEC-type high-efficiency filter and an activated-charcoal gas scrubber before being diluted with clean air, monitored, and ejected up a stack.

III. REACTIVITY MEASUREMENTS

A. Zero-power Reactivity Measurements

1. Loading

After the central superheater core structure, control rods, and control rod drives had been installed and checked out, the loading of fuel assemblies began. The core was completely loaded with boiling fuel assemblies, each containing four flow rods and forty-five 4.95 w/o-enriched fuel rods, in a reverse sequence to that used in unloading boiling core B-2. Then central superheater fuel assemblies were substituted for boiling fuel assemblies in the central 12 positions. A diagram of the final loading in core B-2 containing 40 boron-stainless-steel poison rods is shown in Fig. 8. The progress of the loading was followed by the customary curves of inverse count rate vs number of assemblies for selected configurations of the nine control rods.



ID-103-A3235

Fig. 8. Final Loading, Boiling Core B-2

The central superheater core support structure gave the same positioning of fuel assemblies as the boiling core structure, except that boiling fuel assemblies placed in the central 12 superheating fuel assembly positions rested on top of the core support plate instead of fitting into it. Therefore, they were $3\frac{1}{4}$ in. higher than normal. Before boiling core B-2 was unloaded, adapters were installed on three of the 12 central boiling assemblies in one quadrant to raise them $3\frac{1}{4}$ in. higher than normal for similar positions in the superheater core structure. The reactivity effect of these higher assemblies was found to be negative.

To ensure that the reactor was well subcritical during loading, count rates were measured from three fission counters located in reflector thimbles adjacent to the core. The count rates observed during unloading the boiling core were compared with those found during the loading of the central superheater core. Also, control rod positions for reactor criticality were found for loadings of 60, 35, and 20 fuel assemblies. These were also compared with the values found during unloading. Table II shows the loading sequence of core CSH-1 and the principal critical measurements made during the loading operation.

In Loading No. 118, the core was completely loaded with boiling fuel assemblies and 40 boron-stainless-steel poison rods. The central 12 assemblies were raised $3\frac{1}{4}$ in., and the nine-control-rod-bank position at room temperature was 10.100 in. In core B-2, with 40 poison rods and no fuel assemblies raised, the nine-control-rod-bank position was 9.053 in.

The reactivity worth vs water, at room temperature, of a single superheater fuel assembly in core position 56 was measured to be 0.71% by comparing Loadings Nos. 122 and 123.

After the superheater fuel assemblies were loaded, all poison rods were removed in two steps and replaced with 4.95 w/o-enriched fuel rods. Critical experiments were conducted at room temperature to verify that the reactor would not go critical on the complete withdrawal of any single control rod alone.

2. Adjustment of Fuel-to-water Ratio

Several experiments were conducted at room temperature in which the fuel-to-water ratio in the boiling fuel assemblies was varied by changing the number and arrangement of water-filled flow rods in the assemblies. A flow rod, as shown in Fig. 9, had the same outside geometry and dimensions as a boiling fuel rod, but the in-core portion was made of X-8001 aluminum tubing, $3/8$ -in. OD x 0.20-in. wall thickness, perforated on each end to insure flooding with reactor water. The use of flow rods to increase the moderator fraction of the core prevented bypass of coolant water through a vacant fuel rod location. The objective of these experiments was to increase the available excess reactivity and reduce the value of the

Table II
LOADING SEQUENCE, CORE CSH-1

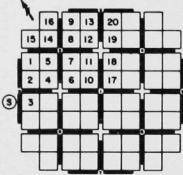
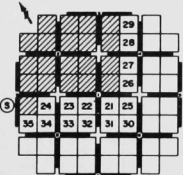
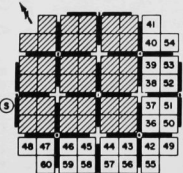
| Loading No. | Configuration | Remarks | Control Rod Critical Positions | |
|-------------|---|--|--|---|
| | | | Core CSH-1 Loading | Core B-2 Unloading |
| 116 |  | <p>a. 14 poison rods 20 boiling assemblies</p> <p>b. Assemblies in positions No. 6, 10, 11, 17, and 18 were $3\frac{1}{4}$ in. high.</p> | <p>Rod No. 2: 23.345 in. Remainder: 16.000 in.</p> | <p>Rod No. 2: 23.730 in. Remainder: 16.000 in.</p> <p>Boiling assemblies No. 6, 10, and 11, $3\frac{1}{4}$ in. high.</p> |
| 117 |  | <p>a. 32 poison rods 35 boiling assemblies</p> <p>b. Additional assemblies, positions No. 21, 22, 23, 25, 26, 31, and 32, were $3\frac{1}{4}$ in. high.</p> | <p>Rod No. 2: 21.660 in. Rods No. 5 and 9: 15.000 in. Remainder: 0.000 in.</p> | <p>Rod No. 2: 22.415 in. Rods No. 5 and 9: 15.000 in. Remainder: 0.000 in.</p> <p>Boiling assemblies No. 6, 10, and 11, $3\frac{1}{4}$ in. high.</p> |
| 118 |  | <p>a. 40 poison rods 60 boiling assemblies</p> <p>b. Assemblies in super-heater positions are $3\frac{1}{4}$ in. high.</p> | <p>Rod No. 1: 10.098 in. Remainder: 10.100 in.</p> | <p>All rods: 9.053 in. No assemblies above normal.</p> |

Table II
(Continued)

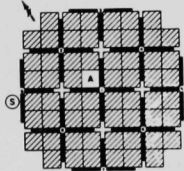
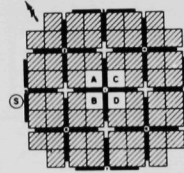
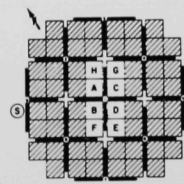
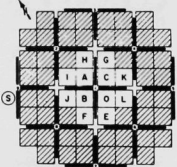
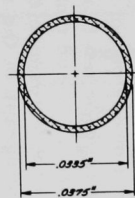
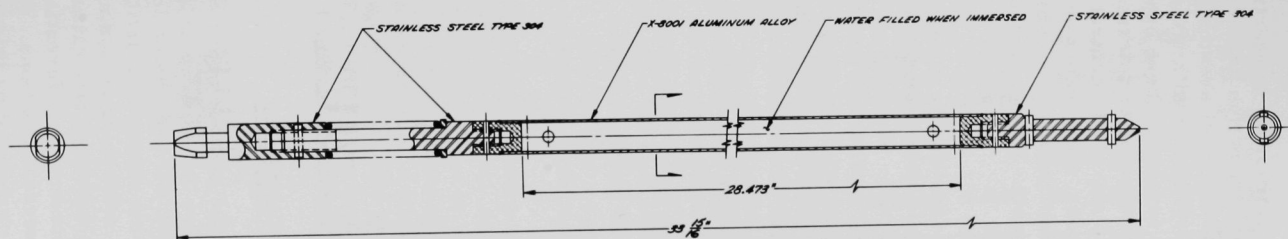
| Loading No. | Configuration | Remarks | Control Rod Critical Positions | Reactivity Change from Previous Configuration, % |
|-------------|--|--|---|--|
| 119 |  | a. 36 poison rods 1 superheater assembly 59 boiling assemblies | Rod No. 1: 10.600 in. Remainder: 10.100 in. $\left(\frac{\Delta\rho}{\Delta h}\right)$ Rod No.1 = 0.32%/in. | -0.16 |
| 120 |  | a. 24 poison rods 4 superheater assemblies 56 boiling assemblies | Rod No. 1: 9.760 in. Remainder: 10.100 in. $\left(\frac{\Delta\rho}{\Delta h}\right)$ Rod No.1 = 0.335%/in. | +0.275 |
| 121 |  | a. 24 poison rods 8 superheater assemblies 52 boiling assemblies | Rod No. 1: 14.170 in. Remainder: 10.100 in. $\left(\frac{\Delta\rho}{\Delta h}\right)$ Rod No.1 = 0.21%/in. | -1.20 |

Table II
(Continued)

| Loading No. | Configuration | Remarks | Control Rod Critical Positions | Reactivity Change from Previous Configuration, % |
|-------------|---|---|--|--|
| 122 |  | <p>a. 24 poison rods 11 superheater assemblies 48 boiling assemblies</p> <p>b. Position L is water.</p> | <p>All rods: 12.410 in.</p> <p>$\left(\frac{\Delta\rho}{\Delta h}\right)_{\text{Rod No.1}} = 0.139\%/in.$</p> | |
| 123 | | <p>a. 24 poison rods 12 superheater assemblies 48 boiling assemblies</p> | <p>a. All rods: 11.705 in.</p> <p>$\left(\frac{\Delta\rho}{\Delta h}\right)_{\text{9-rod bank}} = 1.13\%/in.$</p> <p>b. No. 1 rod: 8.278 in. Remainder: 12.410 in.</p> <p>$\left(\frac{\Delta\rho}{\Delta h}\right)_{\text{Rod No.1}} = 0.188\%/in.$</p> | +0.71 |



SECTION THRU ROD



ID-103-A3324

Fig. 9. Flow Rod

temperature and void coefficients of reactivity. It was also possible to flatten the neutron flux distribution and to modify the neutron energy spectrum within each boiling fuel assembly. The detailed flux plots showing the flatter power distribution within the boiling fuel assemblies are shown in Fig. 49. The results of these experiments are shown in Table III. At each step, checks were made to determine if the reactor would go critical on the withdrawal of any single control rod alone. Because of a temporary shortage of flow rods, water holes or water tubes (made of 1/4-in. OD x 0.028-in.-wall 3003 aluminum) were substituted for some of the flow rods in some of the experiments. No poison rods were in the core during these experiments.

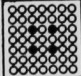
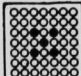
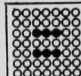
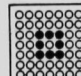
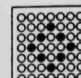
The change in available excess reactivity for each step is not listed because an accurate determination could not be made without a complete control rod calibration. However, it was estimated from control rod positions and differential control rod reactivity worths that the change in available excess reactivity at room temperature from the four- to the five-, six-, or eight-concentrated-flow-rod configurations was negligible. The change to the eight-distributed-flow-rod configuration resulted in a significant increase in available reactivity, but this configuration was not used because substitution of some poison rods in place of fuel rods would have been required to prevent criticality on the withdrawal of any one of intermediate control rods No. 2, 4, or 6. The decision was made not to use poison rods in core CSH-1, and the eight-concentrated-flow-rod configuration was used in the reference loading. Figure 10 shows the reference zero-power fuel loading for this core, and Fig. 11 is a photograph of the reactor loaded for the zero-power, room-temperature experiments.

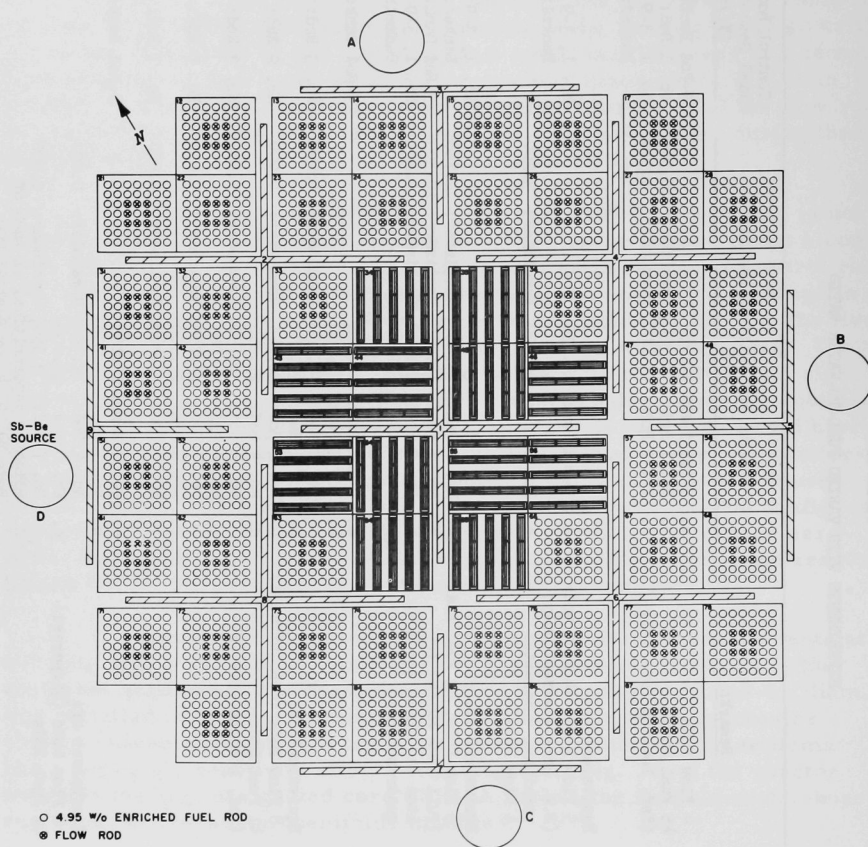
For the zero-power, operating-temperature measurements at 600 psig, 489°F conditions, six flux-wire thimbles were installed in the southeast quadrant of the core. A sheathed thermocouple, 0.040-in. diam, was installed in a boiler coolant channel and another in a superheater coolant channel for accurate temperature measurements. These items had a negligible reactivity effect. A photograph, Fig. 12, of the reactor with this loading, designated core CSH-1A, shows the flexible-metal-hose exit superheated-steam manifolds installed.

3. Control Rod Calibration

The control rod arrangement for the CSH-1 core can be seen in Fig. 10, and is the same as that of the previously reported boiling cores, B-1 and B-2.^(3,4) The control rod was calibrated in the same fashion - that is, the removal of available excess reactivity by the addition of boric acid to the reactor water. This moderator poisoning, at different boron concentrations, permitted the establishment of a critical position at several control rod heights, and correspondingly, differential-control-rod-reactivity-worth measurements at these several positions. Reactivity calibration of the core CSH-1 control rods was performed by this means from approximately 11 in.

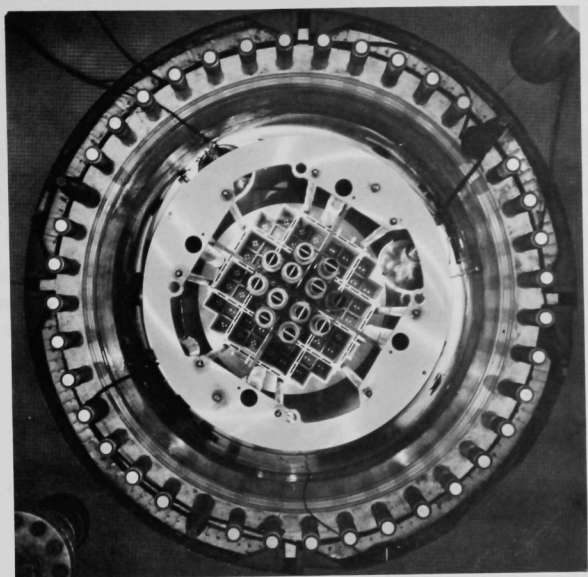
Table III
EXPERIMENTS WITH VARIED FUEL-TO-WATER RATIO

| Loading No. | Configuration | Remarks | Control Rod Critical Positions (in.) | | Control Rod Differential Reactivity Worth (%/in.) | |
|-------------|---|---|--------------------------------------|---|---|-------|
| | | | | | | |
| 125 |  | 4 Flow Rods 45 Fuel Rods (Ref. loading core B-2) | a. | 9-Rod Bank: 10.365 | 9-Rod Bank: | 1.43 |
| | | | b. | No. 1 Rod: 10.370, Remainder: 10.360 | No. 1 Rod: | 0.195 |
| | | | c. | No. 2 Rod: 25.000, Remainder: 4.320 | No. 1, 3-9 Rods Banked: | 0.205 |
| 126 |  | Equivalent of: 5 Flow Rods, 44 Fuel Rods (N.W. core quadrant only, remaining quadrants: 4 Flow Rods) | a. | 9-Rod Bank: 10.330 | No. 1, 3-9 Rods Banked: | 0.162 |
| 127 |  | Equivalent of: 6 Flow Rods, 43 Fuel Rods (full core except for item (a) which was N.W. quadrant only) | a. | No. 2 Rod: 25.000, Remainder: 2.760 | No. 1, 3-9 Rods Banked: | 0.131 |
| | | | b. | No. 1 Rod: 10.268, Remainder: 10.300 | 9-Rod Bank: | 1.400 |
| | | | c. | No. 2 Rod: 25.000, Remainder: 3.684 | No. 1, 3-9 Rods Banked: | 0.182 |
| 129 |  | Equivalent of: 8 Flow Rods (Concentrated) 41 Fuel Rods (Ref. loading core CSH-1) | a. | 9-Rod Bank: 10.366 | 9-Rod Bank: | 1.41 |
| | | | b. | No. 2 Rod: 25.000 | No. 3 Rod: | 0.113 |
| | | | c. | No. 1 Rod: 25.000 | No. 2 Rod: | 0.368 |
| | | | d. | No. 2 Rod: 18.215, Remainder: 0.000 | No. 3 Rod: | 0.111 |
| | | | e. | No. 4 Rod: 25.000 | No. 7 Rod: | 0.110 |
| | | | f. | No. 3 Rod: 8.090, Remainder: 0.000 | No. 7 Rod: | 0.120 |
| | | | | No. 6 Rod: 25.000 | | |
| | | | | No. 7 Rod: 7.760, Remainder: 0.000 | | |
| | | | | No. 8 Rod: 25.000 | | |
| | | | | No. 7 Rod: 8.480, Remainder: 0.000 | | |
| 132 |  | Equivalent of: 8 Flow Rods (Dispersed) 41 Fuel Rods | a. | 9-Rod Bank: 10.160 | 9-Rod Bank: | 1.460 |
| | | | b. | No. 1 Rod: 25.000 | | |
| | | | | No. 2 Rod: 17.390, Remainder: 0.000 | | |
| | | | c. | No. 8 Rod: 25.000 | | |
| | | | | No. 7 Rod: 2.550, Remainder: 0.000 | | |
| | | | d. | Slightly supercritical on each of Rods No. 2, 4, or 6 at 25.000, remaining 8 rods at 0.000. | | |



ID-103-A3236

Fig. 10. Loading Diagram, Core CSH-1



ID-103-3886

Fig. 11

Zero-power, Room-temperature
Loading, Core CSH-1

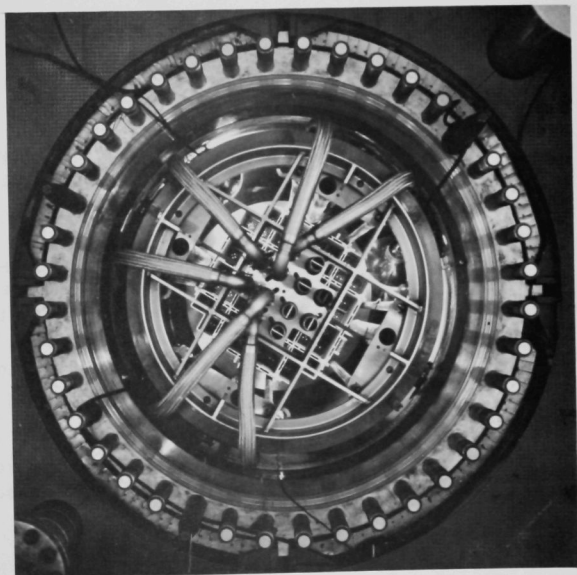


Fig. 12

Zero-power, Operating-
temperature Loading,
Core CSH-1A

ID-103-3887

withdrawn to 22 in. withdrawn, and was accomplished in two temperature ranges: room temperature (76-79°F), and operating temperature (487-489°F). Generally, the operating-temperature reactivity-worth measurements required careful control of electrical and nuclear heating to maintain temperature. The values given here were obtained during periods when the temperature distribution was fairly stable. Samples of boric acid solution were always analyzed at room temperature, and all concentrations are reported for this condition.

Slight changes in control rod critical position occurred as a result of the repair welding on the superheater fuel assemblies, discussed in Section VIII.A. The reactivity measurements reported here were made before the weld repairs. The effect of this welding is discussed in Section III.A.5.

Differential reactivity worths for the nine-control-rod bank, both at room and operating temperatures, with the superheater coolant channels drained and boric acid in the reactor water, are shown in Fig. 13. The curves in the figure are a least-squares quadratic fit to the data and result in the following equations:

$$\frac{\Delta\rho}{\Delta h_{76-79^\circ\text{F}}} = (3.32764 - 0.20348h + 0.0029226h^2) \%/\text{in.} \quad (1)$$

for $10.95 \text{ in.} \leq h \leq 26 \text{ in.}$, and

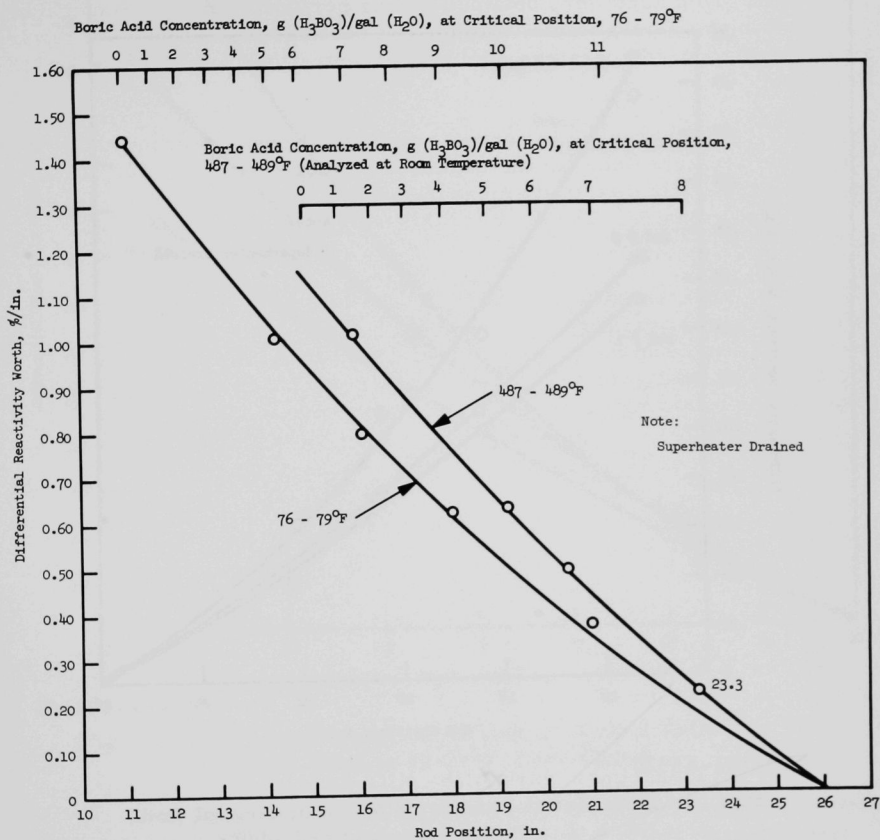
$$\frac{\Delta\rho}{\Delta h_{487-489^\circ\text{F}}} = (3.61969 - 0.20450h + 0.0025170h^2) \%/\text{in.} \quad (2)$$

for $14.76 \text{ in.} \leq h \leq 26.00 \text{ in.}$, where h is the height of the nine-control-rod bank above the bottom of the core. The differential reactivity worth is assumed to be zero at $h = 26 \text{ in.}$

Figures 14 and 15 show the differential-reactivity-worth curves measured at operating and room temperature, respectively, with superheater drained and boric acid in the reactor water, for the central control rod (No. 1), an intermediate rod (No. 2), and the four T-shaped rods in the outer bank (Nos. 3, 5, 7, and 9). These rods were calibrated by withdrawal above the nine-control-rod-bank critical position. The curves, again, represent a least-squares fit to the data.

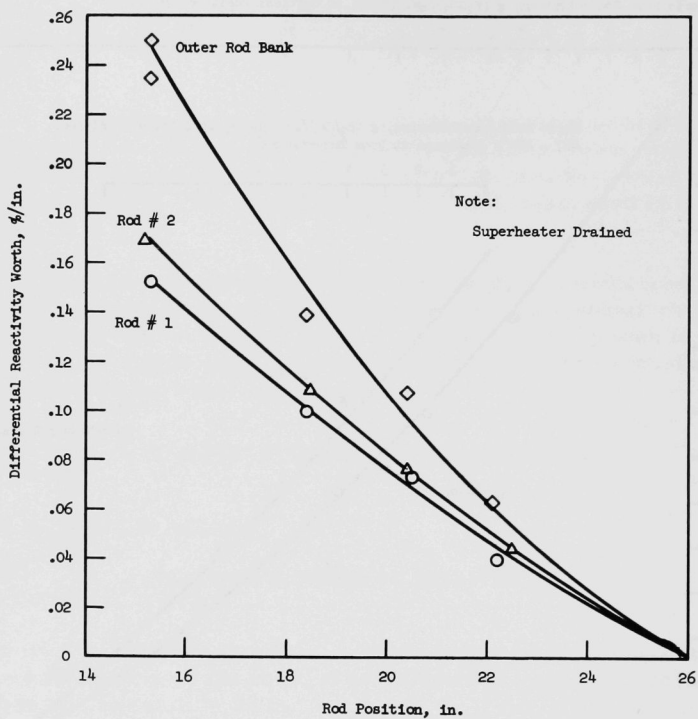
The relative differential reactivity worths of the control rods in Figs. 14 and 15, at the same height and with no boric acid in the moderator water, are compared as follows:

| | Room Temp | Operating Temp |
|-------------------|-----------|----------------|
| <u>No. 1 Rod</u> | 0.74 | 0.90 |
| <u>No. 2 Rod</u> | | |
| <u>Outer Bank</u> | | |
| <u>No. 2 Rod</u> | 1.34 | 1.48 |



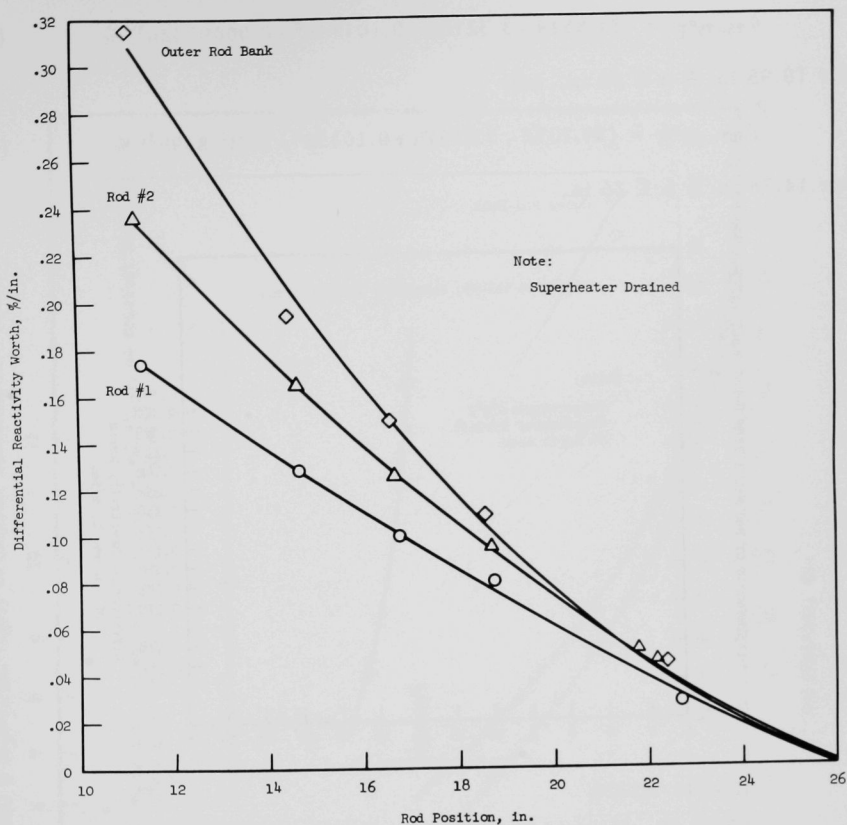
ID-103-A3325

Fig. 13. Differential Reactivity Worth vs Nine-control-rod-bank Position, Cores CSH-1 and CSH-1A



ID-103-A3326

Fig. 14. Differential Reactivity Worth of Control Rods No. 1, 2, and Outer Bank at 487-490°F, Core CSH-1A



ID-103-A3327

Fig. 15. Differential Reactivity Worth of Control Rods No. 1, 2, and Outer Bank at 73-83°F, Core CSH-1

At operating temperature, without boric acid in the moderator and with the superheater coolant channels drained, a determination was made of the differential reactivity worth of the central control rod (No. 1) as a function of its position relative to the remaining eight control rods banked. The differential reactivity worths measured for the central rod above, in, and below the bank are plotted in Fig. 16.

4. Available Excess Reactivity

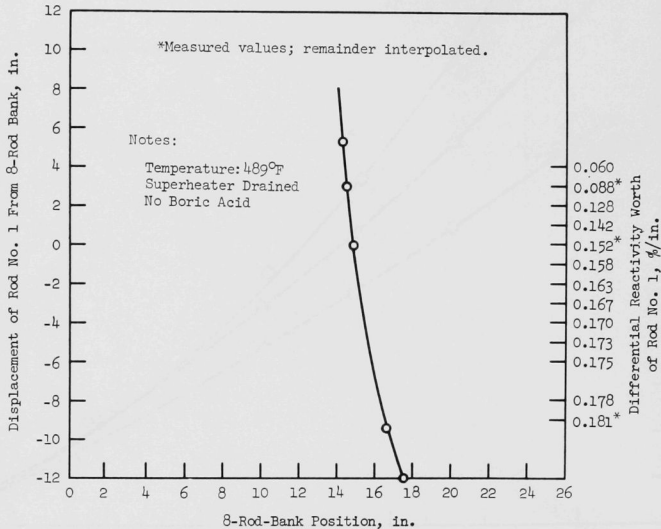
To obtain available excess reactivity at any position, h , of the nine-control-rod bank, equations (1) and (2) were integrated to yield the following equations:

$$\rho_{76-79^{\circ}\text{F}} = (34.8649 - 3.3276h + 0.10174h^2 - 0.0009742h^3) \% \quad (3)$$

for $10.95 \text{ in.} \leq h \leq 26 \text{ in.}$, and

$$\rho_{487-489^{\circ}\text{F}} = (39.7372 - 3.6197h + 0.1023h^2 - 0.000839h^3) \% \quad (4)$$

for $14.76 \text{ in.} \leq h \leq 26 \text{ in.}$

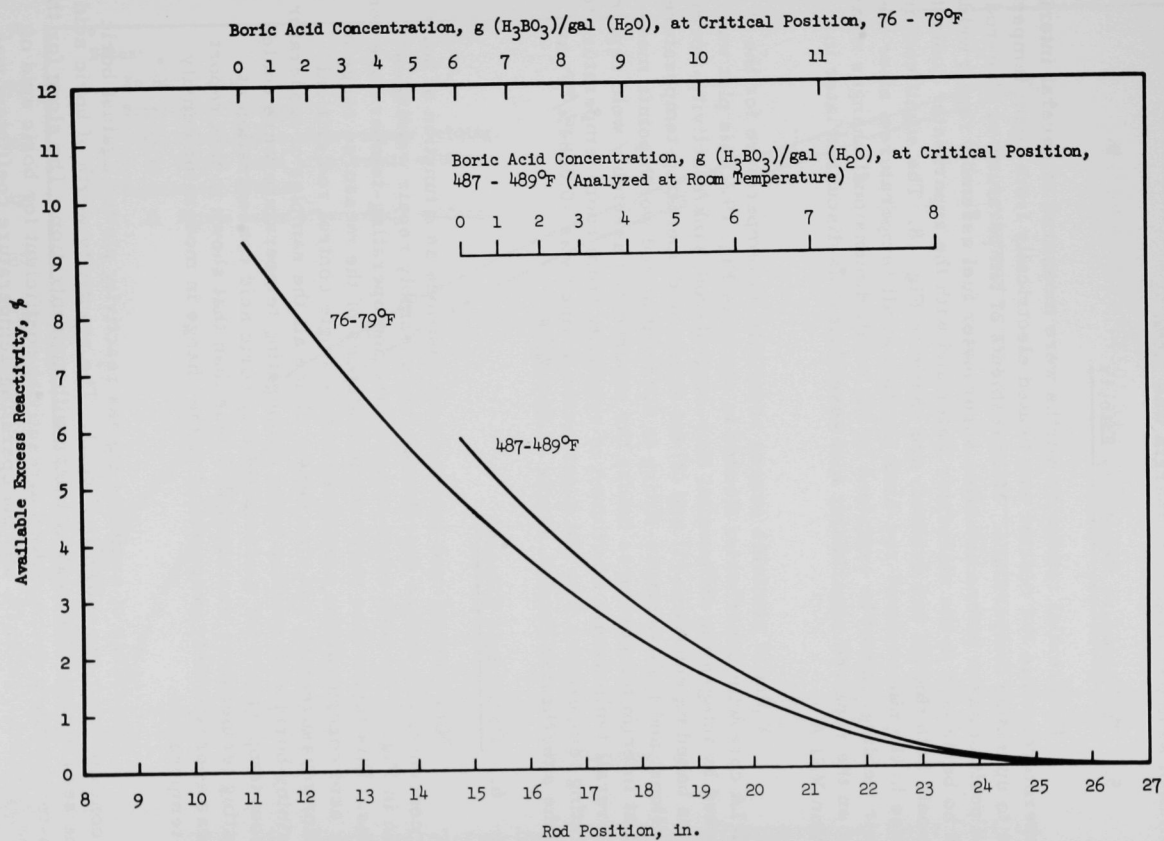


ID-103-A3328

Fig. 16. Critical Position and Differential Reactivity Worth of Control Rod No. 1 with Respect to Eight-control-rod Bank, Core CSH-1

At room temperature, before the superheater fuel assembly weld repairs discussed in Section VIII.A., the available excess reactivity for core CSH-1 was 9.3%; at operating temperature for core CSH-1A, it was 5.8%, for a loss in reactivity due to temperature of 3.5%. Figure 17 shows the curve of available excess reactivity vs nine-control-rod-bank position for both temperature conditions.

The room-temperature shutdown margin, with superheater coolant channels flooded and no boric acid, was estimated roughly by assuming that the nine-control-rod-bank differential reactivity worth peaked at the critical position and the differential worth at this point was double the average. The fact that the differential control rod reactivity worth did not go to zero at the bottom of the core was ignored, as was the



ID-103-A3329

Fig. 17. Nine-control-rod-bank Position vs Reactivity, Cores CSH-1 and CSH-1A

precise shape of the differential-worth curve. The nine-rod-bank differential reactivity worth was $1.44\%/in.$ at the critical position of 10.5 in. The estimated shutdown reactivity margin was 7.6%.

5. Temperature Reactivity Effects

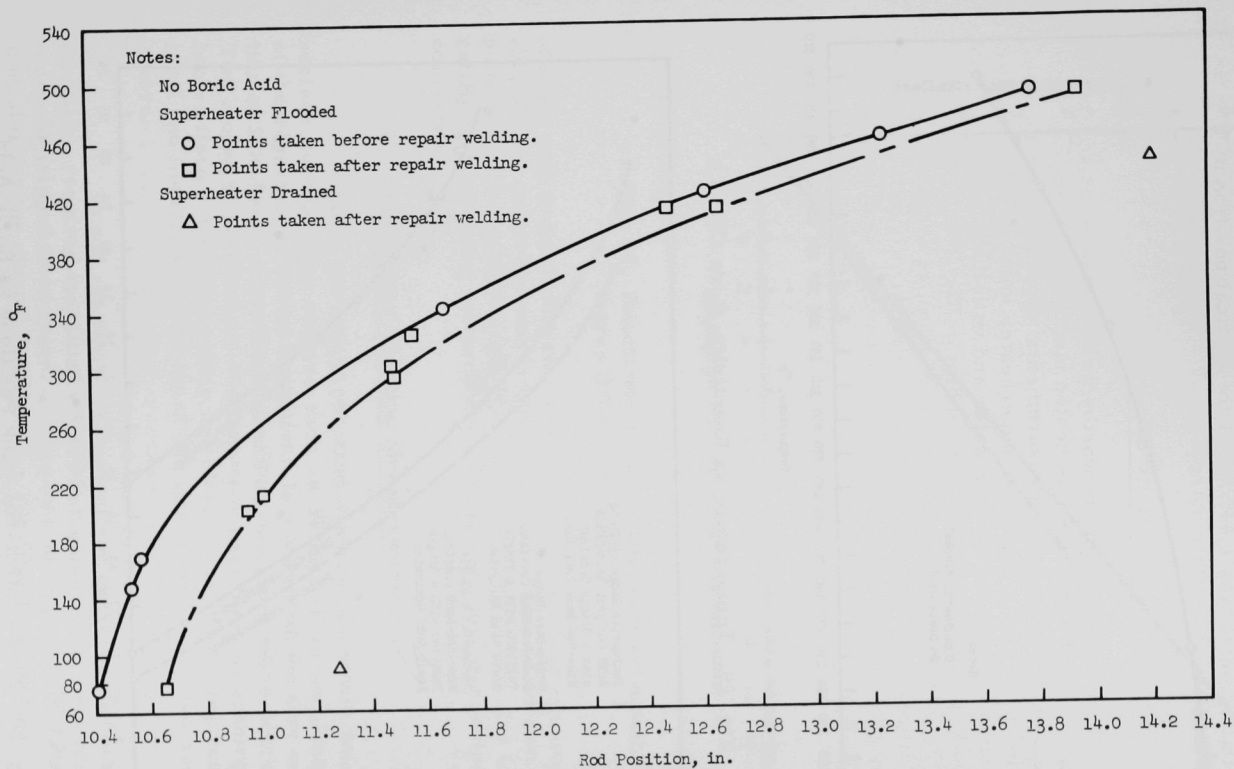
Differential reactivity worths were measured at several interim temperatures while the reactor was heated electrically from room temperature to operating temperature. Measurements of temperature vs nine-rod-bank position taken before and after superheater fuel assembly repair welding, with no boric acid in the moderator water and with the superheater coolant channels both flooded and drained, are shown in Fig. 18. The significant increase in the nine-control-rod-bank position at all temperatures, after the repair welding, cannot be explained by the small dimensional changes measured on the repaired superheater fuel assemblies, as discussed later in Section VIII.A.

A plot of available excess reactivity vs temperature for the CSH-1A core with superheater flooded is shown in Fig. 19. This plot was obtained by integrating differential nine-control-rod-bank reactivity-worth curves based on equations (1) and (2) for room- and operating-temperature conditions, and least-squares-fitting to differential rod worth points measured at interim temperatures before the superheater assembly weld repairs. The overall temperature coefficient of reactivity from room temperature to operating temperature with the superheater drained was $-0.0084\%/^{\circ}F$, and with the superheater flooded, it was $-0.0074\%/^{\circ}F$.

6. Boric Acid Effects

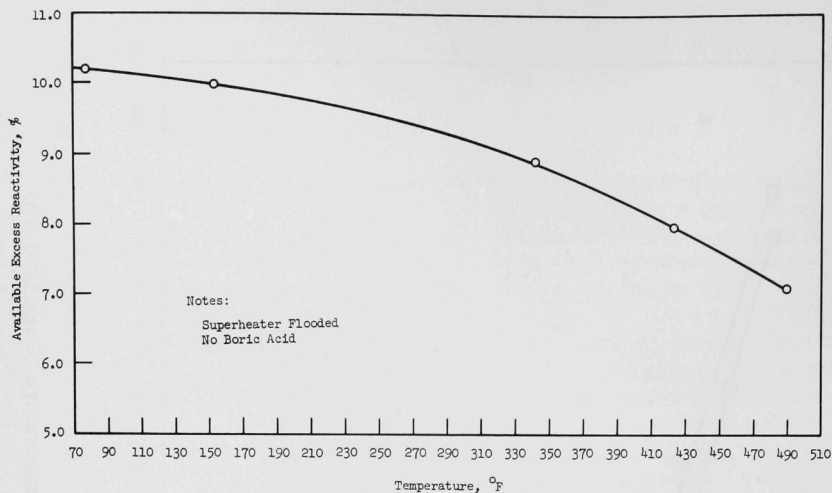
Nine-control-rod-bank critical positions as a function of boric acid concentration, before superheater fuel assembly repair welding, are shown in Fig. 20 for both room-temperature and operating-temperature conditions. This figure also shows some instances of the measured range of boric acid concentrations associated with a single control rod critical position measurement, and vice versa. Since all the samples of moderator containing boric acid solution taken at operating temperature were cooled to room temperature for analysis, the true boric acid concentration at operating temperature was about 20% less than that shown in this report and was approximately proportional to the change in moderator density with temperature.

The values of available excess reactivity plotted against boric acid concentration are shown in Fig. 21. The reactivity worth of boric acid can be seen to be approximately linear with concentration. The slope of the room-temperature curve yielded a reactivity coefficient for boric acid of $-0.77\%/g(H_3BO_3)/gal(H_2O)$, and the operating-temperature coefficient was $-0.86\%/g(H_3BO_3)/gal(H_2O)$, with the samples analyzed at room temperature but the coefficient corrected for operating temperature. The concentration



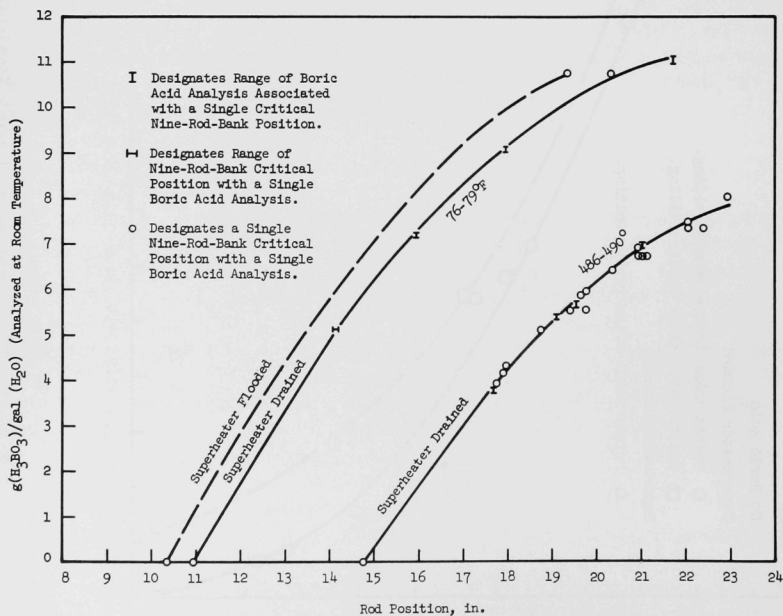
ID-103-A3330

Fig. 18. Nine-control-rod-bank Position vs Temperature, Core CSH-1A



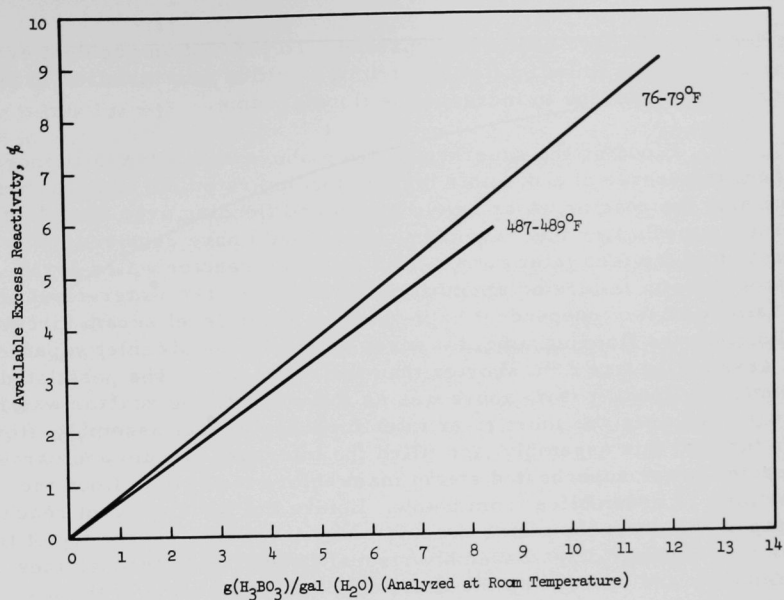
ID-103-A3331

Fig. 19. Temperature vs Reactivity, Core CSH-1A



ID-103-A3332

Fig. 20. Nine-control-rod-bank Positions vs Boric Acid Concentration, Cores CSH-1 and CSH-1A



ID-103-A3333

Fig. 21. Reactivity vs Boric Acid Concentration,
Cores CSH-1 and CSH-1A

of boric acid in the moderator water, which would have removed all available excess reactivity with control rods completely withdrawn, was computed to be 12.2 g(H₃BO₃)/gal(H₂O) at room temperature, and 6.7 g(H₃BO₃)/gal(H₂O) at operating temperature. The latter value was temperature-corrected.

7. Superheater Flooding Measurements

One of the unique potential hazards of a small, integral, boiling-nuclear superheating reactor such as BORAX-V is accidental flooding of the superheater during operation. In a core with the size and composition of BORAX-V, superheater flooding yields a positive reactivity addition. Two modes of superheater flooding were possible: (1) opening a superheater flood valve and flooding from below, and (2) raising reactor water level and flooding over the top of the inlet superheater fuel assembly risers.

To add reactivity by flooding the superheater from below during operation required the lifting of a switch guard on the controls to the solenoid-tripped flood valve, or the removal of a padlock on the remote operator for the manual flood valve. The "flood-valve-open" scram

interlocks would have had to be bypassed. To prevent an accident even if these precautions failed, a flow-restricting orifice was installed in the superheater flood line to increase the flooding time.

Flooding the superheater from above was potentially more hazardous because of a possible higher flooding rate. To add reactivity by raising the reactor water level rapidly and flooding over the top of the inlet superheater fuel assembly risers would have required mal-operation of the feedwater pumps, failure of the reactor water-level control system, failure or ignoring of the high-reactor-water-level alarm, and failure of two independent high-reactor-water-level scram circuits. To lengthen the flooding time, the riser on one of the six inlet superheater fuel assemblies was 2 in. shorter than the remainder. The postulated sequence in flooding from above was as follows: Rising reactor water first flooded over the short riser inlet superheater fuel assembly, flowed down through this assembly, and filled the interpass plenum and parallel-connected lower superheated steam main before it began to flood the remaining 11 assemblies from below. Before the flooding level reached the top of the core, the rising reactor water level reached the top of the other five standard inlet-assembly risers, flooded down through these assemblies, and speeded up the remaining bottom flooding of the six outlet assemblies.

Because of the potential reactor hazard involved in measuring the reactivity addition rate of superheater flooding dynamically while critical, and because of the doubtful feasibility of direct subcritical dynamic measurements, the experiments were performed in two stages: First, the reactivity worth of the flooded central superheater was measured statically by critical experiments; then the rate of flooding was measured with the reactor shut down. The results of these two experiments were then correlated to give reactivity addition rates.

a. Static Reactivity Measurements

The reactivity effect of flooding the superheater coolant channels in the center of the core with demineralized water was evaluated. Two general conditions in both the room- and operating-temperature ranges were studied, one with demineralized moderator water, the other with the moderator water containing boric acid. To measure the reactivity effect, control rod critical positions were determined for the given superheater-flooded condition with all nine control rods banked, and then with the central rod completely withdrawn and the remaining eight control rods banked. Differential control rod reactivity worths for both types of rod banks were measured at each flooded condition, from which the reactivity worth was calculated. Flooded states were achieved by draining the superheater region to the desired level for each static reactivity measurement.

(1) Flooding from Below

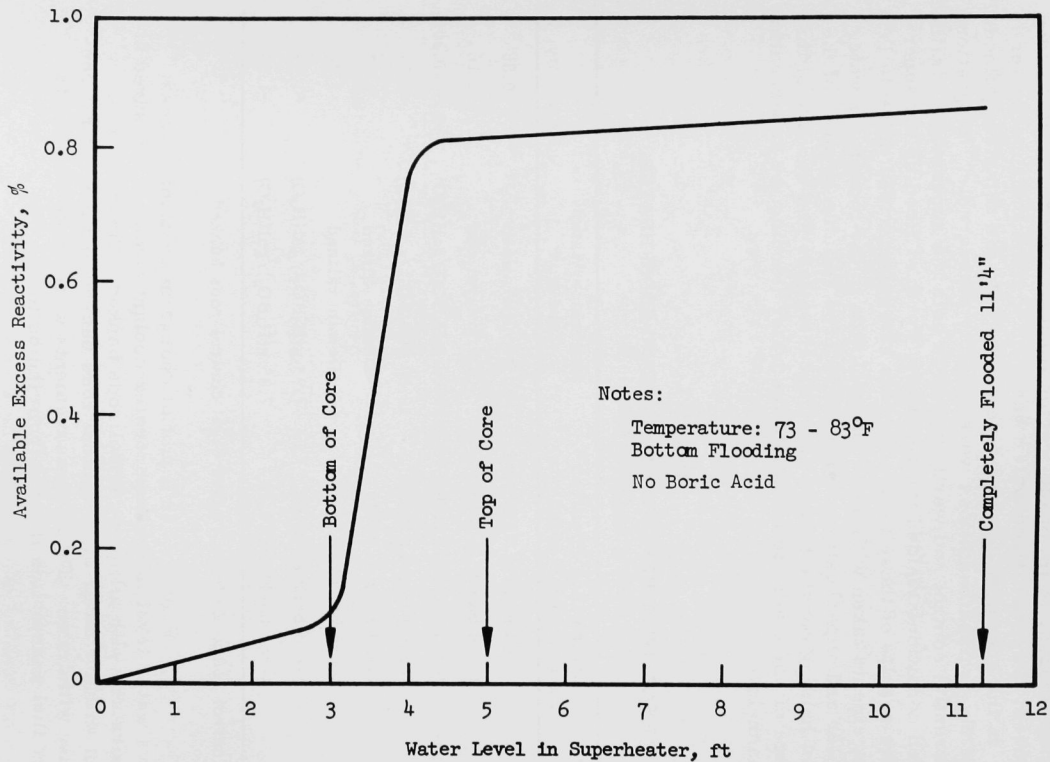
In the room-temperature range, simulating flooding from below through the superheater flood-valve system, five flooded states were investigated: completely drained, 6 in. of fuel region flooded, 12 in. of fuel region flooded, 18 in. of fuel region flooded, and superheater completely flooded. Demineralized water was used to flood the superheater in all cases. In the operating-temperature range, only the completely flooded and completely drained conditions were reliably measurable. Integration of the differential control rod worth curves in both the superheater-drained and -flooded conditions yielded the reactivity worth of flooding the superheater. The results of these measurements are summarized in Table IV. The measurements taken with boric acid solution in the moderator water of both boiler and superheater are not considered reliable because of the difficulty of holding constant boric acid concentrations and because of the slow leakage of boric acid solution into the water flooding the superheater coolant channels.

Table IV
REACTIVITY EFFECTS OF FLOODING SUPERHEATER,
CORE CSH-1

| Temperature, °F | Control Rod Position (Superheater Flooded), in. | Moderator Water Condition | Reactivity, % |
|--------------------|--|--|---------------|
| 70-83 | 9-rod bank at 10.38 | Demineralized | 0.86 |
| 70-83 | 8-rod bank ^a at 9.25 | Demineralized | 1.16 |
| 70-83 | 9-rod bank at 18.99 | 10.88 g(H ₃ BO ₃)/gal(H ₂ O) | ~0.60-0.80 |
| 70-83 | 8-rod bank ^a at 18.51 | 10.88 g(H ₃ BO ₃)/gal(H ₂ O) | ~0.71 |
| 489 | 9-rod bank at 13.77 | Demineralized | 1.27 |
| 489 | 8-rod bank ^a at 12.87 | Demineralized | 1.48 |
| 489 | 9-rod bank at 20.04 | 7.93 g(H ₃ BO ₃)/gal(H ₂ O) | ~1.01 |
| 489 | 8-rod bank ^a at 19.48 | 7.85 g(H ₃ BO ₃)/gal(H ₂ O) | ~1.05 |

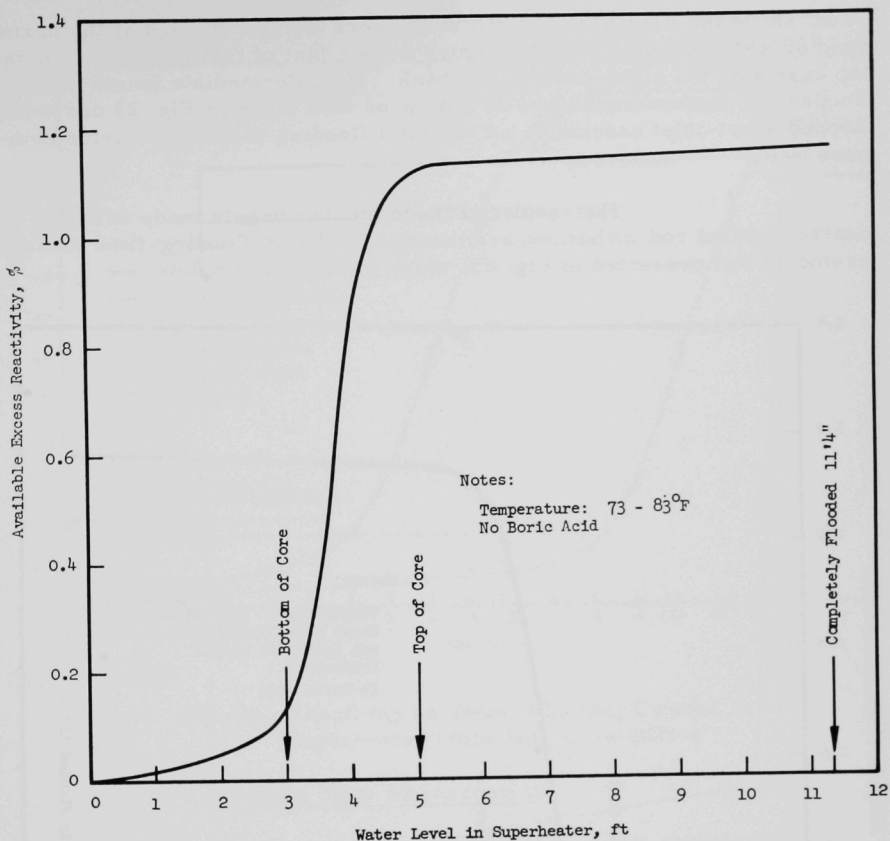
^aNo. 1 control rod at 25.00 in.; other eight control rods banked.

Figure 22 is a plot of change in available excess reactivity vs water level in the superheater coolant channels measured at room temperature with all nine control rods banked. Figure 23 is a similar plot with the outer eight control rods banked and the central control rod fully withdrawn. These measurements were made with all 12 superheater fuel assemblies flooded from the bottom.



ID-103-A3334

Fig. 22. Reactivity vs Superheater Water Level,
Nine-control-rod Bank, Core CSH-1



ID-103-A3335

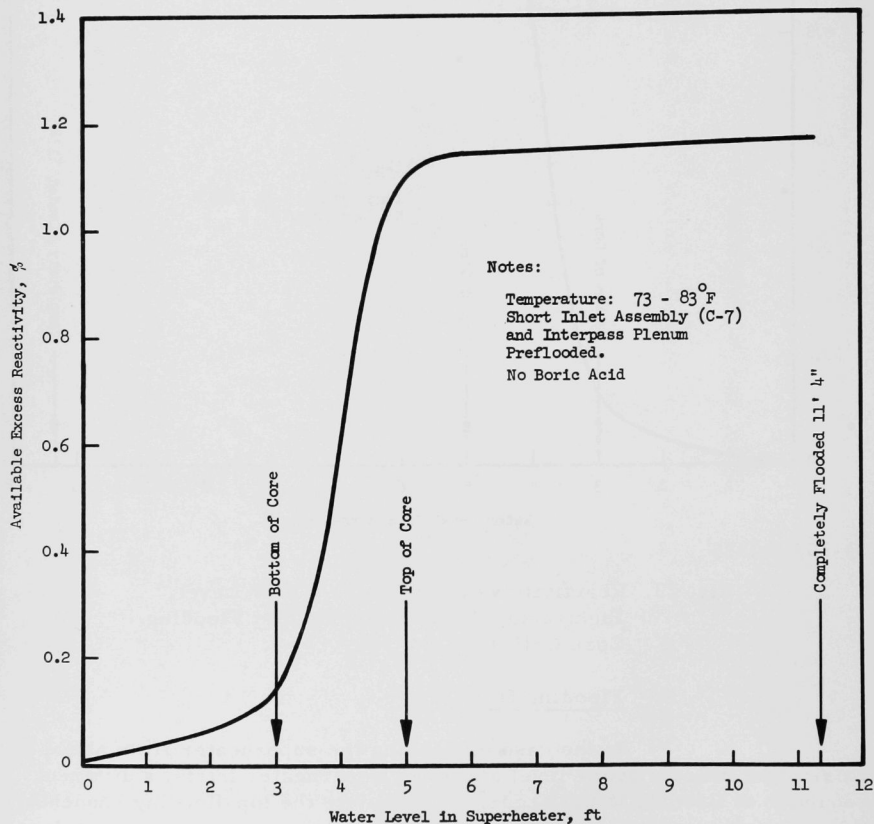
Fig. 23. Reactivity vs Superheater Water Level, Eight-control-rod Bank, Bottom Flooding, Core CSH-1

(2) Flooding from Above

In the case of flooding the superheater from above by raising the reactor water level above the superheater inlets, a different sequence of flooding would occur. To simulate the top-flooding sequence, the reactivity measurements were made at room temperature with only the short-riser-inlet superheater fuel assembly (C-7, core position 53) and interpass plenums flooded. Then measurements were made with the flooding level in the remaining 11 assemblies raised to the base of the core (3.0 ft), 6 in. above the base (3.5 ft), at the core midplane (4.0 ft),

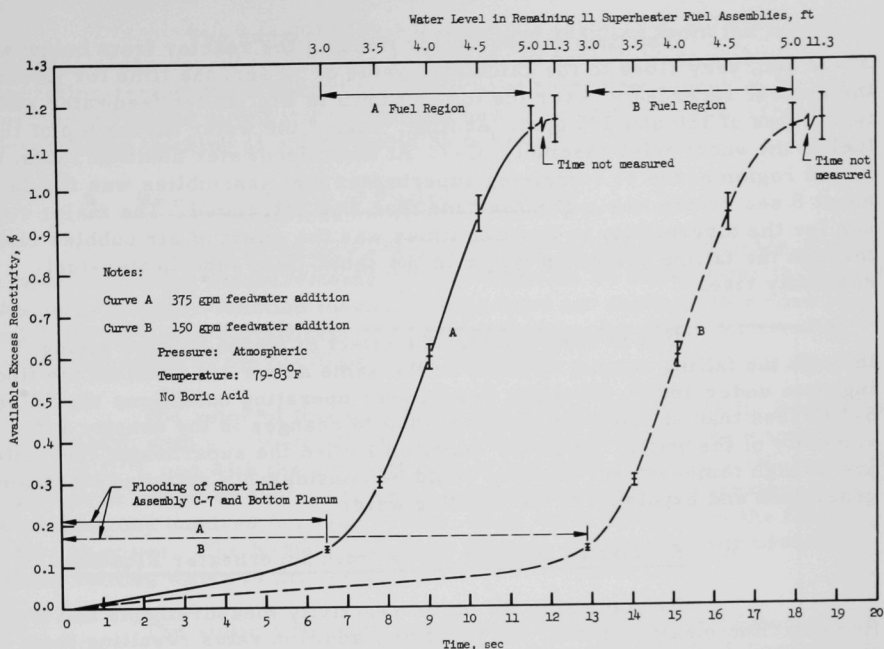
18 in. above the core base (4.5 ft), at the core top (5.0 ft), and at the normal reactor water level of 11.3 ft. Figure 24 is a plot of the flooding-from-the-top case with the eight-control-rod bank. The intermediate points between flooded and drained conditions do not agree with those in Fig. 23 due to the flooded short-inlet assembly, but the total flooding reactivity worths compare well.

The results of these measurements made with the central control rod withdrawn are incorporated with flooding-time measurements and presented in Fig. 25, which is discussed below.



ID-103-A3336

Fig. 24. Reactivity vs Superheater Water Level, Eight-control-rod Bank, Top Flooding, Core CSH-1



ID-103-A3337

Fig. 25. Reactivity vs Time, Flooding Central Superheater from Top, Core CSH-1

b. Flooding Time Measurements

The time required to flood the central superheater was measured, both for the case where flooding occurred from below, using the flood-and-drain system, and for the case of flooding from above, in the event the reactor water level was raised too high. Three superheater assemblies, the short-riser-inlet assembly (C-7), a standard inlet assembly, and an outlet assembly, were each instrumented with two Teflon-insulated wires running axially in coolant channels. One wire in each assembly had uninsulated sensing points at the bottom, midpoint, and top of the fuel region, and the other wire had uninsulated sensing points at the 1/4 and 3/4 points. These wires were connected to a 6.3-Volt ac power supply through an 0.5- or 1-megohm resistor. The return circuit was through the fuel element and water. The ac signal developed across the resistor was rectified and recorded on an oscillograph. Water covering the sensing points produced steps in the signal level recorded. Some difficulty was experienced in the use of the instrumentation in the flooding-from-above tests, but repeated runs gave data that could be satisfactorily interpreted.

The time measured for flooding the reactor from below was 30-32 sec, very close to the calculated value of 30 sec; the time for flooding the central superheater over the top is shown in Fig. 25 for feedwater addition rates of 150 and 375 gpm. At time "zero," the water hit the top of the fuel in the short-inlet assembly, C-7. At these feedwater addition rates, the fueled region of the 11 remaining superheater fuel assemblies was flooded in about 5 sec, which was a greater time than was calculated. The major reason for the discrepancy in flooding times was the effect of air bubbles rising through the falling column of water in the short-inlet superheater-fuel-assembly riser.

If it is assumed that the effect of steam bubbles rising through the falling column of water is the same as for air bubbles, the flooding time under 489°F, 600-psig, zero-power operating conditions should be 5-10% less than at room temperature, due to changes in the density and viscosity of the water. At power conditions when the superheater fuel plates are at high temperature, flooding would be considerably retarded by steam generation and expulsion of the flooding water.

c. Reactivity Addition Rates from Superheater Flooding

By combining the static reactivity measurements and the flooding time measurements, the reactivity addition rates resulting from flooding the superheater coolant channels at room temperature were calculated. The maximum reactivity addition rate from opening the solenoid-tripped flood valve and flooding from below would have been 0.03%/sec.

The reactivity addition from flooding the superheater fuel assemblies over the top is shown in Fig. 25. Because one of the six inlet superheater fuel assemblies, C-7, was 2 in. shorter than the other five, the superheater flooding occurred in two stages. The first flooding, including the short-inlet assembly and one interpass plenum chamber, occurred in 7.8 sec at the 375-gpm feedwater flow rate and would have caused a reactivity increase of 0.14%. At the end of the first stage, the reactor would have been on a 25-sec period if superheater flooding at room temperature had occurred, ignoring the reactivity compensation by the resulting change in power.

The 375-gpm curve in Fig. 25 indicates that the principal reactivity effect would have occurred at the end of the second stage, at which time the remaining 11 superheater fuel assemblies would have been flooded. At this point, approximately 1.0% reactivity would have been added, of the 1.16% total. The flooding in the second stage occurred in about 5.1 sec, and the maximum reactivity addition rate would have been approximately 0.2%/sec. At the point where the water level was at 25% of the fuel height, the reactor would have been on a period shorter than 10 sec, again ignoring the feedback due to the reactor responses. This level was reached 7.8 sec after flooding began and 1.3 sec after the flooding of the remaining superheater assemblies began.

The excursion that would have resulted from the inadvertent flooding of the superheater coolant channels at zero-power, room- or operating-temperature conditions would have been slow enough to be easily terminated by the automatic period and power-level trip scram circuits. Superheater flooding at power would have been even slower.

8. Reactivity Worth of Fueled Oscillator

A fueled oscillator rod was located in reflector thimble C for transfer-function measurements on core CSH-1B, as shown later in Fig. 67. Although transfer-function measurements were not made on this core because of the early curtailment of power operation, the static differential reactivity worth of the oscillator was measured.

The rotor of this oscillator was $2\frac{11}{16}$ in. OD and 26 in. long (25 in. fuel length), with a 1/16-in.-thick, 170° arc of Zr-U containing a total of 100 g of U^{235} , and with the opposite side of the rotor made of 0.030-in.-thick hafnium in an arc of 180°. The rotor housing was made of Zircaloy-2 and contained one hundred fourteen 5/8-in.-diam holes for cooling the fueled rotor at power. The X-8001 aluminum thimble C was also perforated to admit cooling water to the rotor.

The static differential reactivity worth of the oscillator, measured by rotating the oscillator 180° from an orientation of fuel-toward-the-core to an orientation of fuel-away-from-the-core, was 0.05% with the reactor water containing no boric acid at 78°F. The nine-control-rod-bank critical position changed from 10.649 to 10.683 in., as a result of the 180° rotation.

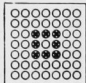
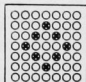
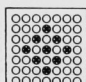
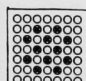
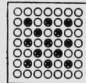
9. Additional Fuel-to-water Ratio Experiments

After the termination of power operation on core CSH-1B and before the changeover to the peripheral superheater core was started, a series of zero-power experiments was performed at temperatures from 70 to 180°F to determine the optimum number of flow rods per boiling fuel assembly. The purpose of the experiments was to achieve smaller negative temperature and void coefficients of reactivity to reach higher power. The results of these measurements were used in planning the peripheral superheater core, PSH-1.⁽¹⁾

Changes were made first in one quadrant only of the boiler zone, without poison rods. The reactivity effect was measured by the change in position and reactivity worth of the intermediate control rod in the opposite quadrant. Very small changes were observed. Table V summarizes the results of these measurements.

Table V

ADDITIONAL FUEL-TO-WATER-RATIO EXPERIMENTS, CORE CSH-1B

| Loading No. | Flow Rod Arrangement | Change in Reactivity Relative to CSH-1B Core | | | Change in Reactivity Heating from 70-180° F % |
|-------------|--|---|-------------------|-------------------------------|---|
| | | 1 Quadrant No Poison Rods | Full Core | | |
| | | | No Poison Rods | 4 Poison ^b Rods | |
| | | | | | |
| 152 |  8 Concentrated (Reference loading core CSH-1) | -- | -- | -- | -0.05 ^a |
| 153 |  8 Dispersed | +0.089 | +0.47 | -0.03 | -0.05 ^b |
| 154 |  9 Dispersed | +0.074 | -- | -- | -- |
| 156,157 |  12 Dispersed (Reference loading core PSH-1) | +0.063 | -- | -0.18 | +0.03 ^b |
| 155 |  13 Dispersed | +0.038 | -- | -- | -- |

^a Extrapolated from experimental data for core CSH-1A for heating from 79 to 129° F with no poison rods.

^b Four poison rods in boiler, adjacent to inner corner of intermediate control rods, to prevent criticality on withdrawal of one intermediate control rod alone.

A system with eight dispersed flow rods per boiling fuel assembly appeared to provide the maximum available excess reactivity at room temperature. A system with 12 dispersed flow rods was calculated to have the maximum available excess reactivity at operating temperature. The reactivity effect of changing from room temperature to 180°F was determined for both arrangements of flow rods in the full boiler zone. The 12-flow-rod arrangement, designated core CSH-1C, was believed to be the one that would yield the greatest power, because the anticipated gain in reactivity due to the lower temperature and void coefficients more than offset the small reduction in reactivity available at room temperature.

10. Experimental Techniques and Error

Before starting control rod calibrations, the performance characteristics of all nuclear instrumentation were examined carefully. Previous difficulties with nonlinearity in period measurements were traced to nonlinear fission-counter circuits. Replacement of the counters resolved this problem.

With the antimony source rod in place in the beryllium, a high neutron-source level resulted. Therefore, to operate at a power level corresponding to a preset indicated current of the linear channel, the nine-control-rod bank was inserted to reduce the multiplication of the source neutrons. For a linear-channel level of 10^{-12} Amp, which was the starting point for control rod calibrations at room temperature, the reactivity change was -1.2%. Indeed, this source effect was significant, at room temperature, in the range of 10^{-12} to 10^{-10} Amp. Therefore, the source rod was withdrawn by means of a remotely operated source drive during reactivity measurements at these low power levels. This effect was negligible at a linear indicated level of 10^{-8} Amp, and at operating temperature the antimony rod was left in the beryllium. In the power range used for criticality measurements at operating temperature, 10^{-9} Amp, the maximum source reactivity effect was less than 0.02% and the source was left inserted. Thus, when the nine-control-rod bank was withdrawn 0.1 in. for period measurements, this resulted in a 20% underestimate of differential reactivity.

The method used to calibrate control rods in the BORAX-V reactor involved the incremental addition of a soluble neutron poison (boric acid) to the moderator water. Specifically, the differential reactivity worth of a set of control rods (one to nine rods in the set) was measured by first establishing a critical configuration of the control rods and then measuring the positive asymptotic reactor period corresponding to a small change in rod positions. Then the boric acid concentration was changed so that the control rods could be moved to new positions and calibrated there by this same "positive-period" technique. A theoretical curve of excess reactivity vs positive asymptotic reactor period was used to obtain the reactivity calibration.⁽⁵⁾

Boric acid has been used for control rod calibration in several other water-moderated reactors as well, including such Argonne reactors as earlier BORAX systems, the EBWR, and the ALPR. It provides a convenient method of obtaining calibrations without introducing large perturbations. While it is recognized that this method, too, perturbs the system and introduces some error, these uncertainties are small in magnitude. A series of one-group control-cell problems with varying boric acid content were run to examine the potential error existing in this method. While these did not take into account such factors as the effect on the disadvantage factor, effects for above-thermal neutrons, etc., an estimate of 15% maximum error in total control rod worth was obtained. Further, the reactivity worth of boric acid remained nearly constant up to a concentration of 10 g(H_3BO_3)/gal(H_2O).

The situation is depicted in Fig. 26, where reactivity, ρ , is plotted against control rod height, h , and boric acid concentration, C_B . Here, the just-critical points lie in the C_B - h plane (a reproduction of the room-temperature curve of Fig. 17), and ρ appears as reactivity added to the system as rods are withdrawn and is related to available excess reactivity, as follows:

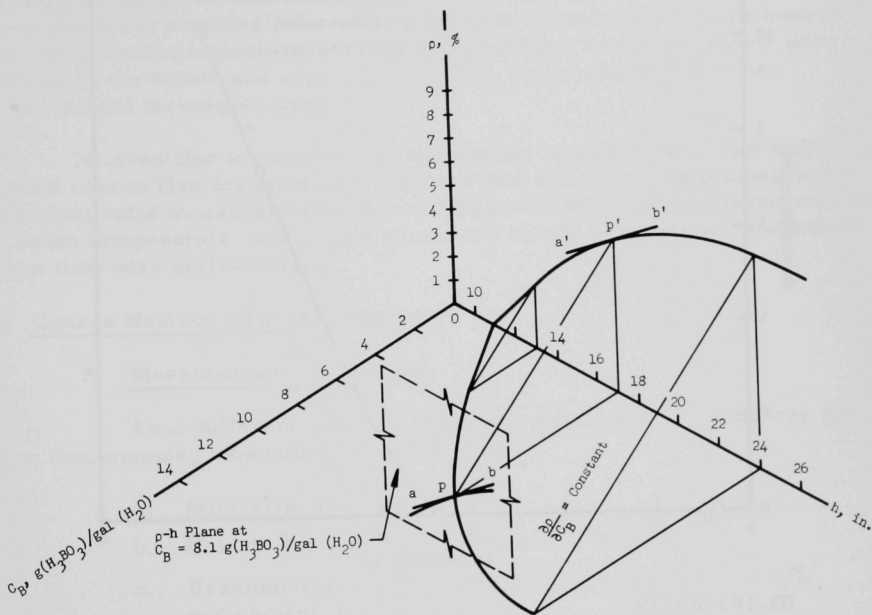
$$\rho_{\text{avail,max}} - \rho(h) = \rho_{\text{avail}}(h).$$

If it is assumed that the ρ - h ($C_B = 0$) curve is correct, it is apparent that to reproduce a slope measurement (differential control rod worth) at p' (slope of tangent $a'-b'$) at or near p (slope of $a-b$) in the plane parallel to the $C_B = 0$ plane, the path $p'-p$ must be a straight line; i.e., $(\partial\rho/\partial C_B)h = \text{constant}$. It is further apparent that the shape of the C_B - h ($\rho = 0$) curve is the same as that of the available excess reactivity curve if $\partial\rho/\partial C_B$ is a constant. A necessary condition for constant boric acid worth is, then, that the slope of the ρ - C_B lines be equal at the various points of measurement, as possibly might be revealed by a series of boric acid dilution measurements. However, it is difficult to achieve accurate results with dilution measurements because of the relatively large reactivity effect associated with a small error in boric acid concentration.

The effect of control rod height on the worth of boric acid is not known at this time. A simple consideration of control rod worth in terms of the small change in diffusion length, L , caused by boric acid might be sufficient for a thermally black rod in a homogeneous reactor. Heterogeneities introduce another problem, however, and are not discussed here.

The technique used to obtain representative reactor water samples for the analysis of boric acid concentration was probably a cause of error as a result of changing solution composition with time. This variation was caused primarily by diffusion of boric acid solution of higher concentration into static regions of the system where the concentration was

less. Examination of data reveals that with an apparent constant temperature the nine-control-rod-bank critical position decreased as rapidly as 0.01 in./hr, for a maximum reactivity change of 0.014%/hr. However, about half of this change occurred over a 24-hr period with $C_B = 0$, probably due to slight temperature heterogeneities in the reactor water. The measurements reported in this report are those taken as near the boric acid sampling time as possible. The error in the critical control rod position measurement vs boric acid concentration should thus be less than 1%.

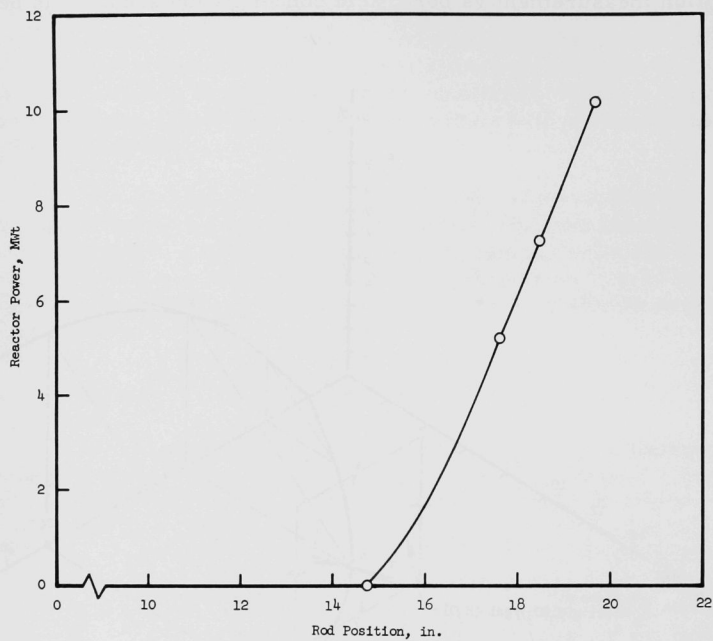


ID-103-A3338

Fig. 26. Relationship between Reactivity (ρ), Soluble Poison Concentration (C_B), and Control Rod Height (h)

B. High-power Reactivity Measurements

Because of the brevity of the power operation on core CSH-1B, the planned reactor transfer-function measurements were not made. Therefore, the value of the power coefficient of reactivity was not obtained. Also, planned measurements of the reactivity effects of xenon, samarium, and burnup were not made. Figure 27 shows a graph of nine-control-rod-bank position vs power for this core.



ID-103-A3339

Fig. 27. Power vs Nine-control-rod-bank Position,
Core CSH-1

IV. NEUTRON FLUX MAPPING

Core physics calculations made during the design of BORAX-V produced smooth neutron flux plots for the central superheater core by using homogenized number densities in various computer codes, and flux-peaking factors within fuel assemblies were obtained from PDQ cell calculations. However, since the central superheater core of BORAX-V was far from homogeneous, it was desirable to determine experimentally the local axial and radial variations in the neutron flux within a fuel assembly, from assembly to assembly, and between the boiler and superheater zones. These measurements provided information on power distribution for the heat engineering analysis, peak-to-average power ratios, fractional power production in the boiler and superheater zones, and verification of the calculational techniques used.

Neutron flux measurements were made at zero power only and included coarse flux distributions, both at room and operating temperature, cadmium ratio measurements, fine radial power distribution measurements at room temperature, and a core symmetry check. All data were obtained from flux-wire activations.

A. Coarse Neutron Flux Distributions

1. Measurement Techniques

Four different detector materials were used in the coarse neutron flux-mapping experiments. They were:

- a. Gold wire, 0.032-in. diam.
- b. Gold-5 w/o iron alloy wire, 0.032-in. diam.
- c. Uranium-zirconium wire, 3.379 w/o uranium, 93.13% enrichment, 0.031-in. diam.
- d. Copper wire, 0.032-in. diam.

These wires were irradiated in both continuous and segmented arrangements. Segmented wires were used for all radial and for some axial measurements, and continuous wires were used for the remainder of the axial traverses.

For the room-temperature irradiations, the flux wires in the boiler region were held in special wire holders inserted into coolant channels of the fuel assemblies. These holders were made of aluminum tubing, 0.125-in. diam x 0.020-in. wall, with a support and guides for reproducible positioning. The reproducibility of wire positioning vertically was assured by the upper shoulder of the holder which rested on the upper grid of the fuel assembly, as shown in Fig. 28. Both continuous and segmented wires could be loaded in these holders. Aluminum spacer wires were used to position the wire segments axially.

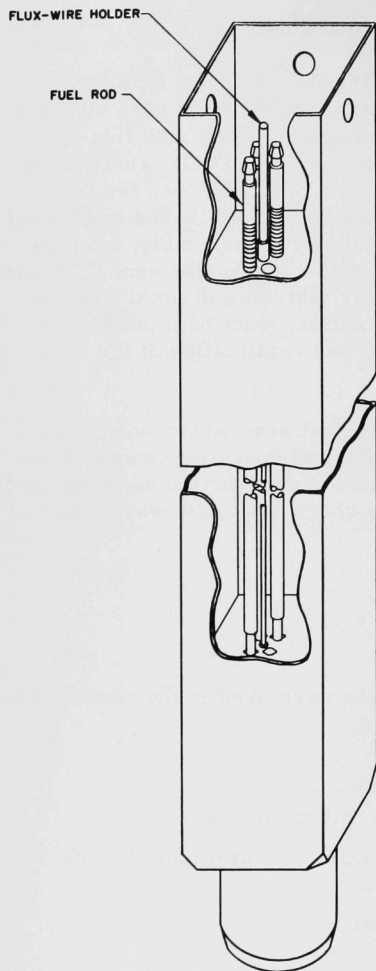
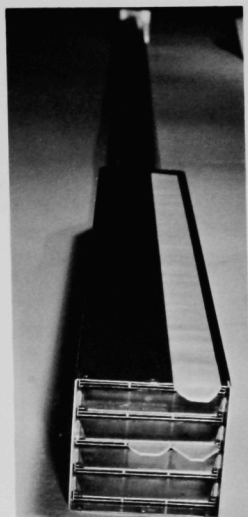


Fig. 28
Flux-wire Holder in
Boiling Fuel Assembly

ID-103-A3252

Room-temperature irradiations in the superheater region were made using the equipment shown in Fig. 29. Teflon strips, 0.050 in. thick, were cut to fit in the coolant channels in a superheater fuel assembly, and a $1/32$ -in. \times $1/32$ -in. groove was cut axially on each strip to hold the flux wires. The strips were inserted from the bottom into the coolant passages of special superheater fuel assemblies with removable lower nozzles. Axial positioning was accomplished by pushing the strips into the coolant channels until their ends were at the same elevation as the bottom of the lower flow vanes.



ID-103-A3066

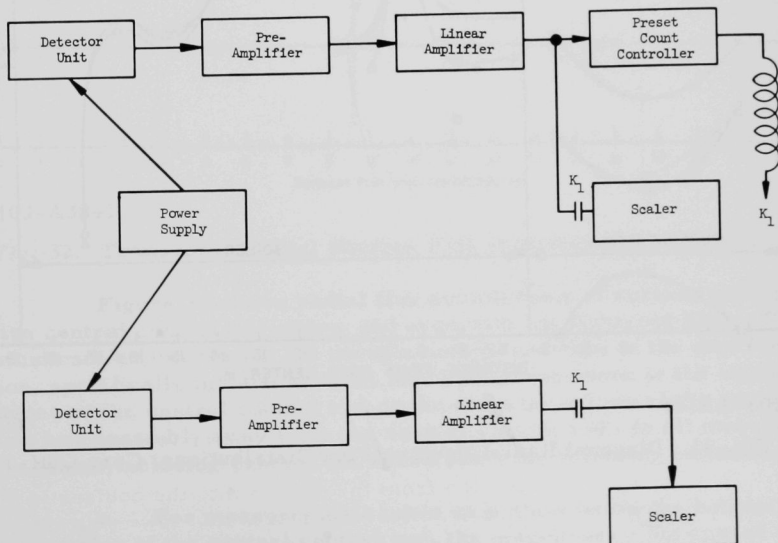
Fig. 29

Flux-wire Holders in
Superheater Fuel Assembly

For the irradiations at operating temperature and pressure, long wires fastened to stainless-steel carrier wires were inserted in six $5/32$ -in.-OD \times 0.020-in.-wall stainless-steel pressure thimbles located as shown later in Fig. 67. These thimbles extended through a reactor head nozzle and top shield, which permitted manual insertion and withdrawal of the flux wires.

The induced activity in the flux wires was gamma-counted, using sodium iodide scintillation crystals and the circuit shown in Fig. 30. Count normalization for purposes of data comparison was accomplished by irradiating a monitor of each wire material being used at the same axial and radial position in each irradiation. Counting to a preset number, using these monitor wires provided automatic normalization and decay correction.

The wire segments were counted in a standard lead pig arrangement, and the long wires were counted in a linear flux-wire scanner. The long wires were fastened in a groove in an aluminum rod and traversed under a vertical, collimated scintillation head in successive steps.

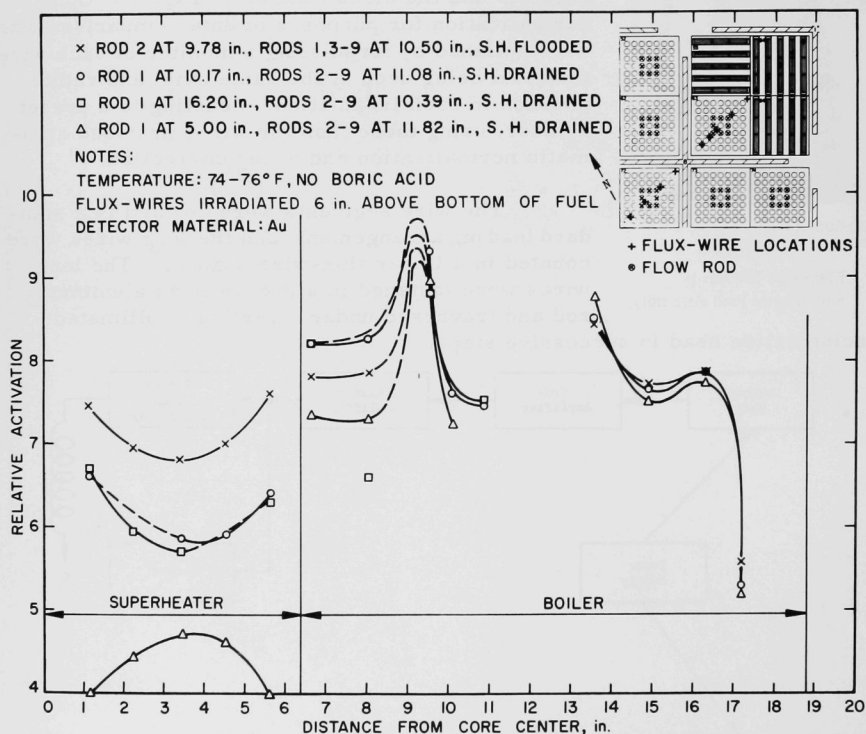


ID-103-A3253

Fig. 30. Block Diagram of Flux-wire Counting System

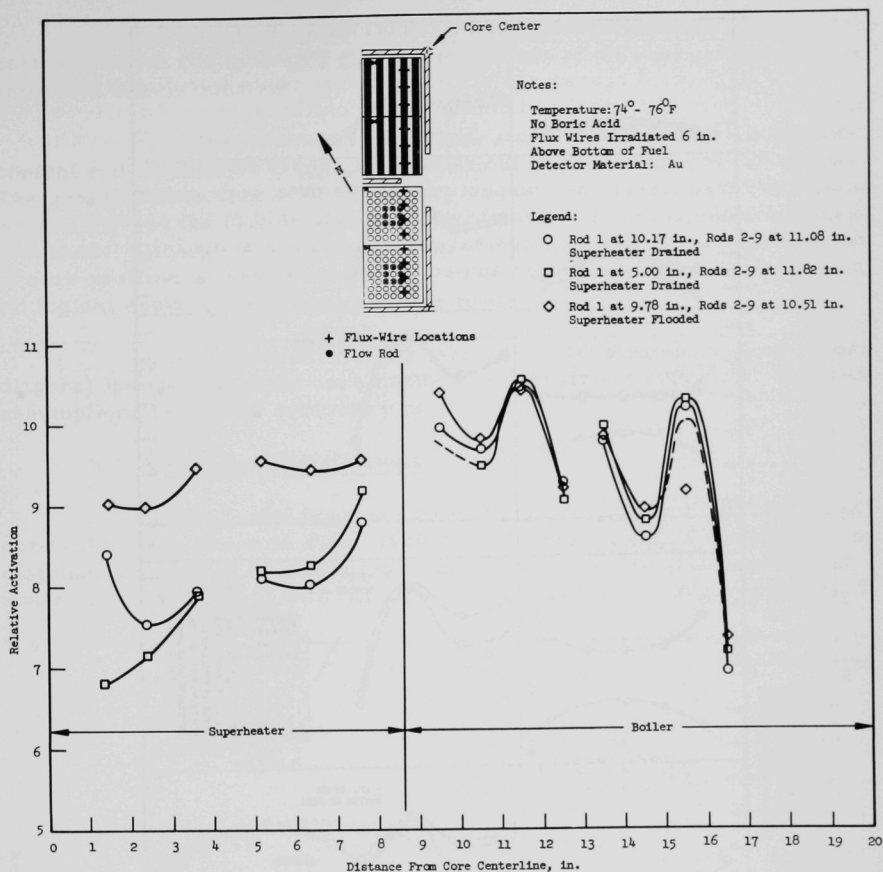
2. Radial Neutron Flux Distributions

Several coarse radial flux measurements were made to determine the effect of control rod configuration on the power split between the boiler and superheater regions. Figures 31 and 32 show plots, obtained from gold wire activation, of the radial flux shapes measured in diagonal and transverse directions, respectively. The data were obtained at a plane 6 in. above the bottom of the fuel, with no boric acid in the system, and indicate that movement of the central control rod has some influence on the power split between the boiler and superheater regions.



ID-103-A3340

Fig. 31. Diagonal Radial Neutron Flux Distributions, Core CSH-1

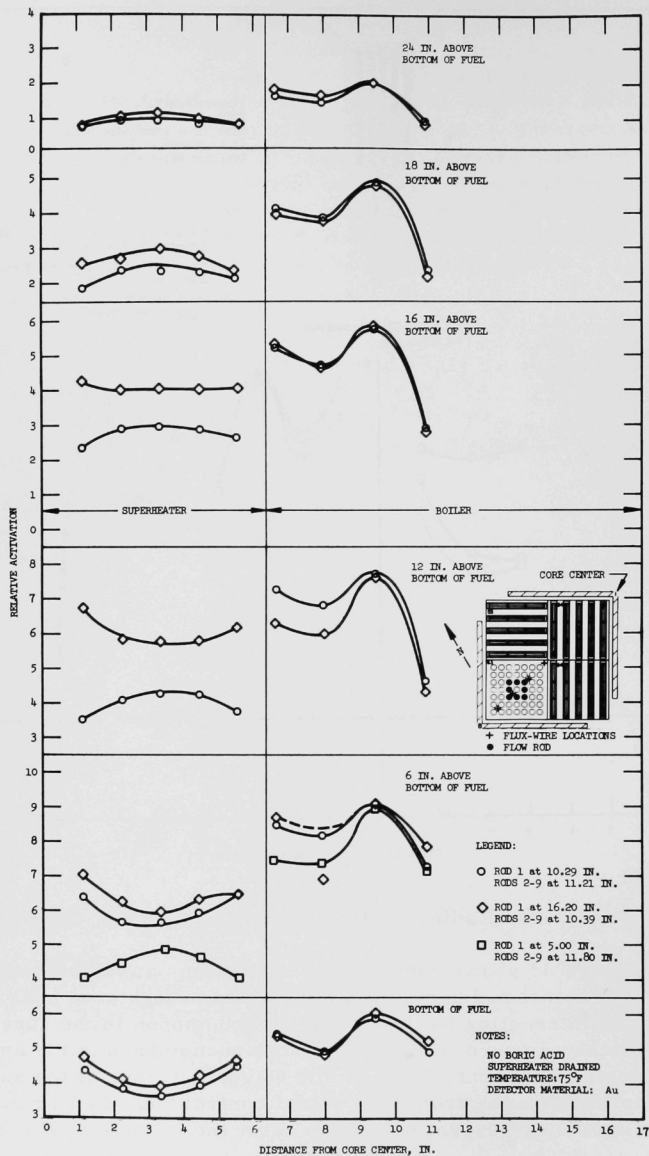


ID-103-A3341

Fig. 32. Transverse Radial Neutron Flux Distributions, Core CSH-1

Figure 33 shows radial flux distributions at various axial planes for the central control rod above, and even with, an eight-rod bank. These data indicate an interesting but unexplained phenomenon in the superheater region, specifically in core position 54. This phenomenon is the apparent influence of the central control rod on the diagonal corner of the superheater fuel assembly away from the central control rod. In all measurements taken, including several not shown here, the following pattern existed:

a. For measurements taken on a plane below the bottom of the poison section of the central control rod, the magnitude of the coarse neutron flux showed a minimum at about the center of the assembly, with a gradual, continual rise in the directions of each diagonal corner.



ID-103-A3342

Fig. 33. Influence of Control Rod Position on Radial Neutron Flux Distribution, Core CSH-1

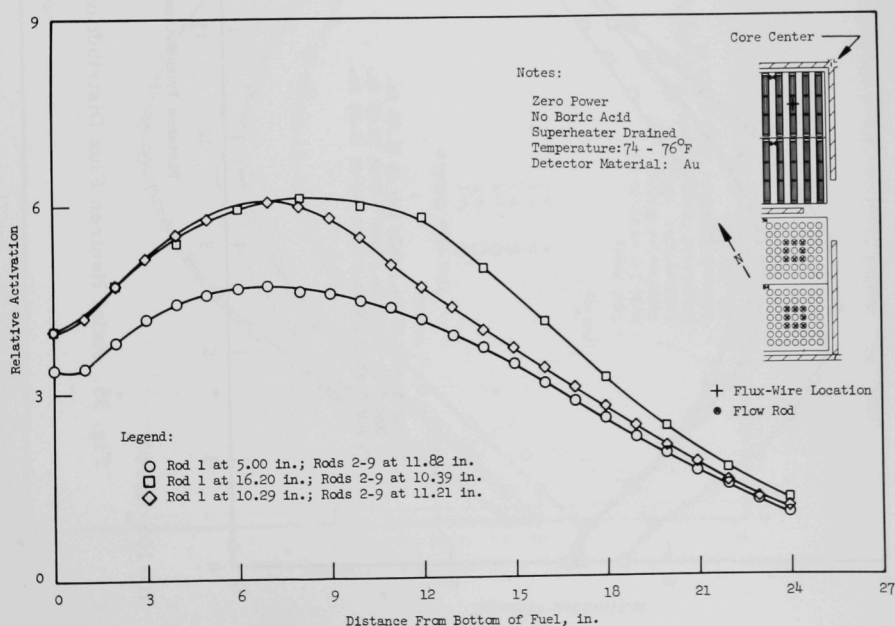
b. Measurements taken on a plane level with the bottom of the central control rod indicated that the magnitude of the coarse neutron flux remained nearly constant.

c. Measurements on a plane above the bottom of the central control rod exhibited a trend just opposite to that described in "a" above. The gross neutron flux in the assembly was at a maximum near the assembly center, and the flux dropped in both directions as the corners were approached. Although this apparent control rod influence in the outer corner of core position 54 seems anomalous, in no case was this trend violated. No logical explanation is known at this time.

A core symmetry check taken in radial directions along a core diagonal indicated that the core exhibited symmetry to within 3%. Further assumptions regarding symmetry cannot be made.

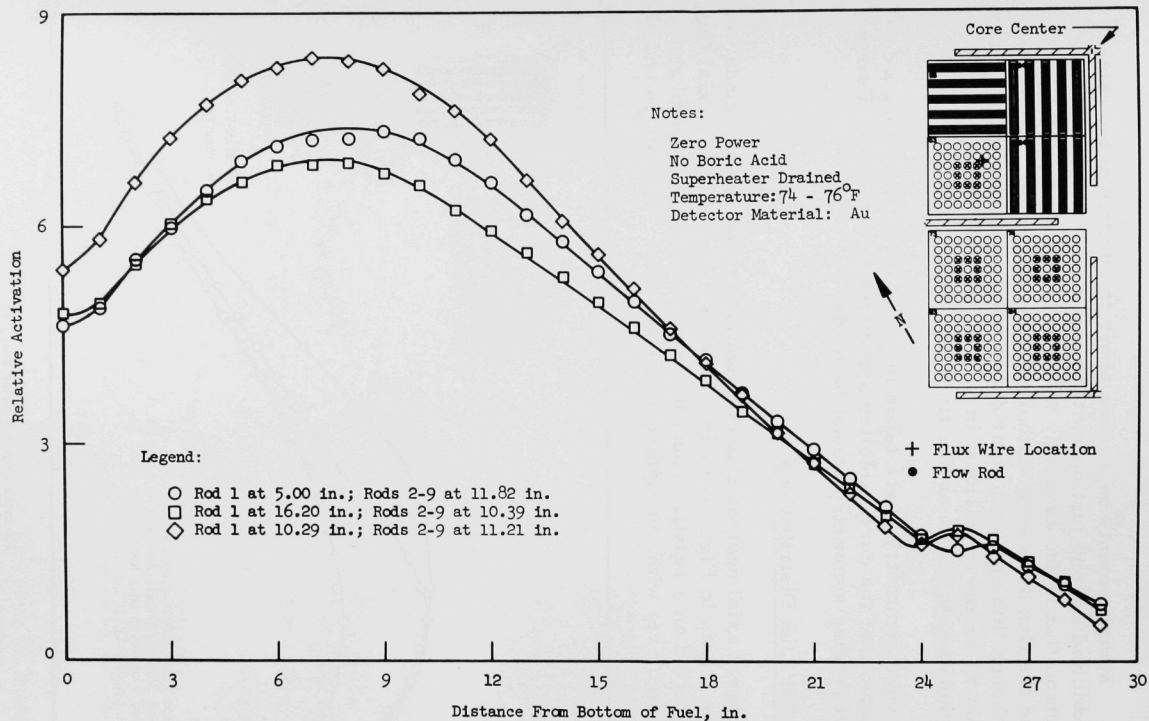
3. Axial Flux Distributions

Several axial neutron flux distribution measurements made in core CSH-1 are shown in Figs. 34 to 38. Figures 34 and 35 show axial flux distributions plotted on a relative count basis for the central control rod above, below, and level with, an eight-control-rod bank. Figures 36 and 37



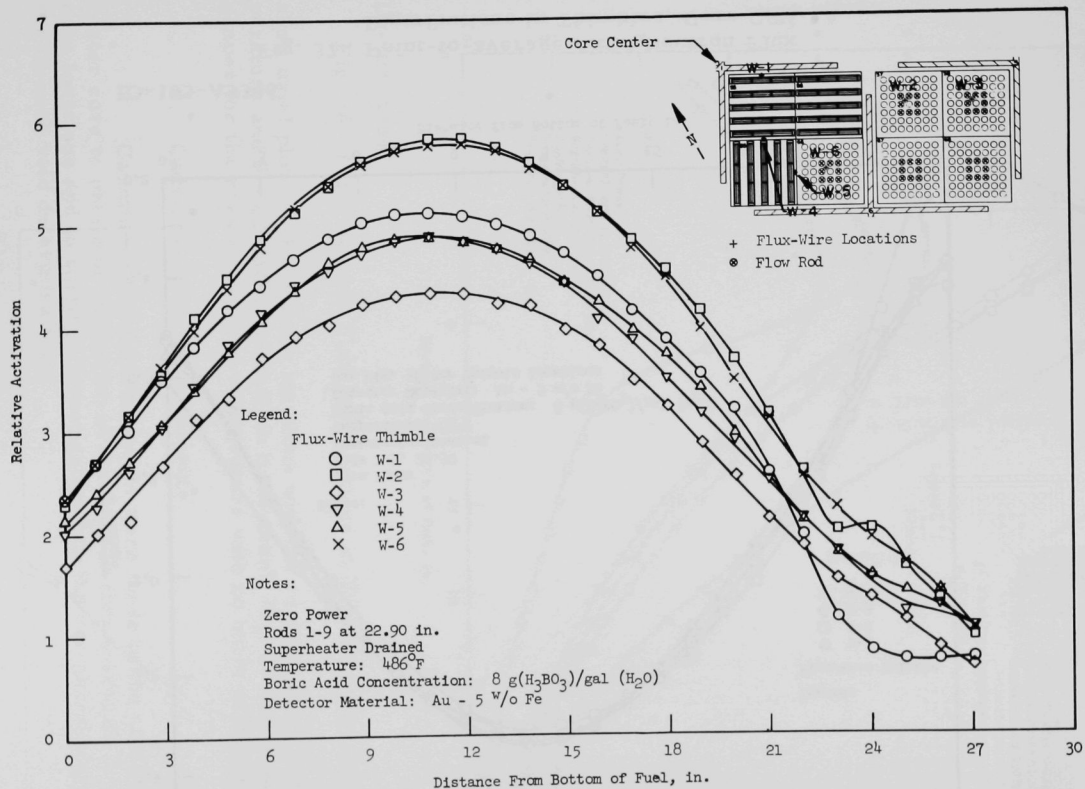
ID-103-A3343

Fig. 34. Axial Neutron Flux Distributions, Core Position 54, Core CSH-1



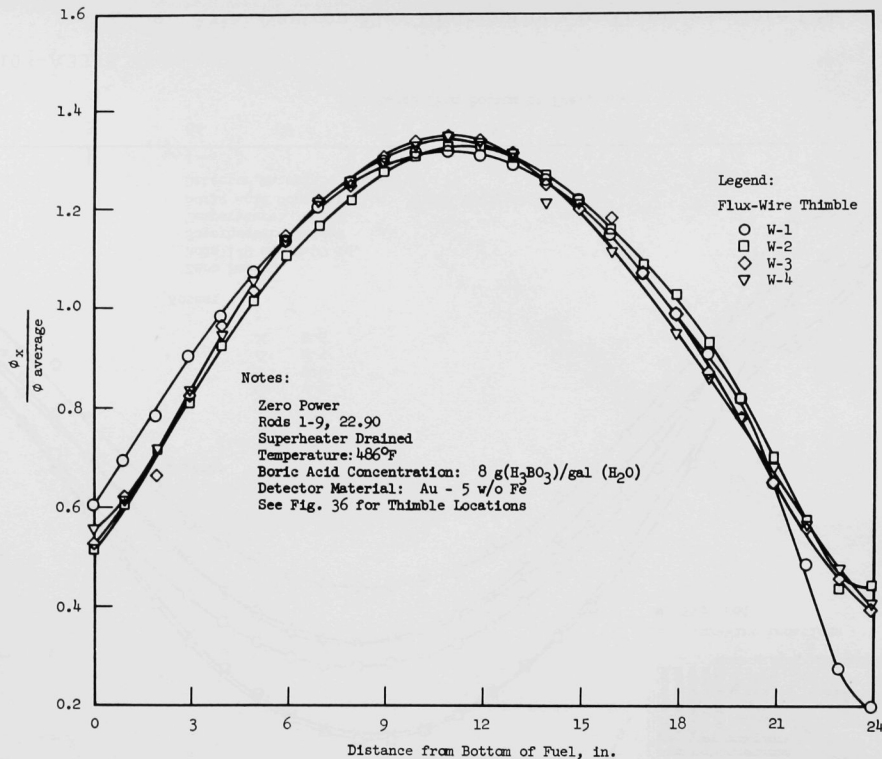
ID-103-A3344

Fig. 35. Axial Neutron Flux Distributions, Core Position 63, Core CSH-1



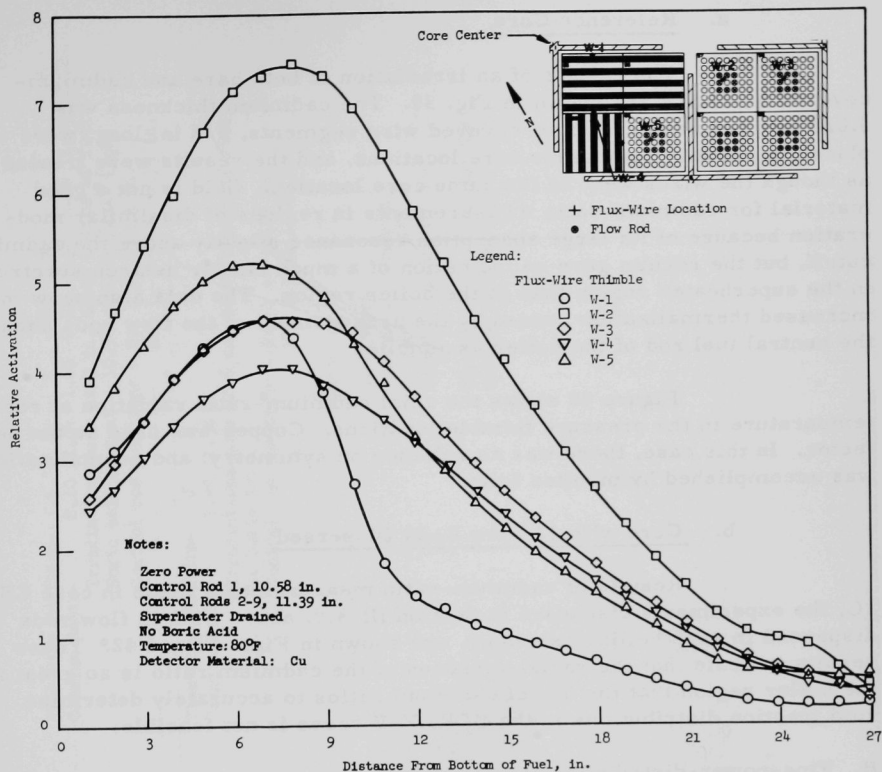
ID-103-A3345

Fig. 36. Axial Neutron Flux Distributions in Thimbles, Core CSH-1A



ID-103-A3346

Fig. 37. Point-to-average Axial Neutron Flux
Distributions in Thimbles, Core CSH-1A



ID-103-A3347

Fig. 38. Axial Neutron Flux Distributions in Thimbles, Core CSH-1

show axial plots in the thimble locations with the reactor at operating temperature and 8.0 g(H_3BO_3)/gal(H_2O) in the system; Fig. 38 shows axial flux shapes for the reactor at room temperature with no boric acid in the system.

4. Cadmium Ratio Measurements

Cadmium ratio measurements were made in the central superheater core to obtain an indication of the neutron flux spectrum at various core locations and to continue investigation into the use of cadmium ratios for in-core void determinations.

a. Reference Core

The results of an irradiation of both bare and cadmium-covered gold wire are shown in Fig. 39. The cadmium thickness was 0.020 in. Bare and cadmium-covered wire segments, $3/8$ in. long, were placed in radially symmetric core locations, and the results were treated as though the wires were in the same core location. Gold is not a good material for cadmium-ratio measurements in regions of dissimilar moderation because of its large absorption resonance slightly above the cadmium cutoff, but the results gave an indication of a much harder neutron spectrum in the superheater region than in the boiler region. The data also show the increased thermalization caused by the arrangement of the flow rods about the central fuel rod of the boiler assemblies.

Figure 40 shows the axial cadmium-ratio variation at room temperature in the pressure thimble locations. Copper was used as the detector. In this case, there was no reliance on symmetry, and normalization was accomplished by monitor foils.

b. Core with 12 Flow Rods Dispersed

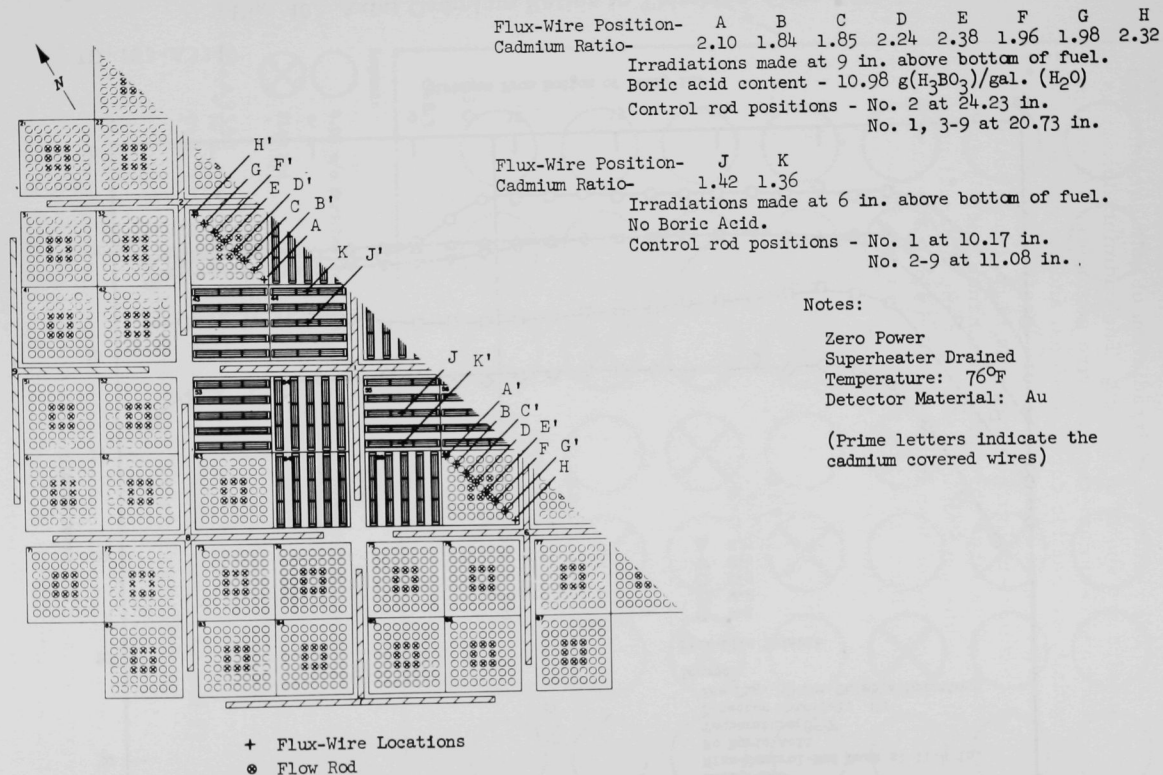
Results of cadmium-ratio measurements made in core CSH-1C, the experiments discussed in Section III.A.9. above with 12 flow rods dispersed in each boiling assembly, are shown in Figs. 41 and 42. These results indicate that the radial variation of the cadmium ratio is so great in the boiler region that the use of cadmium ratios to accurately determine void fraction distributions in the BORAX-V cores is not feasible.

B. Fine-power-distribution Measurements

The original physics calculations for the central superheater core were based on a boiling fuel assembly that contained no flow rods. To determine the fine-power distribution in core CSH-1 for use in heat-transfer analysis, measurements in the boiling fuel assemblies with flow rods and in the superheater fuel assemblies were necessary. Because the techniques used in the measurements blocked the flow passages and utilized materials that were temperature-limited, the fine-power-distribution measurements could be made only at zero-power, room-temperature conditions.

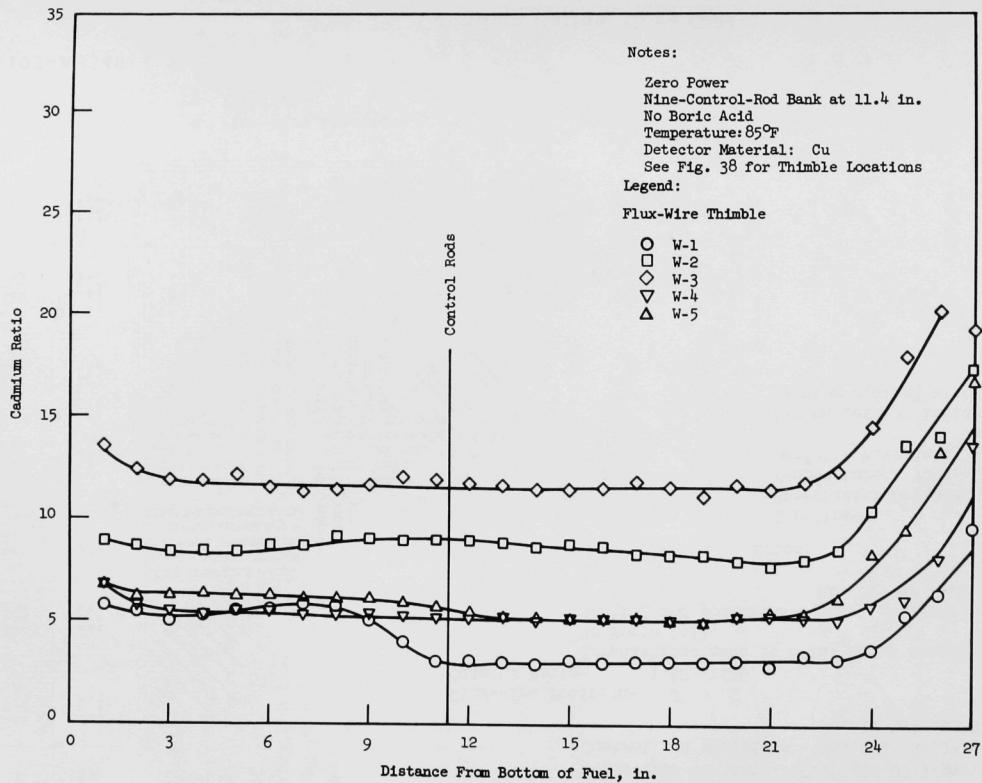
1. Measurement Techniques

The fine-radial-power-distribution measurements in the boiler region were obtained in modified fuel assemblies as shown in Fig. 43. Two boiling fuel assembly boxes were modified by removing replaceable sections of the box sides. Polyethylene blocks, $3\frac{3}{4}$ in. sq x $1/2$ in. thick, were prepared with forty-nine $3/8$ -in. holes on $1/2$ -in. centers so that fuel rods could pass through the blocks. Two holes, $1/32$ in. diam x $1/4$ in. deep,



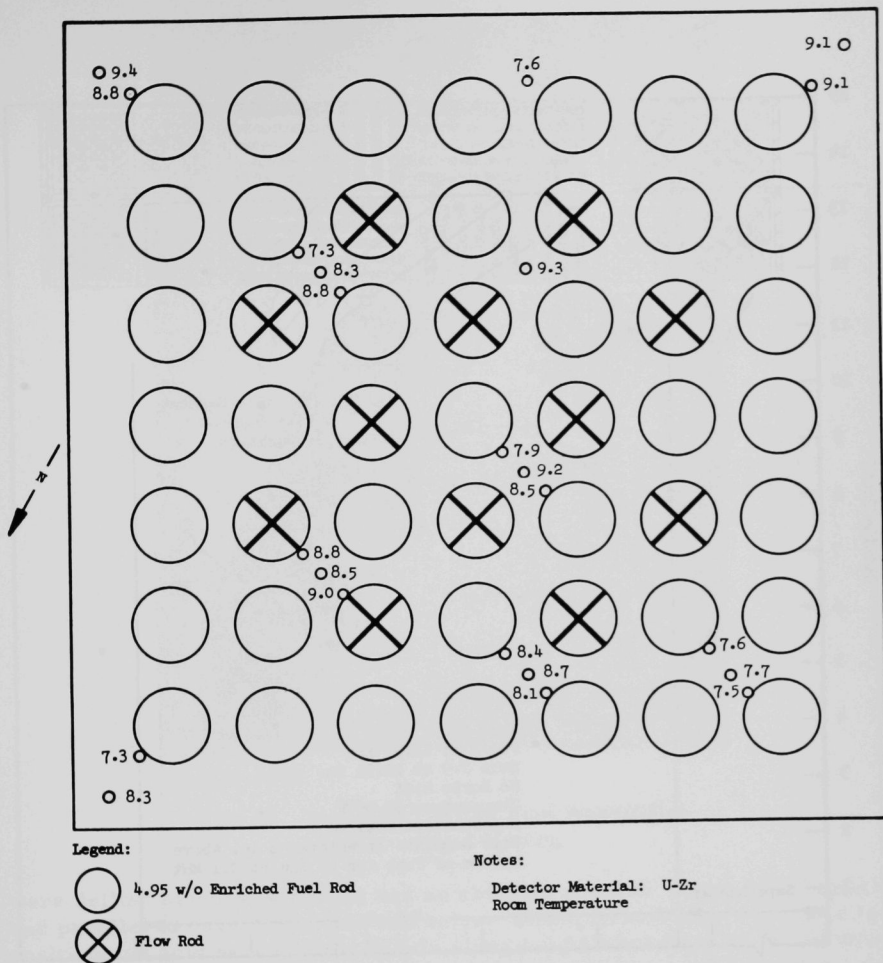
ID-103-A3348

Fig. 39. Cadmium Ratios, Core CSH-1



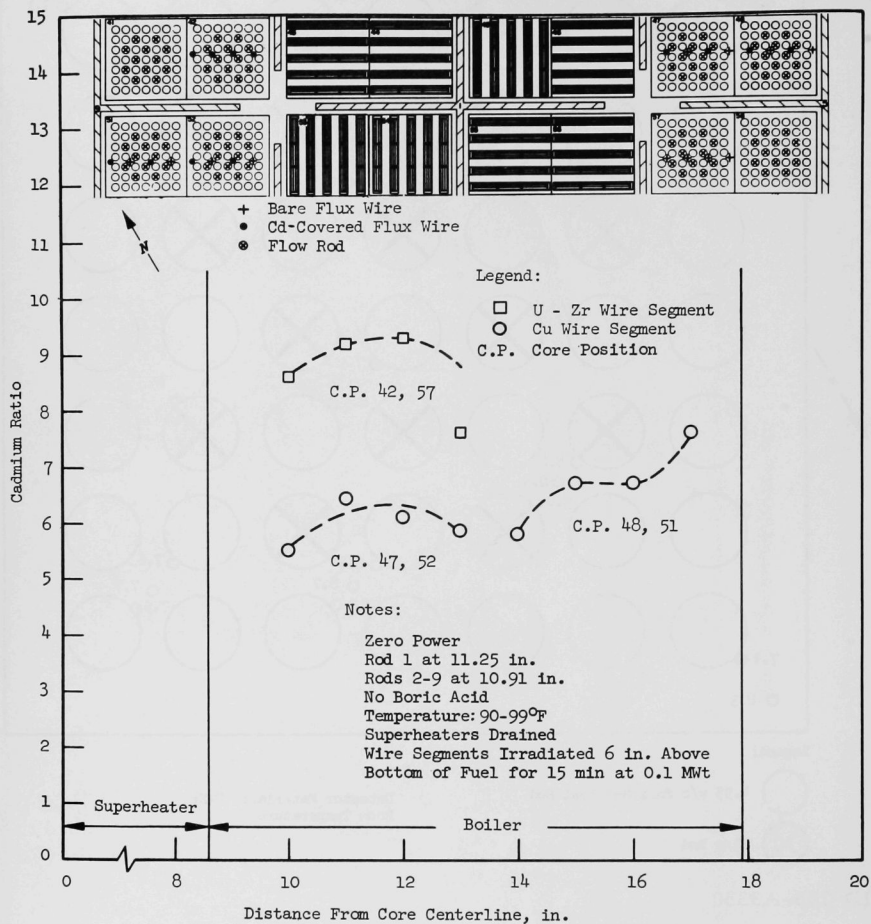
ID-103-A3349

Fig. 40. Axial Cadmium Ratios in Thimbles, Core CSH-1



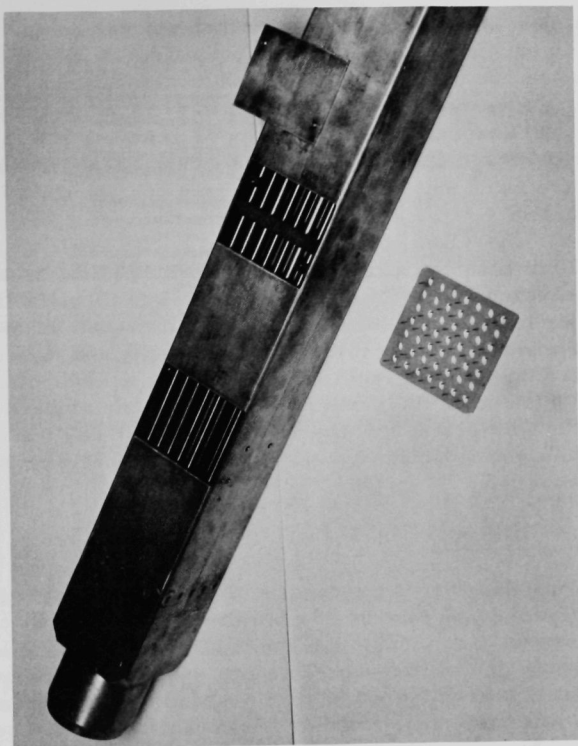
ID-103-A3350

Fig. 41. Cadmium Ratios in Core Positions 42 and 57
(12 Dispersed Flow Rods), Core CSH-1C



ID-103-A3351

Fig. 42. Radial Cadmium Ratio Distribution, Core CSH-1



ID-103-3668

Fig. 43. Modified Boiling Fuel Assembly
for Fine-flux Mapping

were drilled diagonally across and as close as possible (about 10-15 mils) and parallel to each of the fuel rod holes. These small holes were used to position and hold securely the $3/8$ -in.-long x 0.031 -in.-diam Zr-3.379 w/o U (93% U^{235}) wires. Each polyethylene flux-wire tray was loaded with 62 flux wires, two adjacent to each of the 31 fuel-rod holes. The flux-wire trays were positioned near the midplane of the active length of the core. All the measurements were made with a boric acid concentration of $10.8 \text{ g}(\text{H}_3\text{BO}_3)/\text{gal}(\text{H}_2\text{O})$ in the reactor water.

The fine-power-distribution measurements in the superheater fuel assemblies were made in a somewhat similar manner, using the equipment shown in Fig. 29. Teflon strips, 0.050 in. thick, were cut to the width of the steam-coolant channels in the superheater fuel element, and a groove $1/32 \times 1/32$ in. was cut across the strip at a height corresponding to the location of the flux wires in the boiler region. Flux wires, similar to those

used in the boiler, but $1/8$ in. long, were then placed end-to-end in the groove (nine in each of the two edge coolant channels, and eight in the middle one) so that an entire coolant channel, with the exception of the spacer wires, was covered. Corresponding coolant channels in each of the five fuel elements in one fuel assembly were so equipped in each irradiation, so that 15 Teflon strips were inserted into an assembly for one irradiation. Measurements were made only in one octant of the core on the assumption that symmetry existed.

After each day's irradiation, the wires were counted in the equipment discussed in Section IV.A.1. above. One flux wire from each run was used as a monitor. Three wires, the monitor wire and two others, were counted simultaneously, using three counting heads, and the counting time was determined by the time required for a preset number of counts (e.g., 20,000) to be obtained on the monitor wire. The results were thus automatically decay-corrected. All the wires from each day's irradiation in one fuel assembly were counted, using the same counting channel, and each wire was counted twice.

2. Normalization

Normalization of the results of the four fine-flux irradiations had been planned through the use of monitor wires located in the same positions in the core on each irradiation run, but these monitors were inadvertently omitted. It was discovered before the fourth irradiation that no monitor had been used in the same core position on each run and that it would be impossible to correlate the daily irradiations. Consequently, an additional irradiation was performed in which flux wires were placed in the positions occupied by the wires used as daily monitors so that the daily irradiations could be compared.

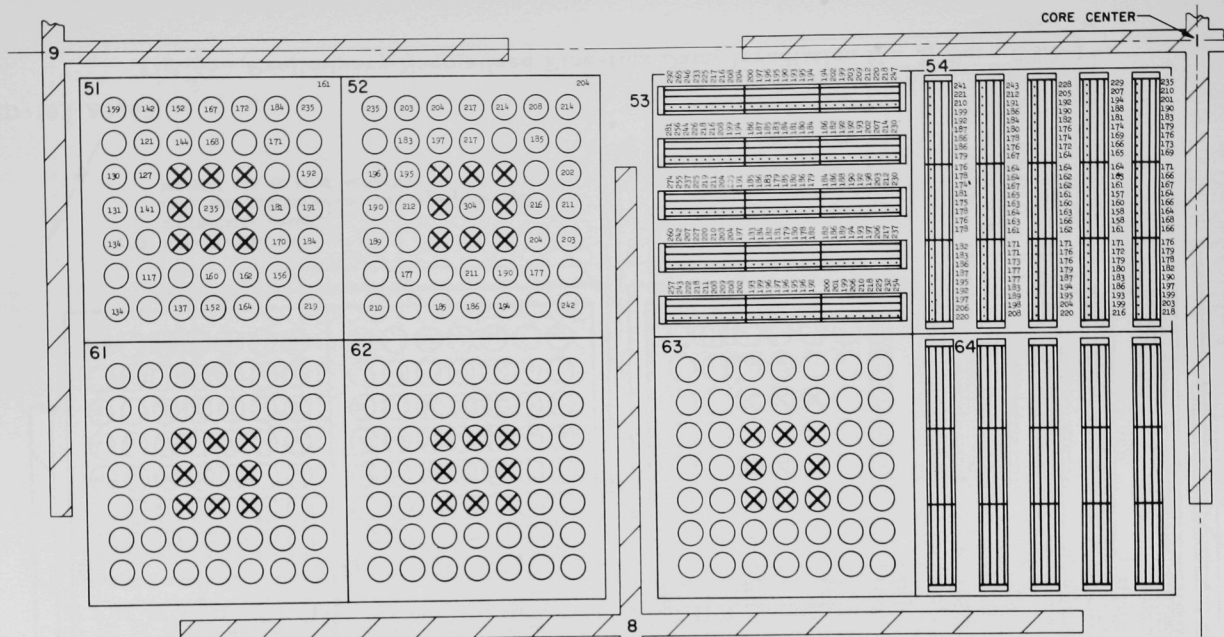
Data from the four irradiations are presented in Figs. 44 through 47. The data in each figure were obtained in the following manner:

a. Measurements in Boiling Fuel Rod Locations

The counts for the two wires adjacent to each fuel rod were averaged, corrected for varying flux-wire weights by normalizing to a wire weight of 31.0 mg, corrected for the daily difference between the two counting channels, normalized to a preset count of 20,000 on the daily monitor, and multiplied by a factor to account for the lack of a common monitor in the four separate irradiations.

b. Measurements Adjacent to Superheater Coolant Channels

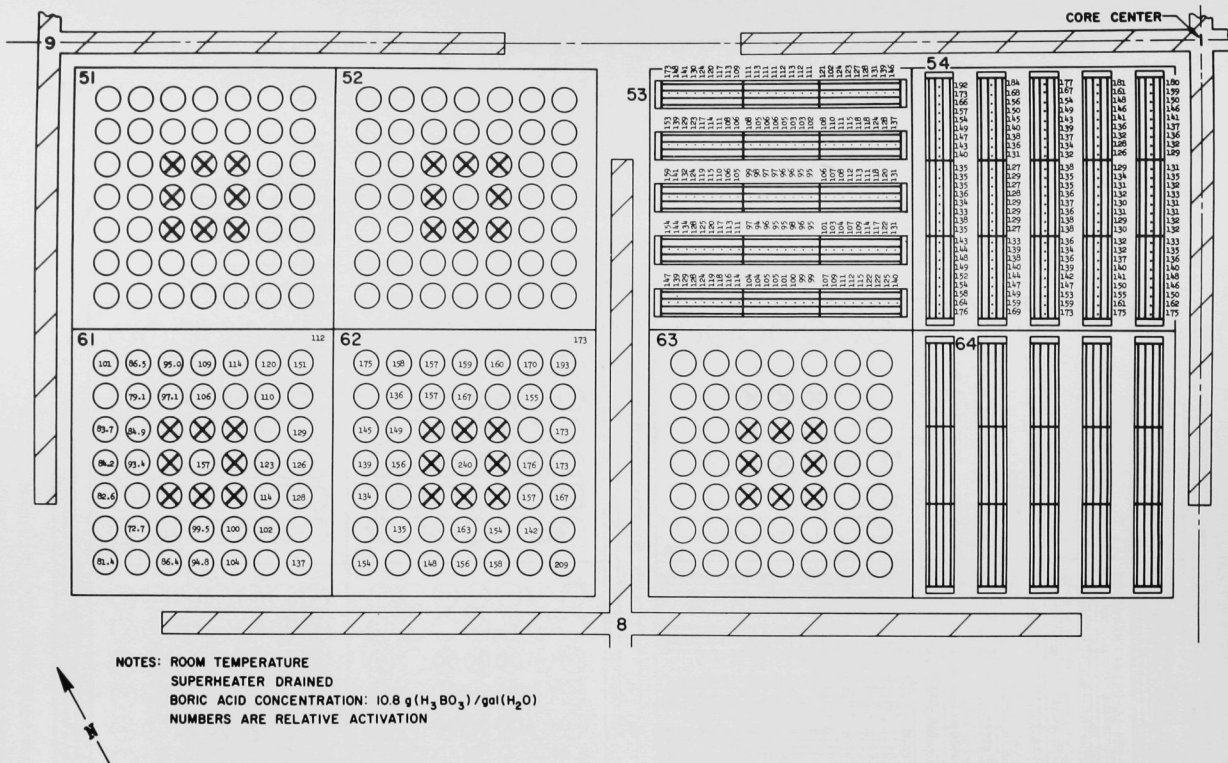
The two counts for each superheater flux wire were averaged, corrected for variations in wire weight by normalizing to a wire weight



NOTES: ROOM TEMPERATURE
 SUPERHEATER DRAINED
 BORIC ACID CONCENTRATION: 10.8 g(H_3BO_3)/gal(H_2O)
 NUMBERS ARE RELATIVE ACTIVATION

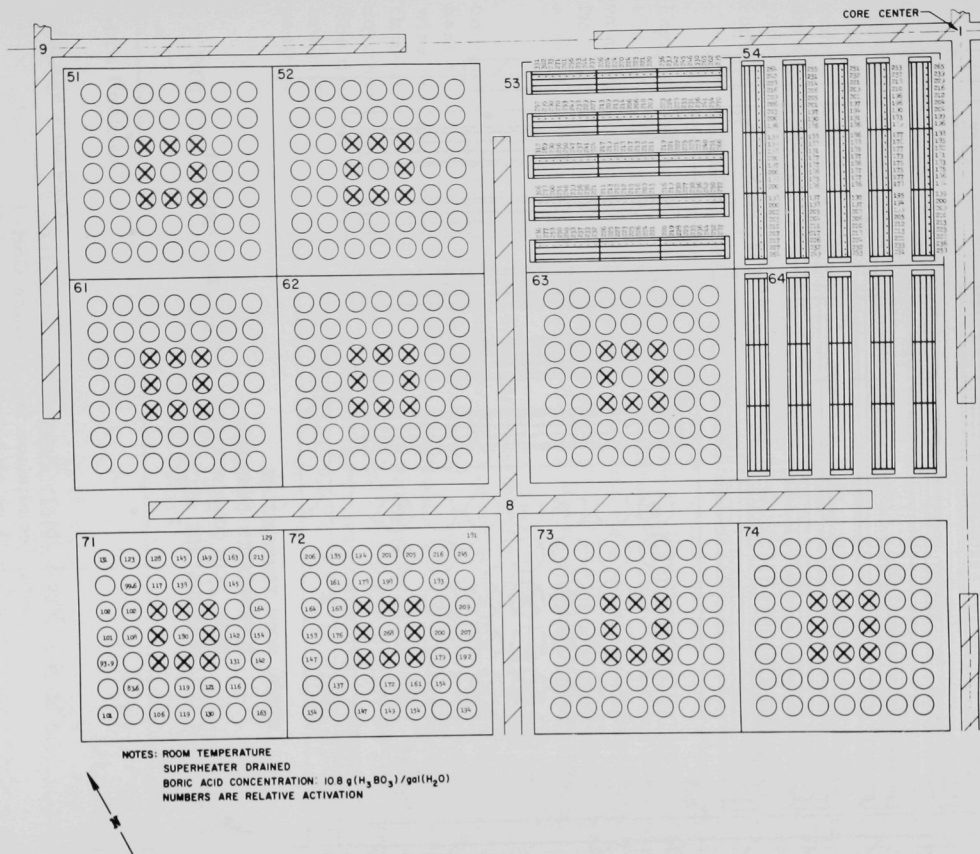
ID-103-A3266

Fig. 44. Preliminary Normalized Fine-flux Data, Irradiation No. 1, Core CSH-1



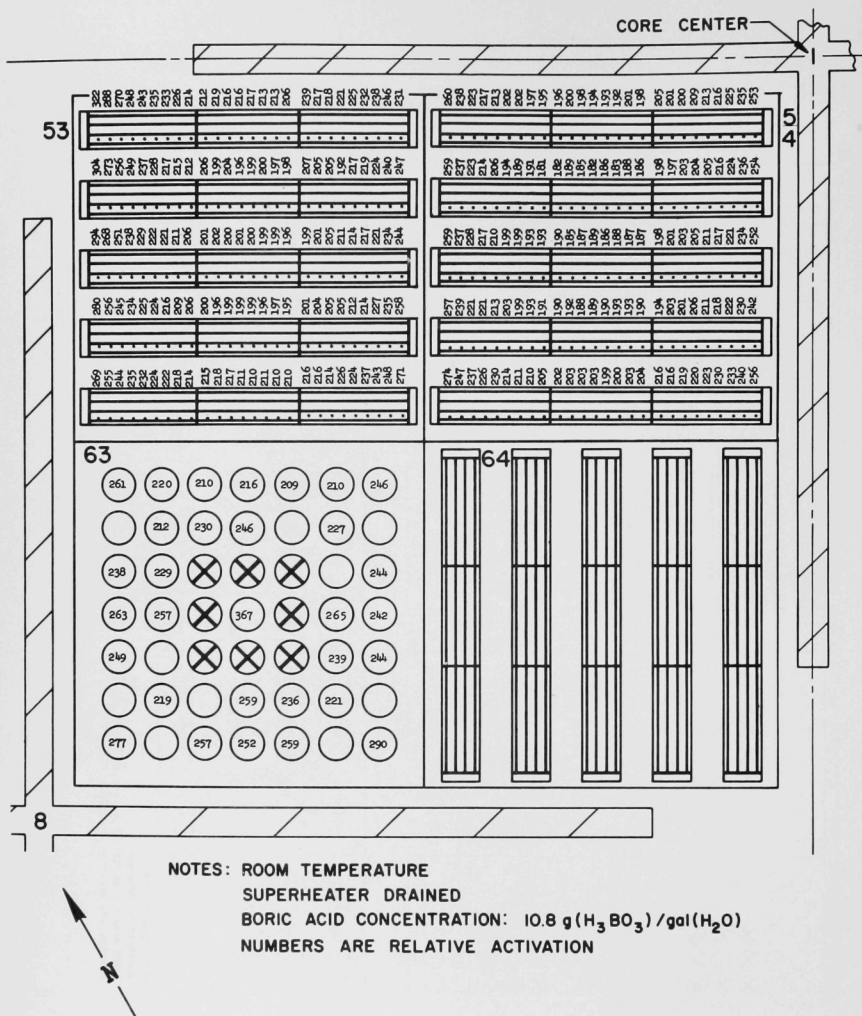
ID-103-A3267

Fig. 45. Preliminary Normalized Fine-flux Data, Irradiation No. 2, Core CSH-1



ID-103-A3268

Fig. 46. Preliminary Normalized Fine-flux Data, Irradiation No. 3, Core CSH-1



ID-103-A3352

Fig. 47. Preliminary Normalized Fine-flux
Data, Irradiation No. 4, Core CSH-1

of 10.6 mg, normalized to 40,000 counts on the monitor wire, multiplied by the proper counting-channel factor, and then multiplied by the factor that normalized the four individual monitor wires. Then, to bring the superheater wires into a common basis with the boiling wires, all superheater

flux-wire counts were multiplied by $20,000/40,000$ (to account for the difference in the preset count on the monitor wires) and by $31.0/10.6$ (to account for the difference in wire weights).

c. Average Activation in Boiling Fuel Assemblies

The number in the upper right corner of the boiling fuel assemblies in Figs. 44-47 represents a weighted average of the numbers appearing within the 31 boiling fuel rod locations, and as such, is the number that would appear in an average boiler fuel rod for that assembly. The average was obtained by adding the numbers from the four corner rods and the center rod to the product of $36/26$ times the sum of the remaining 26 fuel rods containing numbers, and dividing this total by 41, the number of fuel rods in each boiling fuel assembly.

As a result of the above normalization, all the data shown in Figs. 44-47 should be directly comparable. Each number in the four figures should be the number of counts (in hundreds) a flux wire at the given position would yield, compared to an identical flux wire located in water channel No. 1, core position 73, which yielded 20,000 counts. Unfortunately, however, such was not the case and further normalization was necessary.

Figures 44-47 indicate that the four sets of data are not completely compatible. The average flux-wire reading for the boiling fuel assemblies does not behave as expected. Table VI shows the average flux-wire reading for the various core positions. The low value of the average flux-wire reading for core position 61 appears to be too low. An even more noticeable discrepancy appears in the data for the superheater flux wires. The data for the superheater flux wires in irradiation No. 2 appear to be too low compared to data for irradiations Nos. 1 and 3, particularly for core position 53.

Table VI
BOILING FUEL ASSEMBLY AVERAGE FLUX-WIRE ACTIVATION,
CORE CSH-1

| Core Position | 51 | 52 | 61 | 62 | 63 | 71 | 72 |
|---------------------------|-----|-----|-----|-----|-----|-----|-----|
| Average Flux-wire Reading | 161 | 204 | 112 | 173 | 243 | 129 | 181 |

However additional data on flux distribution within a central superheater fuel assembly were available. Critical experiments with the BORAX-V central superheater fuel had been carried out previously in the ZPR-VII reactor at Argonne, Illinois. In the course of these experiments, numerous flux traverses through a four-plate fuel element were made (perpendicular to the fuel plates), and the conclusion was drawn by Plumlee et al. that "it appeared that the traverses plotted in the direction

normal to the fuel plates were independent of lateral position except for a scaling factor, and that the lateral traverses from edge to edge across the fuel plates were similar in shape regardless of position (inner or outer) in the insulating box. This is shown by comparison of many flux profiles in the direction normal to the fuel plates (see Fig. 13)...".⁽⁶⁾ Figure 13 of ANL-6691 is reproduced here as Fig. 48. This figure indicates that flux wires within the two outer coolant channels in any fuel element should have the same relative activation, and flux wires in the center coolant channel should have 93.2% of this activation.

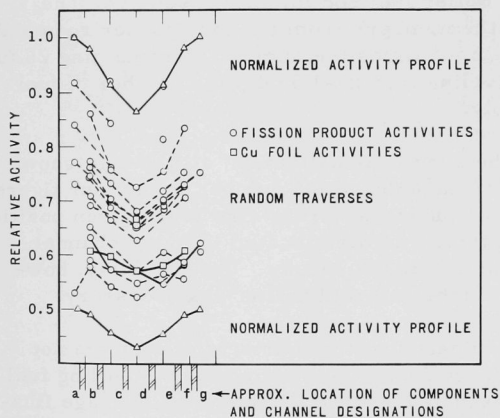


Fig. 48

Foil Activity Depression
through Insulating Box,
Central Superheater
Fuel Element

103-446

Based on the above work, the following procedure was carried out for further normalization of the data:

- (1) The counts of the 26 wires in each coolant channel were averaged.
- (2) A series of ratios was established, by comparing the above average for each of five coolant channels in one irradiation in one assembly to those for corresponding coolant channels in another irradiation or superheater assembly.
- (3) The data from irradiation No. 3 for core position 54 were arbitrarily selected as the datum level.
- (4) The data from irradiation No. 1 for core position 54 were multiplied by the average of five of the ratios obtained in step (2) above (namely, 1.127) to make the averages for the 26 wires in both outer coolant channels of each of the five elements in the assembly in core position 54 equivalent.

(5) The data from irradiation No. 2 for core position 54 were multiplied by the average of another five of the ratios obtained in step (2) and by 0.932 (the combined factor was 1.334) so that the activities of wires in the five center coolant channels in core position 54 were, on the average, 0.932 of the two outer coolant channels in each element. By steps (4) and (5), the data for core position 54 were brought into agreement with the data from Plumlee et al.⁽⁶⁾

(6) The average ratio of the averages found in step (2) for irradiation No. 3, core position 53, to irradiation No. 3, core position 54, was 1.166. The average ratio of the averages found in step (2) for irradiation No. 1, core position 53, to irradiation No. 3, core position 53, was 1.132. Therefore, to get core position 53 on a comparable basis with core position 54, the data from irradiation No. 3, core position 53, were multiplied by 0.985 to make these data 1.149 times as great as those for irradiation No. 3, core position 54.

(7) The data for irradiation No. 1, core position 53, were multiplied by 1.142 to make the averages found in step (2) for the two outside coolant channels in core position 53 equivalent.

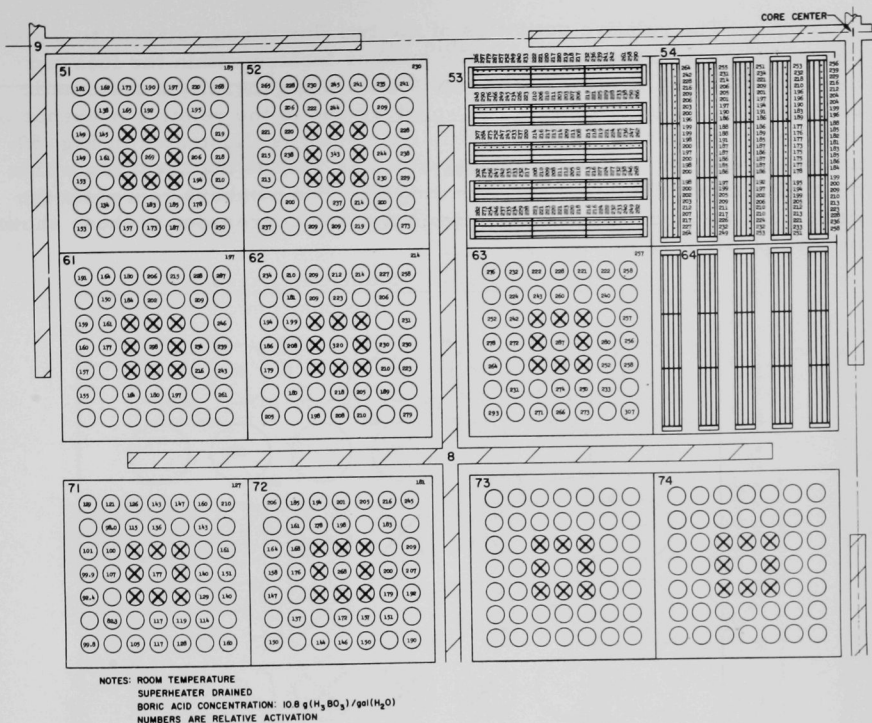
(8) The data from irradiation No. 2, core position 53, were multiplied by 1.898 to make these 93.2% of the values for the outside coolant channels in core position 53.

(9) The data from irradiation No. 4 for both core positions 53 and 54 were multiplied by 1.057 to get the averages [as arrived at in step (2)] for core position 53 in irradiations Nos. 2 and 4 to be equivalent, since the flux wires in the two irradiations were located in the same channels in core position 53.

The above adjustments were made to bring the data from the flux wires in the superheater fuel assemblies into agreement with Plumlee's data.⁽⁶⁾ Why such adjustments were necessary is not clear. The most reasonable explanation is that the counting equipment was not properly adjusted each day (there were daily variations in the discriminator and gain settings on the three counting channels), but the channel factor that was a part of the regular normalization procedure should have accounted for such variations. In any event, such adjustments were necessary; and since they were made for the superheater, corresponding adjustments were made in the boiler flux wires. The same factor was applied to boiler wires as to superheater wires, which were counted on the same day in the same counter. Table VII summarizes the correction factors that were used on the data from Figs. 44-47 to put them in the form presented in Fig. 49, the final normalized data.

Table VII
FINAL NORMALIZATION FACTORS, CORE CSH-1

| Item | Irradiation No. | Core Position | Factor | Explanation |
|------|--------------------|------------------|--------|---|
| 1 | 3 | 54 | 1.000 | Arbitrary datum level |
| 2 | 1 | 54 | 1.127 | Made outer channels of core position 54 equivalent |
| 3 | 2 | 54 | 1.334 | Made core position 54 inner channels 0.932 of outer channels |
| 4 | 3 | 53 | 0.985 | Made core position 53 comparable to core position 54 for both irradiations Nos. 1 and 3 |
| 5 | 1 | 53 | 1.142 | Made outer channels of core position 54 equivalent |
| 6 | 2 | 53 | 1.898 | Made core position 53 inner channels 0.932 of outer channels |
| 7 | 4 | 53 | 1.057 | Made item 7 equivalent to item 5 |
| 8 | 4 | 54 | 1.057 | Conformed with item 7 |
| 9 | 1 | 51 | 1.142 | Counted on same day in same channel as item 5 |
| 10 | 1 | 52 | 1.127 | Counted on same day in same channel as item 2 |
| 11 | 2 | 61 | 1.898 | Counted on same day in same channel as item 6 |
| 12 | 2 | 62 | 1.334 | Counted on same day in same channel as item 3 |
| 13 | 3 | 71 | 0.985 | Counted on same day in same channel as item 4 |
| 14 | 3 | 72 | 1.000 | Counted on same day in same channel as item 1 |
| 15 | 4 | 63 | 1.057 | Counted on same day in same channel as item 7 |



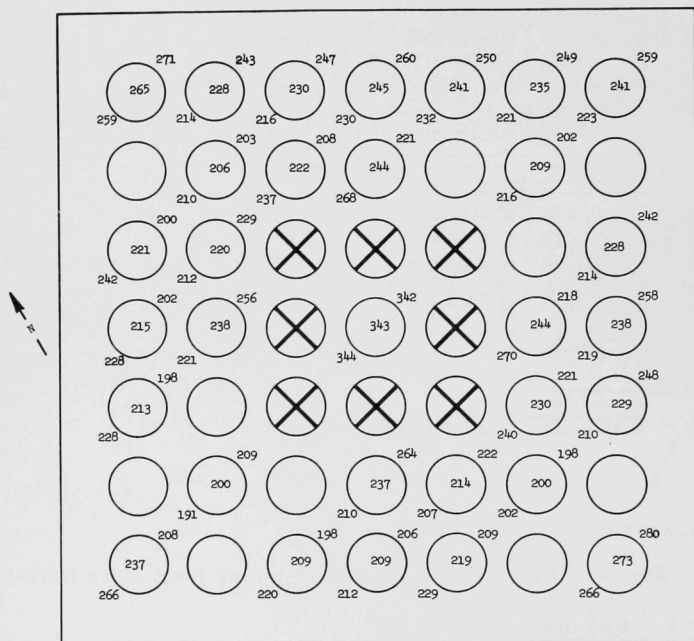
ID-103-A3270

Fig. 49. Final Normalized Fine-power Map, Core CSH-1

3. Results

Figure 49 presents the normalized data for all of the boiling fuel assemblies and for one set of coolant channels in the superheater fuel assemblies. The numbers at the fuel locations represent relative activations of identical flux wires at the locations. The effect of the eight flow rods in each boiling assembly can readily be seen, as the peak power production occurred in the center boiling fuel rod in each case. The number in the upper right corner of each boiling assembly is the average for the 41 fuel rods in that assembly, so an intra-assembly local-to-average fuel rod power production is obtainable. Only one set of superheater flux-wire data is presented, since the remaining outer channels have been made equivalent to the data presented, and the inner channel data have been adjusted to 93% of the outer channel data.

The relative activities of the two flux wires adjacent to a given fuel rod were averaged to obtain the number located within the fuel rod locations in Figs. 44-47 and Fig. 49. There was generally a systematic difference in the activities of the two wires due to the relative presence of water at the flux-wire location. This difference is illustrated in Fig. 50, in which the counts of the individual wires as well as the averages within the fuel rod are shown for core position 52. The numbers represent the finally normalized data of irradiation No. 1 and correspond to those shown in core position 52 in Fig. 49.



Note:

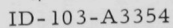
Room Temperature

ID-103-A3353

Fig. 50. Relative Flux-wire Activities and Average for a Fuel Rod (Circled), Core Position 52, Core CSH-1

4. Analysis

Superheater coolant-channel local-to-average fission ratios were obtained in the direction parallel to the fuel plates for core positions 53 and 54. The profiles for ten coolant channels in each of the two superheater fuel assemblies were averaged, and the results are shown in Fig. 51. The two curves are similarly shaped but slightly different. The fission ratio was highest in the region of the superheater adjacent to the boiler.



83

In the direction perpendicular to the fuel plates, the ratio was fairly uniform. The average ratio of fission rate in a given coolant channel in one element to that in a corresponding coolant channel in the center element for core position 53 was 1.023, 0.991, 1.000, 1.000, and 1.061, working from the element farthest from the control rod channel to that closest to the control rod channel. Corresponding ratios in core position 54 were 1.046, 1.000, 1.000, 0.983, and 1.018, with resulting peak-to-average ratios of 1.04 for both assemblies.

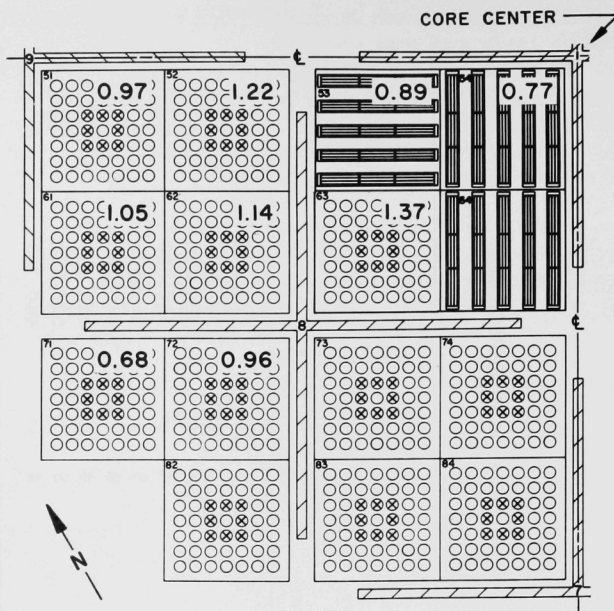
The normalized fine-power-distribution data in Fig. 49 were used, together with earlier experimental data, to determine the relative power produced in various core positions and the fraction of the total core power produced in the superheater.

In an earlier exponential experiment with BORAX-V boiling fuel rods, Kirn and Hagen⁽⁷⁾ found that the average fission rate across a boiling fuel rod was 91% of the fission rate in a flux wire on the surface. Plumlee et al.,⁽⁶⁾ as shown in Fig. 48, determined that the average fission rate in the two outside fuel plates was equal to 0.95, and in the two inside fuel plates was equal to 0.89, based on a figure of 1.00 at the moderator side surface of the insulating tube around a superheater fuel element. On the same basis, the average fission rate at a detector in the outer coolant channels was equal to 0.91, and in the center coolant channel, 0.86.

To determine the relative power production in a fuel assembly, it was necessary to consider the fuel loading as well as the local fission rate. For a boiler fuel assembly containing 41 fuel rods, each rod with 16.3 g of U^{235} , a normalized power-production term is given by $(41)(16.3)(0.91)$ (average normalized fission rate in the assembly), or 608 (average normalized fission rate). A superheater fuel-assembly power-production term was somewhat more difficult to derive. An outside fuel plate contained 53.6% as much fuel as an inner plate and had a relative flux of 0.95. A fully loaded inside fuel plate had a relative flux of 0.89. Therefore, the normalized average flux in all the fuel was equal to 0.91, which coincidentally was the relative flux measured by a detector in the outer coolant channels. Since an average flux-wire activity had been obtained for each superheater coolant channel, the average of the ten outside coolant channels in an assembly was readily obtainable, and this was the normalized average fission flux for the assembly. Each superheater fuel assembly contained 430 g of U^{235} , so a normalized power-production term is given by (430) times (average fission rate in the assembly). Table VIII indicates the procedure used in determining the relative power produced in the various core positions and the superheater region. The local-to-average power ratios for the individual fuel assemblies are also shown in Fig. 52. The power fraction in the superheater at room temperature, zero power, was thus about 17%.

Table VIII
LOCAL-TO-AVERAGE FUEL ASSEMBLY POWER PRODUCTION,
CORE CSH-1

| Core Position | Average Flux-wire Reading | Normalized Power Production in Assembly | | Number of Similar Assemblies in Core | Normalized Power Production in Similar Assemblies | Local-to- average Power Production |
|------------------|---------------------------------|--|-----------------------------------|---|---|---|
| | | 608 Times Average Flux Wire | 430 Times Average Flux Wire | | | |
| 51 | 183 | 111,000 | | 8 | 888,000 | 0.97 |
| 52 | 230 | 140,000 | | 8 | 1,120,000 | 1.22 |
| 53 | 236 | | 101,000 | 8 | 808,000 | 0.89 |
| 54 | 206 | | 89,000 | 4 | 356,000 | 0.77 |
| 61 | 197 | 120,000 | | 8 | 960,000 | 1.05 |
| 62 | 214 | 130,000 | | 8 | 1,040,000 | 1.14 |
| 63 | 257 | 156,000 | | 4 | 624,000 | 1.37 |
| 71 | 127 | 77,000 | | 8 | 616,000 | 0.68 |
| 72 | 181 | 110,000 | | 4 | 440,000 | 0.96 |



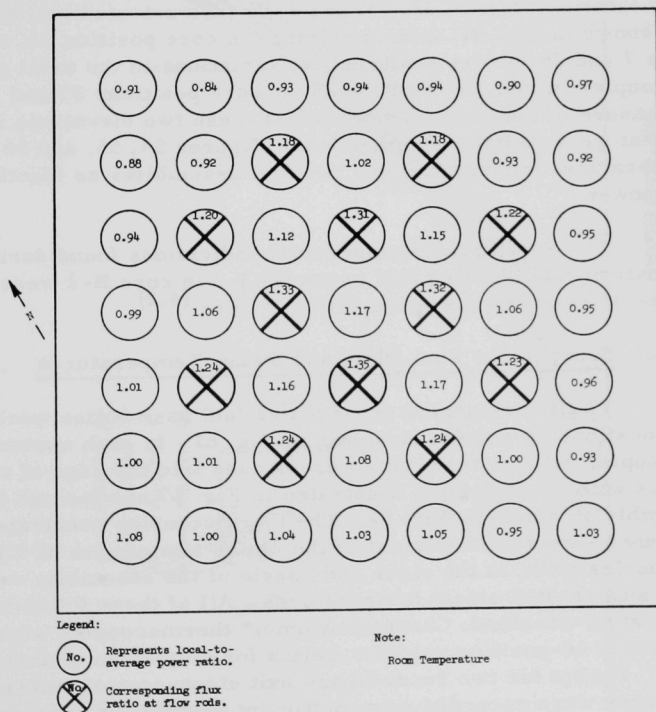
ID-103-A3355

Fig. 52. Local-to-Average Ratio of Power Produced in Individual Fuel Assemblies, Core CSH-1

One purpose of irradiation No.4 was to determine the effect of rotating the superheater fuel assembly in core position 54 by 90°. The effect can be observed in Figs. 44 and 47. The relative activity of flux wires from core position 53 to those in core position 54 was 1.132 in irradiation No. 1, and was 1.065 in irradiation No. 2, a difference of 7%. As can be seen from Fig. 10, turning the fuel assembly in core position 54 by 90° provided an uninterrupted row of superheater elements through core positions 53, 54, 55, and 56. The resultant increased possibility of neutron steaming may have been the cause of the 7% decrease in relative power production in core position 54.

5. Flux Distribution in 12-flow-rod Boiling Fuel Assembly

As one of the final experiments with the central superheater core after initial power operation was completed, a room-temperature experiment was conducted to determine the local-to-average power distribution in a boiling fuel assembly containing 12 flow rods dispersed regularly through the assembly, designated core CSH-1C, in contrast to the core CSH-1 reference loading with eight flow rods concentrated about the center fuel rod. Core position 57, adjacent to a superheater assembly and symmetrical with core position 52, was used. The results are shown in Fig. 53. The greater number and the dispersal of the flow rods resulted in a lower peak-to-average flux, a maximum of 1.17 in this case, compared to 1.49 with the eight bunched flow rods. This experiment indicated that at a given reactor power level the peak heat flux in the boiler would be reduced, using assemblies with 12 flow rods, to 87% of that using eight flow rods.



ID-103-A3356

Fig. 53. Fine-power Distribution in Core Position 57
(12 Dispersed Flow Rods), Core CSH-1C

V. IN-REACTOR-VESSEL INSTRUMENTATION MEASUREMENTS AND DEVELOPMENT

A. Reactor Data

Measurements were made using permanent in-vessel instruments and instrumented fuel assemblies during all major power operation periods of the reactor with core CSH-1B. The measurements are listed below, along with the techniques used to obtain the data. Locations of most instruments are indicated later on Fig. 67.

1. Boiling Fuel Rod Temperatures

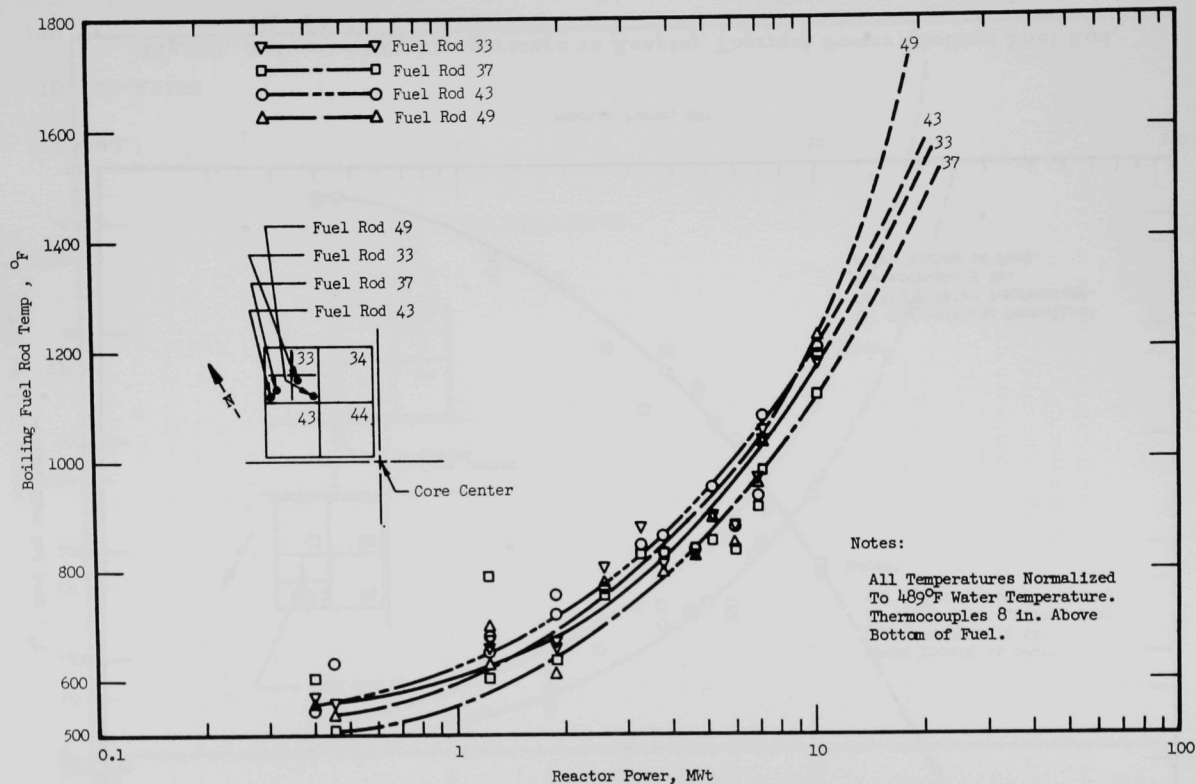
Data were obtained from W/W-26 w/o Re thermocouples installed in the axial center of UO_2 pellets in boiling fuel thermocouple rods. Fuel rod locations 25, 33, 37, 43, and 49 in instrumented boiling fuel assembly I-1, shown in Fig. 67, were monitored in core position 33, and individual fuel rods 7 and 25 in core position 36. Variations in the axial positions of thermocouples in fuel rod location 25, at core positions 33 and 36, gave some measure of the power production at these two elevations in core positions that were radially symmetrical. Figures 54, 55, and 56 illustrate the temperatures measured in the two fuel assemblies as functions of reactor power.

The erratic fuel-temperature indications found during irradiation of instrumented boiling fuel assembly I-2 in core B-2 were not observed during the brief power operation with this core.^(4,8)

2. Superheater Fuel Plate and Steam Temperatures

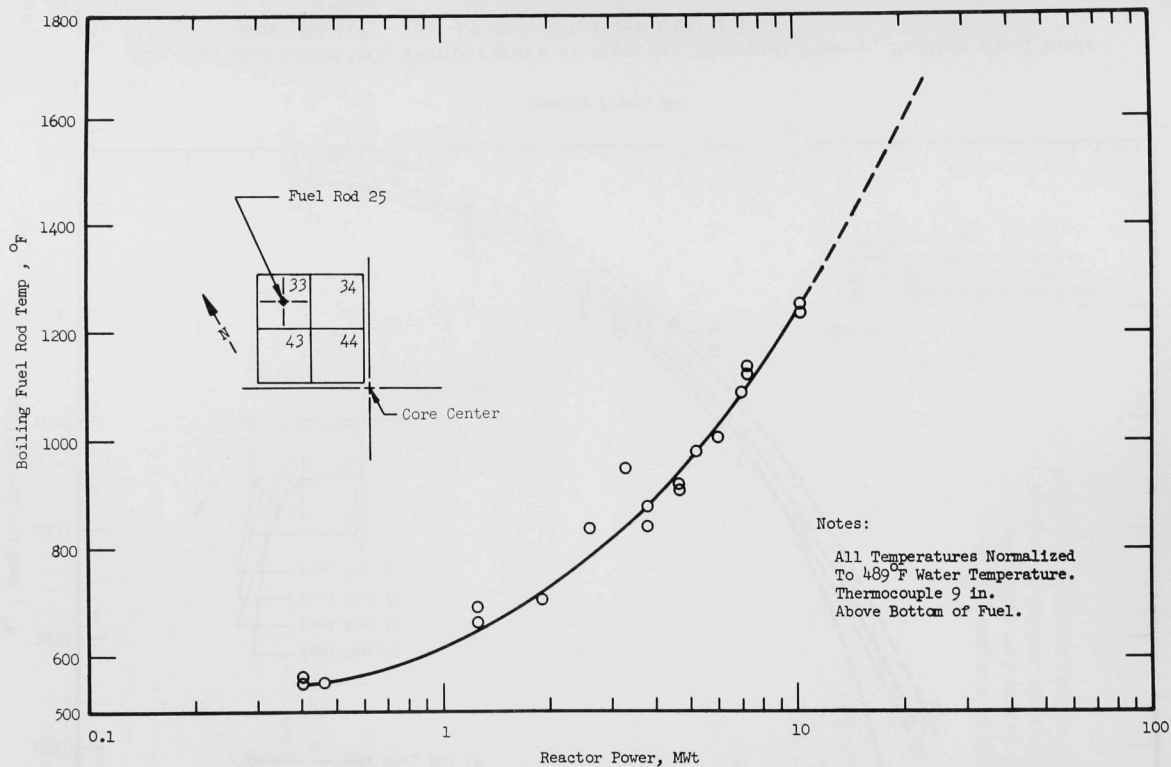
Two instrumented superheater fuel assemblies were mounted in core locations 44 and 45, as shown in Fig. 67. In each assembly, 20 thermocouples with flattened tips were brazed into the edge of selected fuel plates with the technique illustrated in Fig. 57 and located throughout the assembly as shown in Fig. 58. The thermocouples penetrated into the UO_2 -stainless-steel cermet meat of the plates a minimum of 0.115 in. Two thermocouples each, in the riser and nozzle of the assembly, were used to measure superheated steam temperatures. All of these 0.040-in. diam, stainless-steel-sheathed, Chromel-Alumel* thermocouples were monitored by means of a 40-position selector switch for display on a circular chart recorder. Except for two second-pass exit steam temperatures, steam temperatures were recorded on a multipoint instrument. One second-pass exit steam temperature was recorded on a circular chart recorder, and the second was made available on the 40-point selector switch in place of a failed fuel plate thermocouple.

*Hoskins Manufacturing Co. trade name.



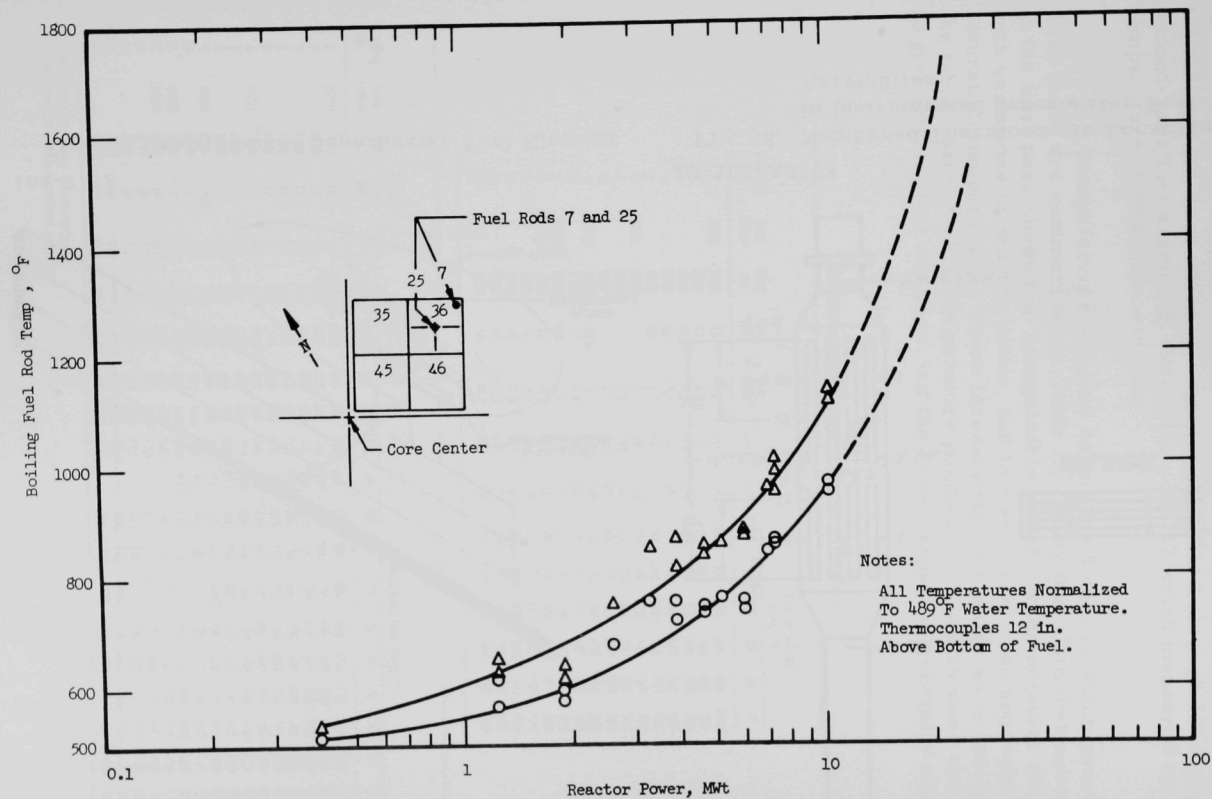
ID-103-A3357

Fig. 54. Indicated UO₂ Temperature vs Reactor Thermal Power, Boiling Fuel Rods Nos. ZA-17, -18, -19 and -20, Core CSH-1B



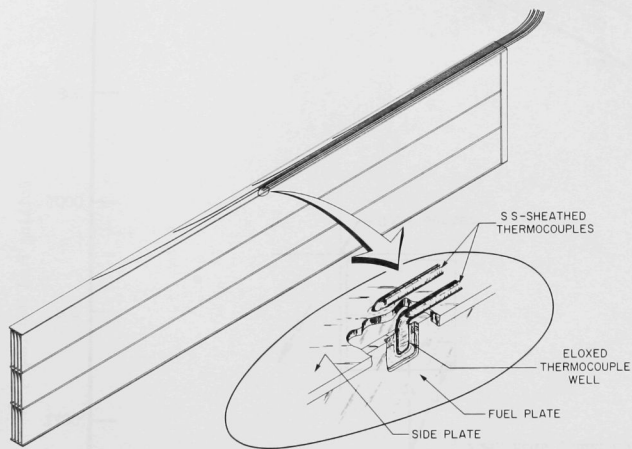
ID-103-A3358

Fig. 55. Indicated UO_2 Temperature vs Reactor Thermal Power, Boiling Fuel Rod No. YA-15, Core CSH-1B



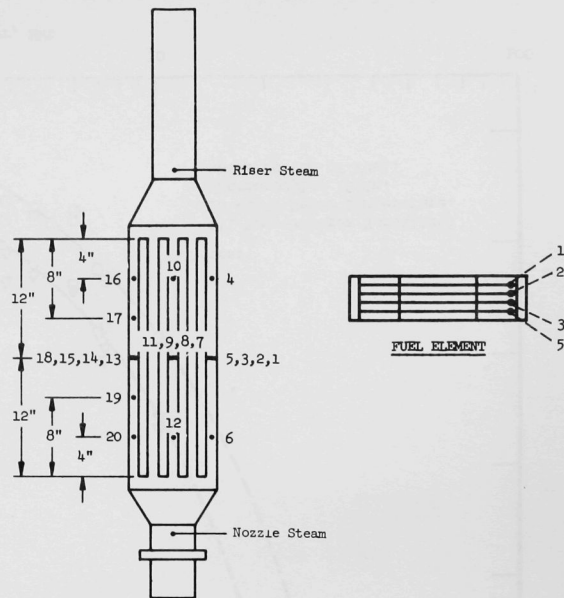
ID-103-A3359

Fig. 56. Indicated UO_2 Temperature vs Reactor Thermal Power, Boiling Fuel Rods Nos. VA-1 and VA-2, Core CSH-1B



106-7172

Fig. 57. Instrumented Superheater Fuel Element



ID-103-A3278

Fig. 58. Numbered Thermocouple Locations in Instrumented Superheater Fuel Assemblies

The selector switch was wired so that the first 20 temperatures corresponded with like-numbered points in Fig. 58, and the next 20 (21 through 40) were wired in sequence to points 1 through 20 on the second-pass fuel assembly, except for point 27 which measured exit steam temperature from the second pass.

Temperatures obtained during the 5 days in which power runs were made are summarized in Table IX. Many fuel plate thermocouples in the first pass showed no recognizable pattern of temperature changes with variations in reactor power, and in many cases read approximately saturation temperature. These inconsistent data points were deleted from the table. Second-pass temperature points 25, 27, and 29 were observed to give intermittent readings, but the values appeared generally consistent.

Table IX
SUPERHEATER FUEL AND STEAM TEMPERATURES, CORE CSH-1B

| Reading No. | Date (1963) | Time, hr | DM-1 ^a Flow, gpm | Power, MWt | First-pass Steam Temp, °F | | First-pass Fuel Temp, °F | | | | | | |
|-------------|-------------|----------|-----------------------------|------------|---------------------------|--------|--------------------------|-----|-----|-----|-----|-----|--|
| | | | | | Inlet | Outlet | 4 | 9 | 10 | 14 | 16 | 17 | |
| 1 | 10/10 | 2005 | 12 | 1.4 | 507 | 650 | 475 | 560 | 500 | 595 | 480 | 505 | |
| 2 | | 2010 | 12 | 1.4 | 511 | 632 | 475 | 560 | 510 | 585 | 485 | 515 | |
| 3 | | 2100 | 12 | 4.8 | 506 | 625 | 485 | 560 | 505 | 590 | 510 | 540 | |
| 4 | | 2130 | 12 | 3.7 | 512 | 600 | 495 | 550 | 505 | 585 | 505 | 540 | |
| 5 | | 2142 | 12 | 3.7 | 510 | 633 | 505 | 560 | 520 | 610 | 525 | 550 | |
| 6 | 10/11 | 1448 | - | 4.1 | 493 | 654 | 505 | 590 | 520 | 620 | 505 | 530 | |
| 7 | | 1540 | - | 5.8 | 489 | 647 | 500 | 570 | 505 | 595 | 500 | 525 | |
| 8 | | 1555 | - | 6.9 | 491 | 675 | 500 | 580 | 505 | 605 | 505 | 535 | |
| 9 | 10/14 | 1500 | 16.5 | 5.5 | 486 | 590 | 505 | 550 | 500 | 610 | 510 | 560 | |
| 10 | | 1550 | 6 | 5.8 | 495 | 628 | 480 | 515 | 480 | 595 | 490 | 480 | |
| 11 | 10/15 | 1300 | ~10 | 2.1 | 487 | 627 | 500 | 560 | 520 | 590 | 475 | 450 | |
| 12 | 10/16 | 1218 | 10 | 6.9 | 491 | 641 | 495 | 565 | 490 | 570 | 490 | 500 | |
| 13 | | 1315 | 10 | -5.2 | 491 | 639 | 500 | 570 | 495 | 575 | 500 | 510 | |
| 14 | | 1437 | 10 | -7.3 | 493 | 650 | 500 | 570 | 500 | 600 | 500 | 520 | |
| 15 | | 1515 | 10 | -7.3 | 493 | 637 | 500 | 570 | 495 | 580 | 500 | 525 | |
| 16 | | 1620 | 10 | 10.2 | 493 | 637 | 505 | 570 | 500 | 600 | 505 | 530 | |

| Reading No. | Date (1963) | Time, hr | DM-1 ^a Flow, gpm | Power, MWt | Second-pass Steam Temp, °F | | Second-pass Fuel Temp, °F | | | | | | | | | | | | | | |
|-------------|-------------|----------|-----------------------------|------------|----------------------------|------------------|---------------------------|-----|-----|------------------|-----|-----|-------------------|-----|-----|-----|-----|-----|-----|-----|-----|
| | | | | | Inlet | Outlet | 22 | 23 | 24 | 25 | 26 | 28 | 29 | 30 | 32 | 33 | 34 | 36 | 37 | 39 | 40 |
| 1 | 10/10 | 2005 | 12 | 1.4 | 663 | 785 | 650 | 660 | 770 | 850 | 650 | 905 | 820 | 700 | 700 | 770 | 720 | 700 | 750 | 670 | 725 |
| 2 | | 2010 | 12 | 1.4 | 650 | 780 | 645 | 660 | 710 | 780 | 650 | 800 | 735 | 670 | 745 | 680 | 655 | 650 | 690 | 640 | 650 |
| 3 | | 2100 | 12 | 4.8 | 648 | 760 | 660 | 665 | 745 | 800 | 655 | 750 | 725 | 715 | 690 | 710 | 680 | 690 | 740 | 660 | 650 |
| 4 | | 2130 | 12 | 3.7 | 692 | 760 | 655 | 670 | 745 | 770 | 655 | 750 | 730 | 770 | 680 | 695 | 680 | 695 | 725 | 655 | 650 |
| 5 | | 2142 | 12 | 3.7 | 650 | 770 | 660 | 670 | 770 | 750 | 670 | 750 | 740 | 790 | 685 | 700 | 680 | 725 | 730 | 675 | 655 |
| 6 | 10/11 | 1448 | - | 4.1 | 667 | 820 ^b | 665 | 690 | 780 | 770 | 695 | 810 | 780 | 760 | 660 | 750 | 700 | 720 | 745 | 675 | 680 |
| 7 | | 1540 | - | 5.8 | 607 | 780 | 670 | 685 | 775 | 750 | 690 | 780 | 760 | 745 | 650 | 740 | 700 | 735 | 760 | 675 | 680 |
| 8 | | 1555 | - | 6.9 | 600 | 790 | 665 | 700 | 795 | 770 | 700 | 790 | 765 | 750 | 655 | 745 | 705 | 750 | 780 | 675 | 675 |
| 9 | 10/14 | 1500 | 16.5 | 5.5 | 578 | 805 | 690 | 750 | 790 | 850 | 750 | 800 | 1140 ^b | 730 | 660 | 710 | 670 | 690 | 730 | 645 | 660 |
| 10 | | 1550 | 6 | 5.8 | 620 | 775 | 670 | 690 | 765 | 765 | 705 | 780 | - | 720 | 675 | 730 | 690 | 715 | 755 | 660 | 675 |
| 11 | 10/15 | 1300 | ~10 | 2.1 | 593 | 725 | 660 | 660 | 690 | 825 ^b | 675 | 730 | - | 675 | 620 | 640 | 630 | 640 | 660 | 610 | 615 |
| 12 | 10/16 | 1218 | 10 | 6.9 | 618 | 690 | 625 | 625 | 680 | - | 640 | 730 | 625 | 710 | 650 | 720 | 680 | 730 | 750 | 660 | 650 |
| 13 | | 1315 | 10 | -5.2 | 613 | 755 | 600 | 675 | 750 | - | 675 | 775 | 1000 | 725 | 650 | 710 | 675 | 720 | 740 | 660 | 650 |
| 14 | | 1437 | 10 | -7.3 | 607 | 775 | 675 | 680 | 775 | - | 675 | 780 | 725 | 740 | 650 | 715 | 675 | 730 | 755 | 660 | 630 |
| 15 | | 1515 | 10 | -7.3 | 618 | 770 | 670 | 675 | 760 | - | 670 | 780 | 900 | 730 | 655 | 715 | 675 | 730 | 770 | 660 | 635 |
| 16 | | 1620 | 10 | 10.2 | 608 | 770 | 670 | 680 | 790 | - | 675 | 790 | 800 | 750 | 655 | 730 | 680 | 760 | 780 | 670 | 640 |

^aDM-1: Reactor-water demineralizer.

^bThermocouple gave intermittent readings.

Calculation of fuel plate temperatures based on entrance and exit steam temperatures indicated that the measured values were about 100°F too low. Such errors might be attributed to thermal conduction out the edge of the fuel plate via the thermocouple, loss of fuel due to the thermocouple slot, and creation of a "cooling fin" on the plate due to the bulge (about 0.002 in. total plate thickness increase) caused by swaging the thermocouple slot. Reproducibility of individual fuel plate thermocouples was found to be about $\pm 10^\circ\text{F}$ at 489°F.

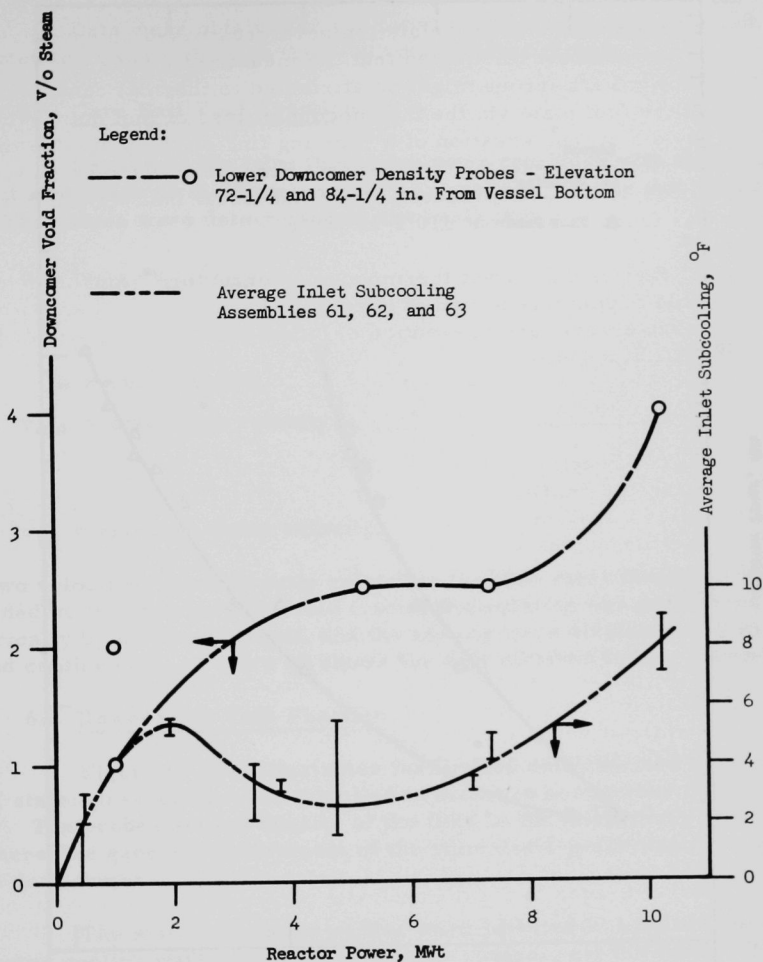
Errors due to wet thermocouple conductors might also have been possible during this period of core CSH-1 operation. A known instance of such errors, and prevention of future occurrences, are discussed in Section VII.B.3. below.

3. Reactor Water Subcooling

The reactor water subcooling temperature differentials were obtained using 1/8-in. OD, stainless-steel-sheathed, Chromel-Alumel thermocouples installed as a removable group in core positions 61, 62, and 63. Two thermocouples at each core inlet and exit location were monitored, and the reactor vessel steam dome thermocouple was also used. The coolant water-temperature thermocouples, installed as part of instrumented boiling fuel assembly I-1, did not give sufficient reproducibility to permit their use. The exit water-temperature thermocouples were not used either because of the difficulties of correcting for calibration changes. The seven subcooling thermocouples were all intercalibrated at zero reactor power conditions while at 600 psig, and the calibration errors determined were later applied to the data. Calibration errors as great as 10°F were found.

Subcooling data were derived by taking the average temperature differences between each inlet water thermocouple and the steam dome thermocouple at various reactor power levels. These values were then compiled and averaged to get the subcooling rate in the reactor core at the different power levels. The curve shown in Fig. 59 is based on these average values.

The unusual shape of the curve is attributed to the effect at low powers of the reactor-water-demineralizer return-water flow and feed-water injection through the control rod drive seals, the downcomer probe cooling system, and the circulating pump seal. These sources introduce relatively large quantities (20-30 gpm maximum) of cool water into the vessel. At higher powers, the relative mass flow rate of water injected becomes small compared to that of recirculated water in the downcomer.

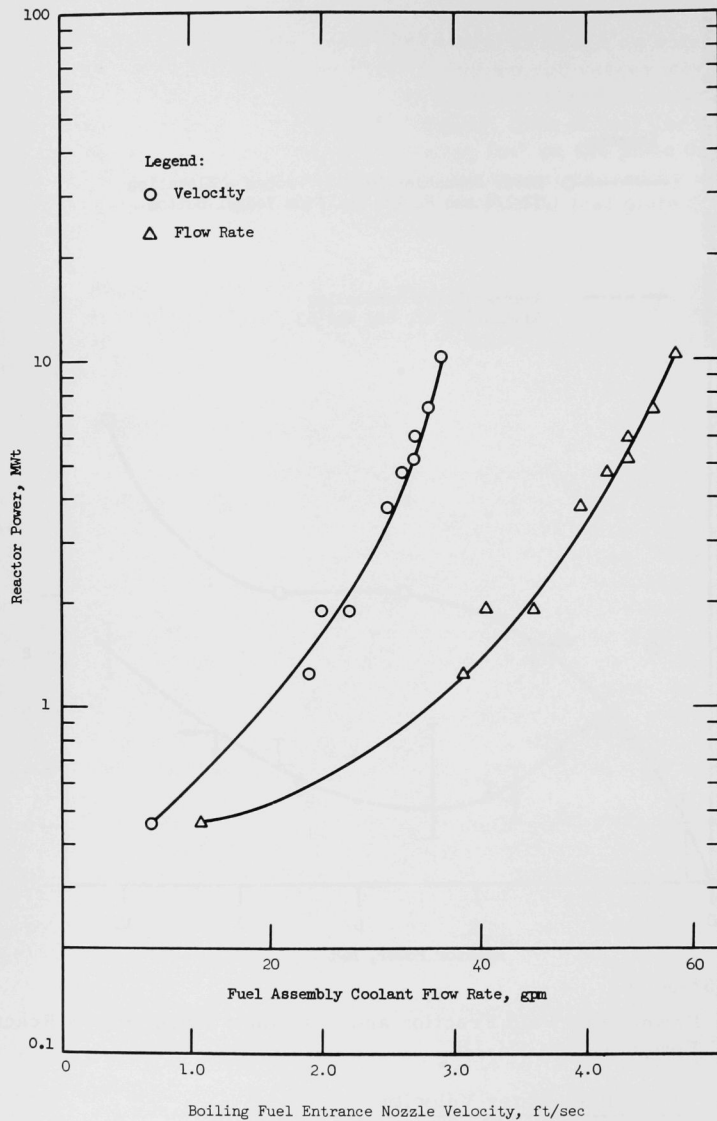


ID-103-A3360

Fig. 59. Downcomer Void Fraction and Core Inlet Subcooling vs Reactor Power, Core CSH-1B

4. Core Inlet Water Velocity

The inlet turbine-type flowmeter on instrumented boiling fuel assembly I-1 was utilized to obtain the data presented in Fig. 60. Note the indication of the trend toward constant inlet velocity as a function of power in the region of 10 MWt.



ID-103-A3361

Fig. 60. Inlet Velocity and Flow vs Reactor Power,
Instrumented Boiling Fuel Assembly I-1,
Core CSH-1B

Data were obtained in the form of volumetric flow rate and converted to velocity through the 3-in.-diam meter throat.

5. Core Exit Void Fraction

Data from the inlet flowmeter were combined with those from the exit flowmeter on the instrumented assembly to provide exit void fraction. The values were determined on the basis that

$$\alpha = (v_{\text{out}} - v_{\text{in}})/v_{\text{out}},$$

where

α = void fraction,

v_{out} = exit water velocity,

and

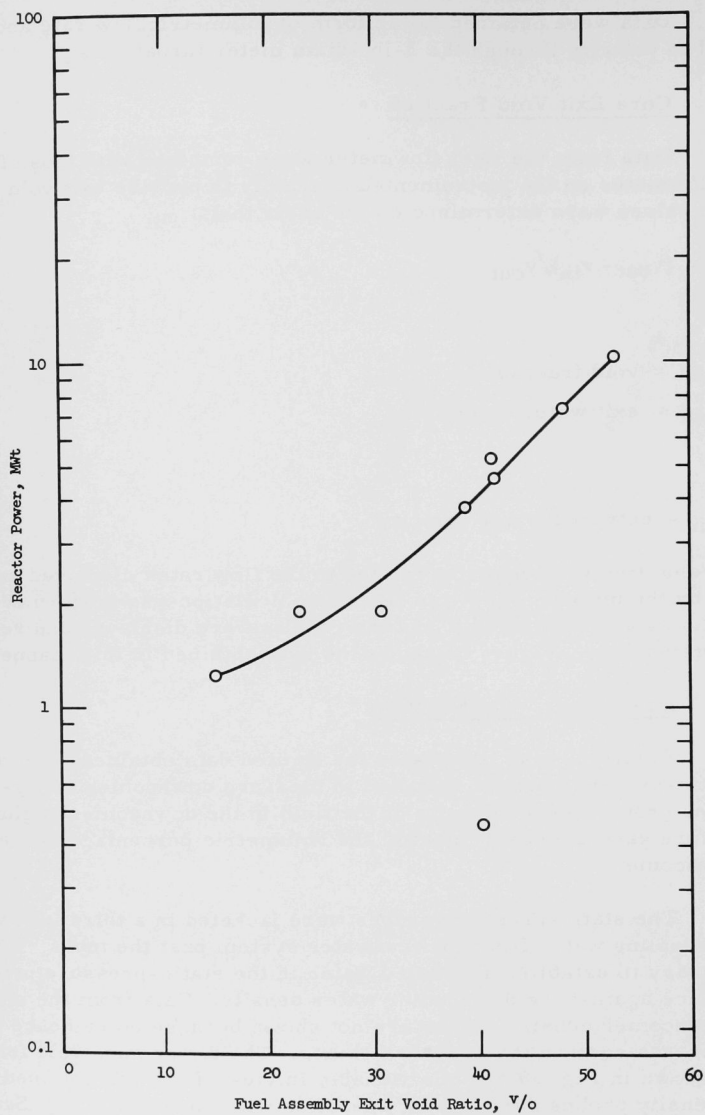
v_{in} = entrance water velocity.

The two velocities were directly related to the flow rates displayed and recorded by the meters. The void fraction calculation was performed electrically by a bridge circuit, and the results were displayed and recorded continuously. Figure 61 shows the data obtained in this manner.

6. Downcomer Void Fraction

Figure 59 also illustrates the limited data obtained from one set of static-pressure probes installed to measure downcomer carryunder. The probes sensed density of the fluid in the downcomer region and therefore gave a measurement of the volumetric percentage of steam in the downcomer.

The static-pressure probes were jacketed in a third tube which conducted cooling water from the feedwater system past the tubes. This was necessary to establish subcooled water in the static-pressure probes for reference against the downcomer water density. Data from the other pair of downcomer density probes are not shown because no evidence of carryunder was seen on the recorder charts. The downcomer void fraction data shown in Fig. 59 are questionable in view of results obtained with the density probes during later operation with core PSH-1.⁽¹⁾ Scatter in the data of $\pm 5\%$ of full scale was found to be common.



ID-103-A3362

Fig. 61. Exit Void Ratio vs Reactor Power, Instrumented Boiling Fuel Assembly I-1, Core CSH-1B

7. Calibration and Use of the Downcomer Stauscheibe Tube

A mock-up of the water-velocity-sensing Stauscheibe probe, duplicating the one installed in the reactor vessel downcomer, was calibrated in the BORAX airwater test loop. The probe was constructed of 7/8-in.-diam bar stock, 4 in. long, with two taps spaced 180° apart and centered on the probe length. All tests were made with 70°F water at atmospheric pressure.

Several traverses were made to determine the water-velocity profile in the loop test section. When mounted 3/4 in. from the wall to the centerline of the probe (simulating the reactor installation), the flow calibration coefficient was found to be 2.69, based on average stream velocity. At the point of average stream velocity, the coefficient was 1.88. The coefficient is defined as

$$h = Cv^2/2g,$$

where

C = calibration coefficient;

h = measured differential pressure, ft of flowing fluid;

v = velocity, ft/sec;

and

g = local acceleration due to gravity, ft/sec².

Data obtained from the probe during reactor operation were found to exhibit variations of about the same magnitude as the anticipated velocity signal. During the short period of reactor operation with core CSH-1B, no meaningful data were provided by the probe.

8. Measurement of Reactor-water Level

The true water level (or, actually, the steam-boiling water mixture interface level) in a boiling-water reactor is difficult to measure accurately with conventional out-of-reactor-vessel techniques. Most such devices rely on measurement of the differential pressure produced by the column of fluid in the vessel. Since the differential pressure is related to fluid density, a vessel containing saturated water will indicate an entirely different level from one filled to the same level with a steam-water mixture.

During operation with the B-2 core, a movable steam sampling probe was used to detect the steam-boiling-water interface elevation at various core powers.⁽⁴⁾ The level-measurement errors determined through use of the probe can be of the order to 26 in. at 15 MWt if the differential-pressure devices are not properly compensated. The sampling probe was accordingly used again with core CSH-1B to set reactor water-level scram trip points to insure against accidental flooding of the superheater.

An acoustic water-level probe was also used to determine the steam-boiling-water interface elevation during operation of the central superheater core. Both the acoustic device and the steam sampling probe were installed to measure the level of points at a radius of 16 in. from the vertical axis of the vessel. Agreement of $\pm 1/2$ in. was found between the acoustic and steam sampling probes. Table X illustrates the data obtained from the acoustic probe and the normal water-level measuring instruments.

Table X
REACTOR WATER-LEVEL MEASUREMENTS,
CORE CSH-1B

| Reactor Power, MWt | Water Level (LR-1 ^a) | Elevation of Interface between Steam and Water-steam Mixture (Acoustic Probe) | Water ^b Level (Acoustic Probe) |
|-----------------------|-------------------------------------|--|--|
| 5.2 | 12 ft, 10 in. | 13 ft, 0 in. | 12 ft, 6 in. |
| 7.32 | 12 ft, 8 in. | 12 ft, 11 $\frac{1}{2}$ in. | 12 ft, $\frac{1}{2}$ in. |
| 10.2 | 12 ft, 9 in. | above 13 ft, 2 in. ^c | above 13 ft, 2 in. ^c |

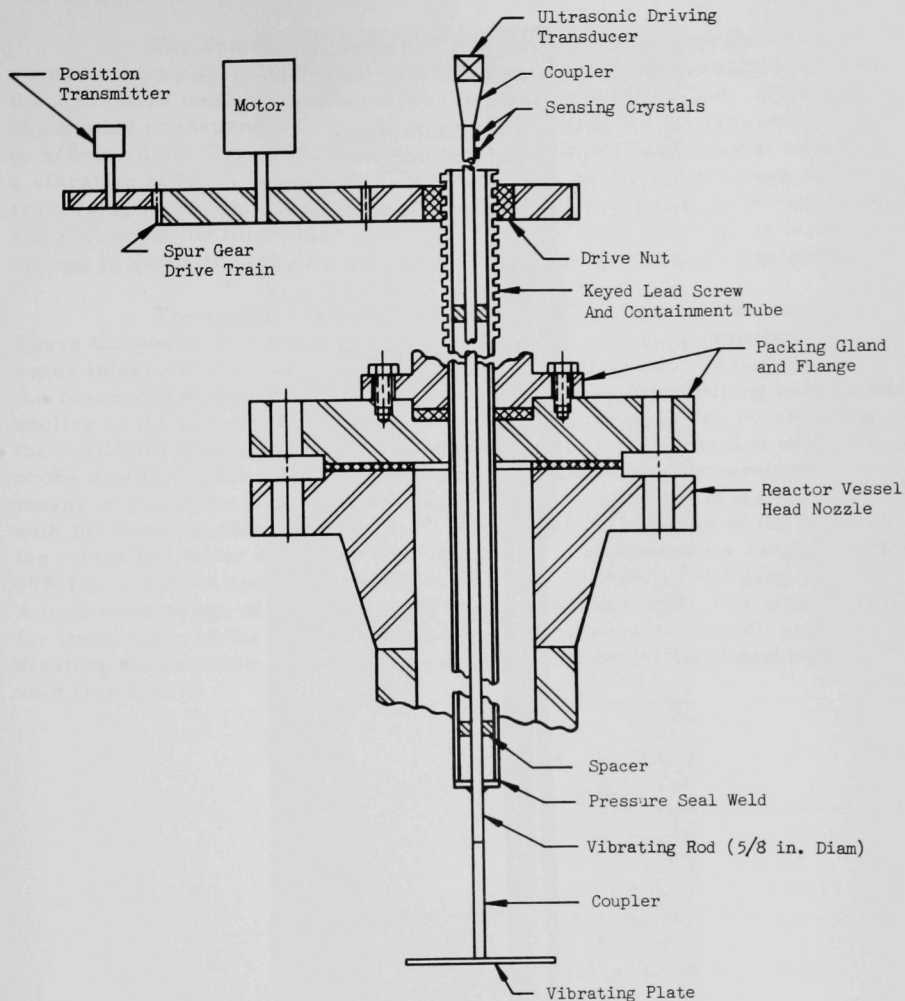
^aOperating instrument. Saturation pressure-compensated, differential-pressure sensor, and circular chart recorder.

^bElevation at which water-steam mixture density approached that of saturated water, as evidenced by constant readings on acoustic probe indicator.

^cUpper limit of probe travel.

B. Acoustic Water-level Probe

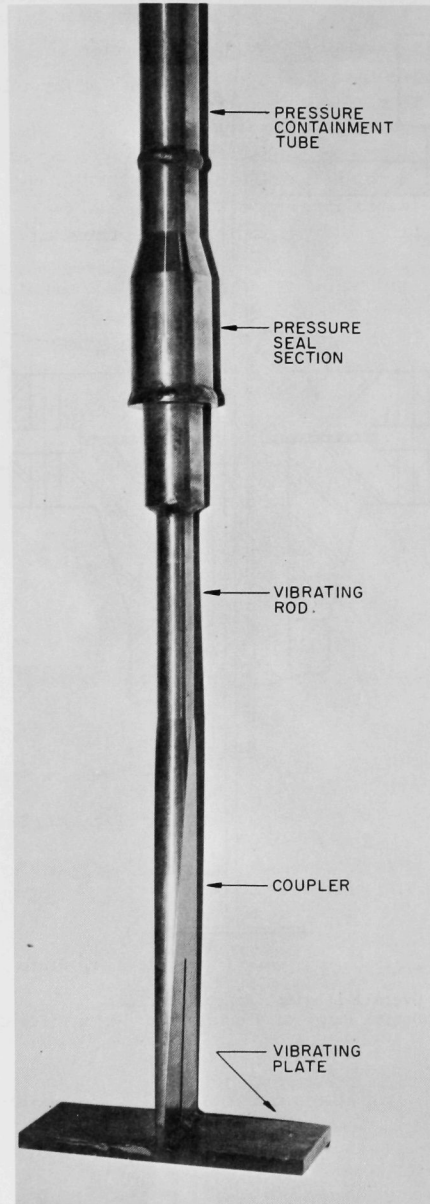
The acoustic water-level probe was designed and developed by Aeroprojects Company of West Chester, Pennsylvania, and adapted to a mechanical drive and pressure seal provided by BORAX personnel. The unit is shown schematically in Fig. 62, and a photograph of the lower end is shown in Fig. 63.



Overall Length: Approx. 15 feet
 Useful Range of Measurement: 28 in. (For Core CSH-1B)

ID-103-A3363

Fig. 62. Schematic Diagram of Acoustic Water-level Probe



ID-103-A3105

Fig. 63. Details of Acoustic
Water-level Probe

The device was basically an acoustic impedance meter which sensed the boundary conditions at the end of an acoustic transmission line through phase measurements on the standing wave in the line. Operation at elevated pressures was accomplished by sealing the transmission line (a 5/8-in.-diam Type 304 stainless-steel rod) into a containment tube at a vibration node. The tube was then moved by the lead screw-and-nut traversing mechanism through a pressure seal on the reactor vessel head, and the steam-boiling-water interface was detected by noting the large change in acoustic coupling indicated by a panel meter on the equipment.

The equipment was first tested in a 600-psi, 489°F autoclave where the position of the probe and the conditions of the steam-boiling-water interface could be observed through sight glasses. Variations in the resonant frequency of the probe assembly were noted during heating and cooling of the autoclave, but this factor was compensated for by adjusting the oscillator frequency to give minimum acoustic transmission when the probe was fully withdrawn from the water. Water-level determination by means of the probe was as accurate as visual observation of its contact with the water surface would allow - about 1/16 in. Change of the indicating meter for water or steam immersion of the sensing plate ranged from 50% full scale, at room temperature, to 58% full scale at 600 psig, 489°F. A maximum range of 34% full-scale change in meter indication was noted for immersion of the probe in nonboiling or boiling water at 600 psig, indicating the possible use of this technique to determine fluid density or void fraction.

VI. WATER CHEMISTRY MEASUREMENTS AND CATALYTIC RECOMBINATION EXPERIMENT

A. Water Chemistry Measurements

The measurements obtained in routine monitoring of chemical parameters during the brief period of power operation of core CSH-1B are summarized in Table XI. The differences in resistivity and pH between reactor water and saturated steam are believed to be due to CO_2 which strips out into the steam. The differences in these parameters between saturated steam and superheated steam are also believed to be due to CO_2 . It is postulated that the CO_2 is reduced to CO on the superheater plates. The CO does not give a conductive solution in samples of condensed steam; hence, an apparent difference in steam purity is indicated. A check on steam radioactivity at the entrance and exit to the superheater showed no differences before the detection of the first fission products.

Table XI
WATER CHEMISTRY MEASUREMENTS,
CORE CSH-1B

| | Reactor Water | Saturated Steam | Superheater Steam |
|---------------------------|---------------|-----------------|-----------------------------|
| Resistivity, megohm-cm | 2.0-2.8 | 0.9-1.2 | 1.1-1.6 |
| pH | 6.5-7.0 | 5.2-5.6 | 5.9-6.2 |
| Cl^- , ppm | 0.02-0.04 | <0.04 | - |
| Suspended solids, av, ppm | 0.13 | - | - |
| O_2 , ppm | 0.1-0.3 | 23-30 | 8 initially, 21-41 later |

The differences in oxygen concentration between reactor water and saturated steam were as expected, due to the stripping action of the steam.

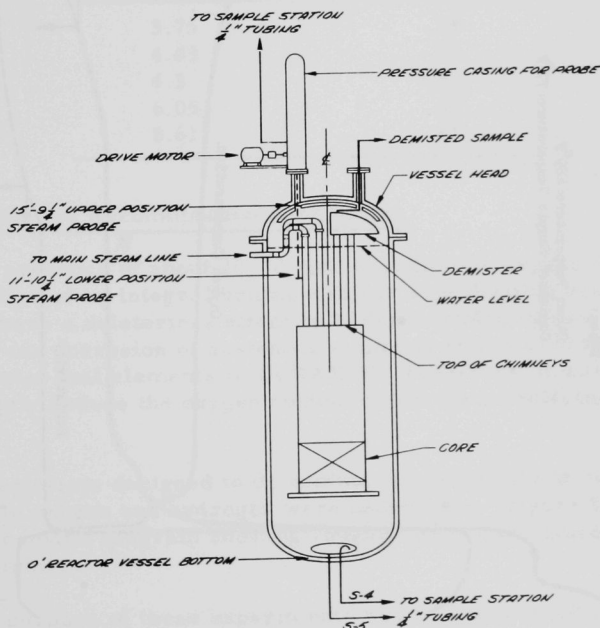
The change in oxygen concentration with time in the superheated steam is believed to be due to one or both of two possible processes: (1) The radiolytic gases were recombining on the fresh superheater cladding surfaces; or (2) the oxygen was being removed by a corrosion mechanism.

The chloride and suspended solids concentrations were as expected from previous operation with core B-2 and presented no problems.⁽⁴⁾

B. Steam Dome Tests

A test with core CSH-1B demonstrated a method of determining how the gas in a steam dome changes in concentration with axial position from below the boiling water-steam interface to the top of the steam dome.

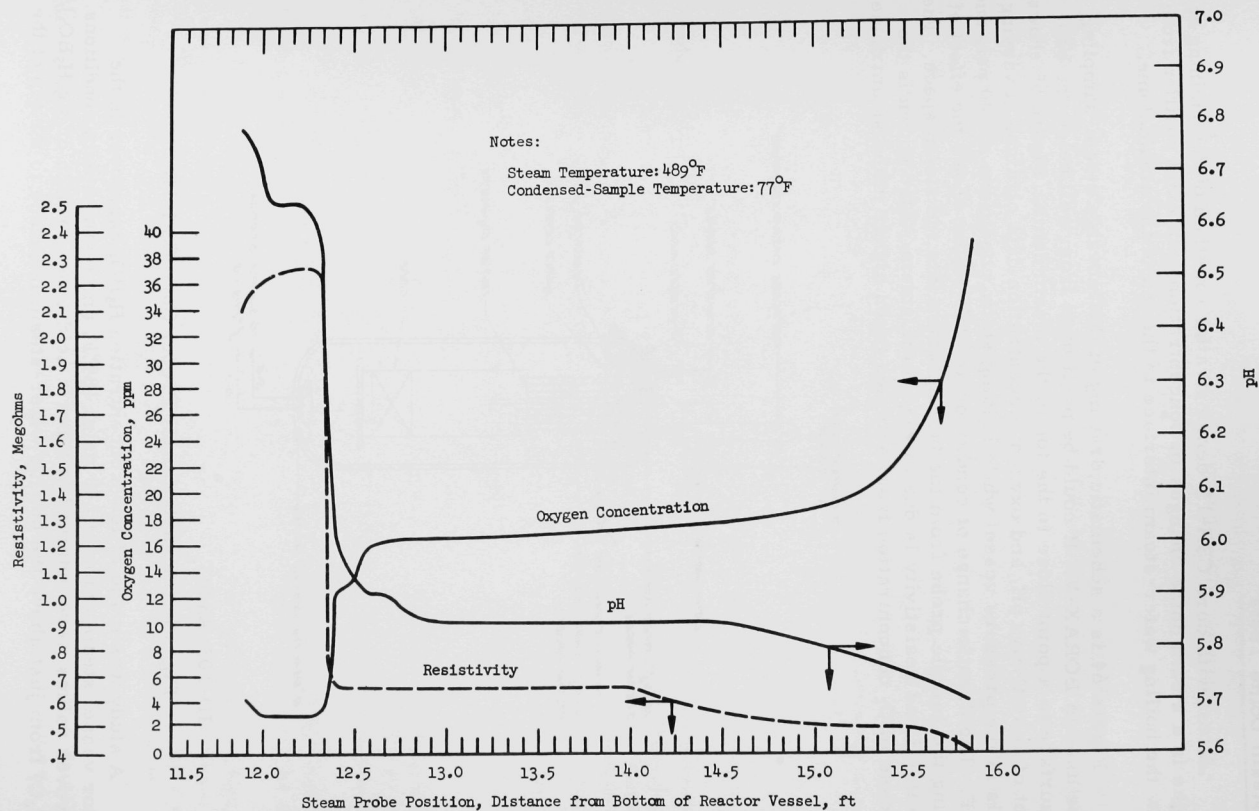
Figure 64 is a schematic drawing of the movable steam-sampling probe used in BORAX-V. It could be positioned from well below the boiling surface to a point close to the top of the steam dome. Figure 65 shows a plot of resistivity, pH, and oxygen concentration data obtained at varying levels in the pressure vessel while holding static conditions at 600 psig and 489°F. The drastic change of conditions at 12 ft-4½ in. shows the effect of moving the sample probe from the boiling water into the steam space. The drop in pH and resistivity is due to CO₂ in the steam. Also shown is the increase in O₂ concentration from samples taken higher in the steam dome.



ID-103-A3283

Fig. 64. Movable Steam Probe, Core CSH-1B

A study was made of low-concentration H₃BO₃ carryover in the reactor vessel steam dome at 600 psig, 489°F, and static-steam conditions. Carryover values were obtained at a boric acid concentration of 8 g(H₃BO₃)/gal(H₂O) from just above the boiling water-steam interface to the top of the



ID-103-A3364

Fig. 65. Measurements on Condensed Static Steam from Steam Dome, Core CSH-1B

steam dome, using the movable steam probe. This concentration in the reactor water resulted in a concentration of 78-80 ppm at all positions of the steam probe from the interface to the top of the steam dome.

The concentrations obtained from samples of condensed steam taken from the top of the steam dome and correlated with boric acid concentrations in reactor water are shown in Table XII.

Table XII
BORIC ACID CONCENTRATION IN
STEAM DOME, CORE CSH-1B

| Reactor Water, $\text{g}(\text{H}_3\text{BO}_3)/\text{gal}(\text{H}_2\text{O})$ | Steam Dome, ppm of H_3BO_3 |
|--|---|
| 3.75 | 28 |
| 4.03 | 31 |
| 4.3 | 35 |
| 6.05 | 53 |
| 8.61 | 85 |

C. Radiolytic Gas Recombination Experiment

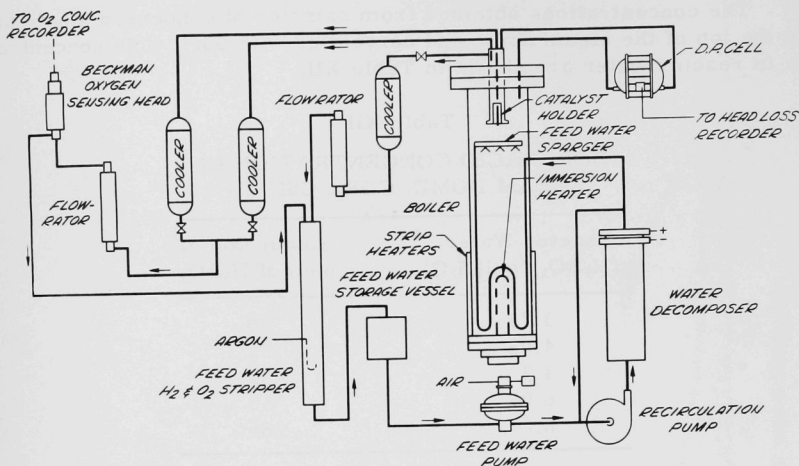
The presence of about 20-30 ppm of radiolytic oxygen in the steam from the boiler of an integral boiling-nuclear superheating reactor was believed to have a deleterious effect on both the oxidation rate and the chloride stress corrosion of austenitic stainless steels used for cladding the superheater fuel elements in BORAX-V. Therefore, it was desirable to significantly reduce the oxygen content of the steam entering the superheater.

Experiments designed to determine the feasibility of recombining the radiolytic oxygen and hydrogen were undertaken. Figure 66 is an abridged schematic diagram showing roughly the major components of the test equipment.

The purpose of these experiments was to find a catalyst suitable for use in the internal steam dryer of BORAX-V which would cause recombination of the hydrogen and oxygen present in the saturated steam. Criteria established for suitability of the catalyst were that it would

1. Allow full flow of steam at 10,000 lb/hr/ft², with a pressure drop of 1 psig or less through a 4-in. bed depth.

2. Recombine a large percentage of the radiolytic gases.
3. Retain physical integrity and catalytic activity for at least one year.



ID-103-A3285

Fig. 66. Abridged Schematic Diagram, Radiolytic Gas Recombination Test Apparatus

The catalysts were tested under the following conditions:

| | |
|-------------------------|----------------------------|
| Temperature: | 489°F |
| Pressure: | 600 psig |
| Oxygen concentration: | 20-30 ppm |
| Hydrogen concentration: | Stoichiometric |
| Steam flow rate: | 9000 lb/hr/ft ² |
| Bed depth: | 4 in. |

Six catalysts were tested, as follows:

1. Low-surface-area copper mesh.
2. Platinized, low-surface-area copper mesh.
3. Palladium oxide on activated alumina pellets (Girdler T-308*).
4. 0.7% palladium on low-surface-area alumina pellets (Girdler T-661*).

*Girdler Catalyst Dept., Chemetron Corp., Louisville, Ky.

5. Platinum oxide on activated alumina pellets (Girdler T-309*).
6. 0.5% palladium on activated alumina pellets (Girdler T-961*).

The first five catalysts tested gave no detectable recombination. Girdler T-961, however, gave 22-27% recombination. This catalyst was tested for 30 hr and showed no sign of changing efficiency. The pressure drop across the 4-in. bed of T-961 was about 16 in. of 70°F water.

After 7 hr of testing, a sample of T-961 was removed and analyzed spectrographically. The analyses showed that the catalyst had taken up some traces of copper and zinc from the brass catalyst holder. Of further importance was the evidence that the γ - Al_2O_3 (gamma alumina) had hydrated to form α - $\text{Al}_2\text{O}(\text{OH})_2$, or Boehmite. The new samples of unused catalyst contained no crystalline palladium; however, after the 7-hr test, the amorphous palladium had apparently changed to a crystalline form.

Planned testing of other catalysts was not performed because of early project termination.

VII. PLANT PERFORMANCE

A. General

In preparation for central superheat operation, the boiling core fuel, the control rods, and the boiling core structure were removed from the reactor vessel. The central superheater core structure was then installed, and the superheater flood-and-drain piping was welded into position, hydro-tested, and test-operated. Control rods were then reinstalled and their operation tested. Reloading of the boiling fuel proceeded as described in Section III.A.1. and 2.

During the first tests of central superheater fuel assemblies for leak-tightness, an excessive leakage rate was found. On six fuel assemblies, the static-steam insulating tubes were found to be leaking moderator water into the steam space at the point where they were welded to the flow vanes. These leaks were repair-welded and the assemblies made sufficiently leak-tight to proceed with the remainder of the zero-power experiments. At the completion of the zero-power experiments at operating temperature, all superheater fuel assemblies were removed from the reactor vessel for further repair work. The repair work and experience with the superheater fuel assemblies are discussed in detail in Section VIII.

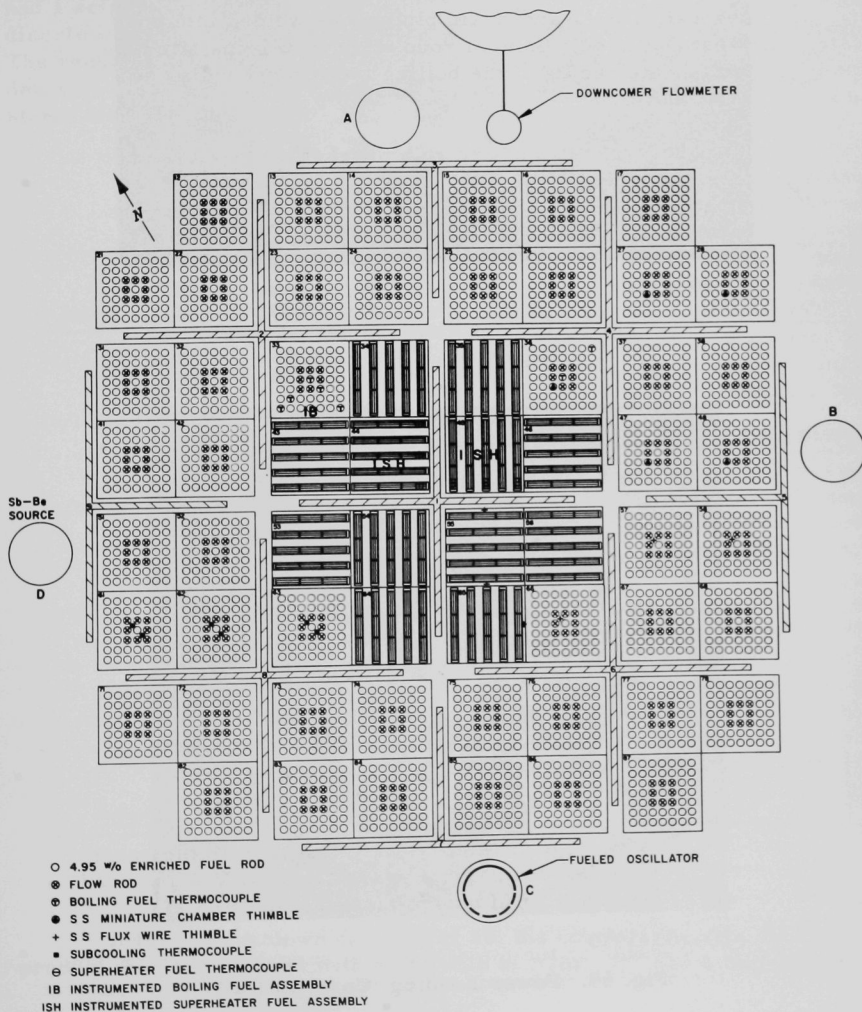
After the superheater fuel was reloaded, a test of leakage rate showed the system to be satisfactory. The reactor was then brought to operating temperature, using electric preheaters. Flooding, draining, and venting were tested to assure that these systems were in proper operating order before power operation.

The following items were installed in the reactor in preparation for power operation: one instrumented boiling fuel assembly; two instrumented superheater fuel assemblies; two individual boiling fuel thermocouple rods; six stainless-steel flux-wire thimbles in boiler coolant channels; five, 3/8-in.-OD, miniature, ion chamber thimbles in place of flow rods; 12 sub-cooling thermocouples, six below the core and six above; and a fueled oscillator rod. The location of these items is shown in Fig. 67, the loading diagram for core CSH-1B.

An internal steam separator was also installed in the reactor at this time. Steam from the steam dome passed through a 4-in.-thick Inconel Yorkmesh Demister* pad before entering the inlet superheater assemblies. The steam separator, a bottom view of which is shown in Fig. 68, fitted closely over the top of the inlet superheater risers and was supported by them and by four pads which rested on the hold-down grid.

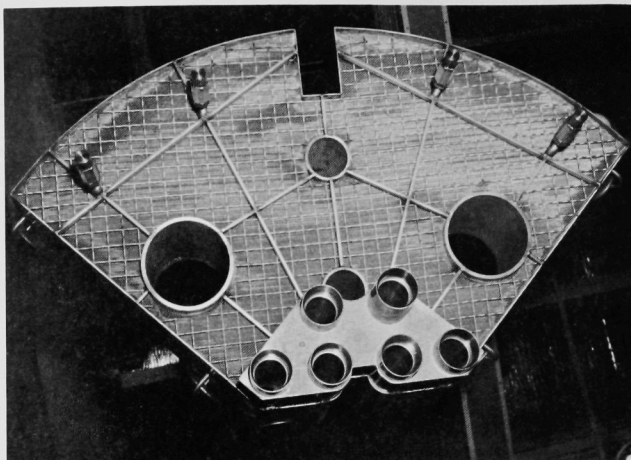
*Otto H. York, Inc., trade name.

The demister pad was held between wire screens. Holes lined with sleeves were provided through the demister so that access to the core was permitted from the nozzles in the reactor vessel head. Because of the brief period of power operation, no measurement was made to determine the effectiveness of this steam separator. A photograph of the top of the reactor, with central superheater core CSH-1B loaded for power operation, is shown in Fig. 69.



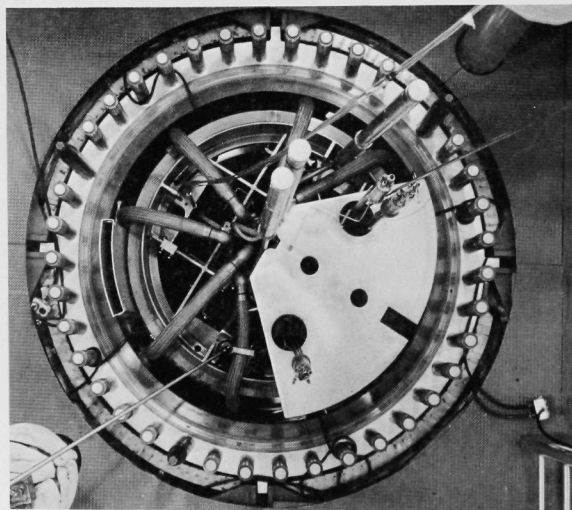
ID-103-A3365

Fig. 67. Loading Diagram, Core CSH-1B



ID-103-3913

Fig. 68. Bottom View of Internal Steam Separator, Core CSH-1



ID-103-3910

Fig. 69. Power Loading, Core CSH-1B

On October 10, 1963, power operation began and was terminated on October 16 because leakage of moderator water into the superheater steam passages was found to be excessive (50 gal/hr) and a low level of fission products was detected in the superheated steam.

The presence of fission products was first noted on the fission product monitor sampling superheated steam. This instrument, which had a scintillation detector monitoring a small ion-exchange column, was discriminated for the energy of gamma rays produced by iodine isotopes. The readings from this monitor are summarized in Table XIII. No evidence of fission products was found in the monitor sampling saturated steam from the boiler.

Table XIII
DATA FROM SUPERHEATED-STEAM FISSION-PRODUCT MONITOR,
CORE CSH-1B

| Date | Time, hr | Power Level, MWt | Monitor Reading, counts/min | Date | Time, hr | Power Level, MWt | Monitor Reading, counts/min |
|---------------------------------|-------------|------------------------|-----------------------------------|------------------------------------|-------------|------------------------|-----------------------------------|
| 10/10/63 | 1415 | 0.0 | 30 | 10/15/63 | 1446 | 0.8 | 400 |
| | 2030 | 3.0 | 30 | | 1450 | 0.8 | 1000 ^b |
| | | | | | 1456 | 0.8 | 1700 |
| 10/11/63 | 1400 | 4.0 | 70 | Monitor-ion-exchange Resin Changed | | | |
| | 1500 | 4.0 | 380 | | | | |
| | 1545 | 4.0 | 450 | | | | |
| 10/14/63 | 1500 | 5.6 | 50 | 10/15/63 | 1530 | 0.0 | 1200 |
| | 1700 | 0.0 | 148 | | 1540 | 0.0 | 1000 |
| | 1800 | 0.0 | 100 | | 1600 | 0.0 | 220 |
| | 2300 | 0.0 | 63 | | 2348 | 0.0 | 60 |
| 10/15/63 | 0900 | 0.8 | 200 | 10/16/63 | 1050 | 0.8 | 350 |
| | 1000 | 0.8 | 125 | | 1131 | 0.8 | 300 |
| | 1010 | 0.8 | 560 | | 1300 | 1.8 | 550 |
| | 1100 | 0.8 | 70 | | 1330 | 5.2 | 600 |
| | 1200 | 2.5 | 425 | | 1415 | 5.2 | 660 |
| | 1300 | 2.5 | 600 | | 1420 | 7.3 | 900 |
| | 1330 | 2.5 | 750 | | 1508 | 7.3 | 1000 |
| | 1352 | 0.0 | 450 ^a | | 1557 | 7.3 | 1700 |
| Superheater Flooded and Drained | | | | | 1600 | 10.3 | 1700 |
| | | | | | 1620 | 10.3 | 1700 |
| | | | | | 1630 | 0.0 | 1600 |

^aFalse scram.

^bAlarm.

After the shutdown on October 16, the count rate on the fission product monitor decayed with a half-life of ~7hr. I^{135} has a half-life of

6.7 hr. An iodine chemical separation was made on a sample of the resin from the monitor, and a gamma-ray spectrometer analysis indicated the presence of I^{131} .

A maximum power of 10.3 MWt was reached at a nine-control-rod-bank position of 19.67 in. as compared with the full-travel position of 25 in. During the 7 days of power operation, the integrated power, during five heat-ups with the superheater flooded, was 7.3 MW-hr, and was 47.75 MW-hr with steam flowing through the superheater. Various parameters and power levels measured during the brief operating time, totaling 15 hr, are summarized in Table XIV.

Table XIV
POWER OPERATION, CORE CSH-1B

| | Power, MWt | | |
|---|------------|------|------|
| | 5.2 | 7.3 | 10.3 |
| Saturated steam temperature, °F | 487 | 487 | 485 |
| First-pass superheater fuel assembly, exit steam temperature, °F | 632 | 635 | 640 |
| Second-pass superheater fuel assembly, exit steam temperature, °F | 755 | 760 | 760 |
| Steam line temperature, 62 ft from reactor, °F | 640 | 660 | 725 |
| Maximum second-pass fuel temperature, °F | 785 | 790 | 820 |
| Steam line radioactivity, 42 ft from reactor, mR/hr | 50 | 50 | 75 |
| Power produced in superheater, % of total in core | 14.8 | 15.0 | 15.2 |

As can be seen from Table XIV, the percent of power produced in the superheater, relative to the total core power, increased slightly with increasing power. Because of early termination of power operation, the planned experiments on the changes produced in the superheater-boiler power division by control rod manipulations were not performed. However, one test was made at lower power. To raise the outlet steam temperature, the central control rod was raised to the full-out position, with the remainder of the control rods banked at 16.7 in. Of the resulting total power of 3.5 MWt, 15.2% was produced in the superheater.

The reactor and superheater startup and shutdown procedures functioned as designed and were satisfactory. The superheater steam-coolant channels were drained and flooded ten times with the reactor at about 600 psig. Draining was accomplished on startup by closing the superheater flood valves that interconnected the reactor vessel water with the superheater steam-coolant region, and then opening the drain valve, which caused

the water to be driven by the reactor vessel pressure through the superheater drain line to the main condenser. By venting steam through the superheater vent valve during the time required to regain operating pressure after draining, the superheater fuel temperatures were maintained below a maximum of 1050°F. With the steam system at operating temperature and the reactor at 600 psig, main steam flow was then started and the superheater vent valve was closed. During shutdown, the reactor power was reduced by lowering control rods, and as power level was reduced, steam flow was reduced by automatic closing of the back-pressure control valve. Superheater fuel temperatures decreased with the reactor power level, and very little steam venting was required to maintain them below 1050°F. The superheater flood valve could be opened immediately after the control rods were fully inserted.

Finally, the superheater fuel, boiling fuel, and central superheater core structure were unloaded in preparation for installation of the core with peripheral superheater.

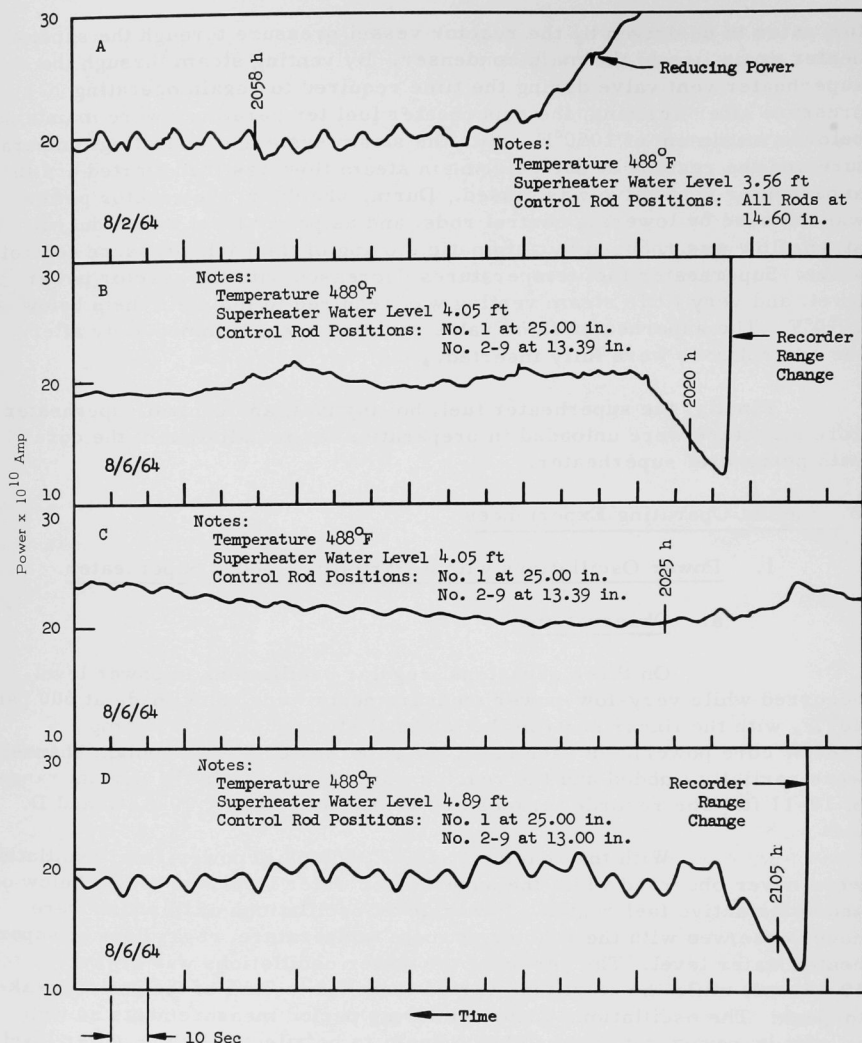
B. Special Operating Experiences

1. Power Oscillations with a Partially Flooded Superheater

a. Observations

On three occasions, regular oscillations in power level occurred while very-low-power measurements were being made at 600 psig, 489°F, with the linear neutron flux channel at about 0.2×10^{-8} Amp (~ 80 W core power). In each case, the superheater steam-coolant channels were partially flooded and the reactor water level was in the normal range of 10-11 ft. The recorded traces are reproduced in Fig. 70 A, C, and D.

With the reactor at 489°F, 600 psig, power-level oscillations were never observed while the superheater water level was either below or above the active fuel region. Power-level oscillations of this kind were never observed with the reactor at room temperature, regardless of superheater water level. The period of the power oscillations was always 10 ± 1 sec, while the amplitude varied from 3.8 to 7.5% of the power, peak-to-peak. The oscillations occurred during period measurements as well as steady-power runs and did not seem to be affected by the power level in the range of 0.2×10^{-9} to 0.8×10^{-7} Amp (8 to 3200 W) on the linear neutron flux channel. The superheater water-level indicator and temporary recorder never showed any oscillations in the superheater water level. However, the sensitivity and response of the superheater water-level-indicating system was inadequate for the magnitude and frequency of the apparent water-level oscillations observed. Thus, the linear neutron flux channel gave the only clear indication of the oscillatory disturbance, but the relatively insensitive log flux recorder also indicated some disturbances during the oscillations.



ID-103-A3366

Fig. 70. Oscillations with Partially Flooded Superheater, Core CSH-1B

b. Analysis

A study and analysis were made in an attempt to determine the cause of the power oscillations. Although the cause has not been proved,

it is suspected to be cyclic variations in the superheater water level, i.e., the two superheater flow passes oscillating together as a unit, or separately and 180° out of phase. As may be seen in Fig. 7, two separate "U"-tubes are present in the reactor system: (1) The superheater, lower superheated steam main to the subreactor room, and connecting flood-and-drain piping from two sides of a U-tube, assuming both passes of the superheater are lumped into one region and oscillate in phase; and (2) the first and second passes of the superheater form two sides of a U-tube, connected through the interpass plenum. If the latter U-tube oscillates, the assumption was made that the six assemblies in each pass oscillate as a whole, the passes being 180° out of phase.

For this analysis, these two modes of oscillation were assumed. It was further assumed that the shapes of the curves of superheater flooding reactivity worth vs superheater water level at 600 psig, 489°F, were similar to the curves in Figs. 22 and 23 at room temperature. A curve of differential flooding reactivity worth vs superheater water level was then derived. (This curve is not shown.)

Since the reactor was at very low power, power feedback was not responsible for the oscillatory behavior. Thus, the cause must have been an "external" mechanism driving a bare reactor, i.e., no feedback. The linearized zero-power reactor kinetics can be written as follows:

$$\frac{\Delta n}{n_0 \Delta k}(s) = G_0(s) = \frac{1}{\ell^* s \left[1 + \sum_{i=1}^6 \frac{\bar{\beta}_i}{\ell^* (s + \lambda_i)} \right]}, \quad (5)$$

where

$\Delta n/n_0$ = peak-to-peak power oscillation, % of power;

Δk = reactivity amplitude, β ;

$G_0(s)$ = zero-power transfer function;

ℓ^* = effective prompt neutron generation time;

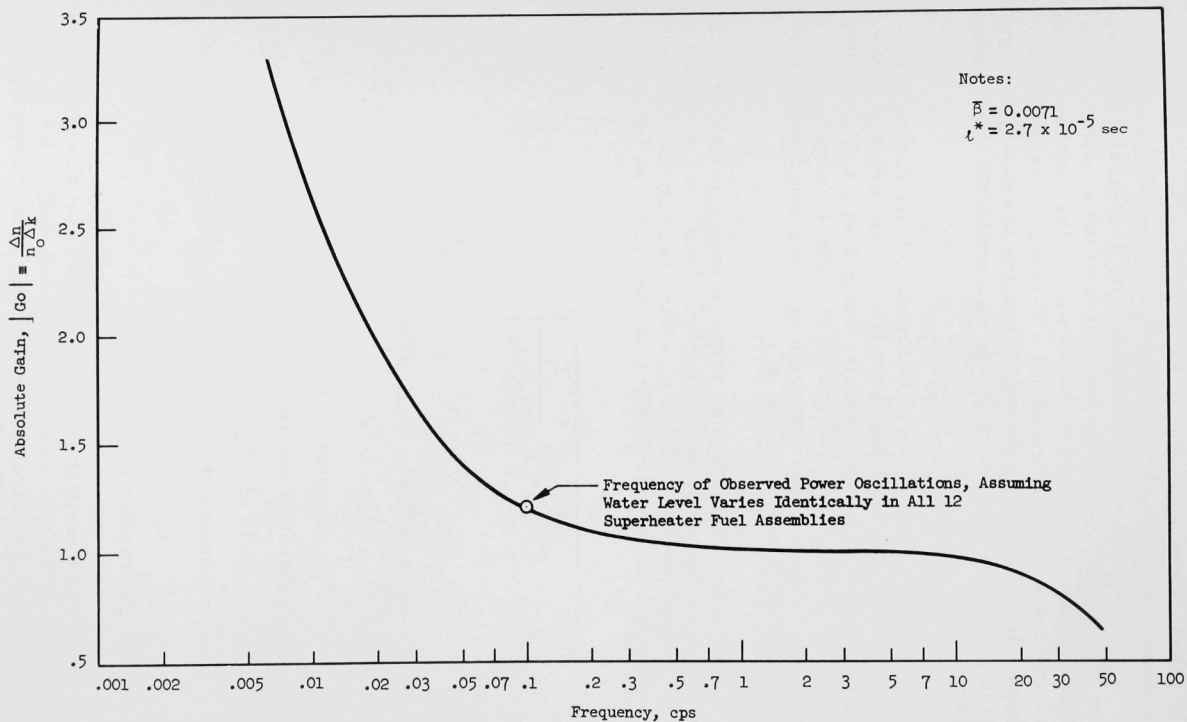
$\bar{\beta}_i$ = effective yield of i^{th} group of delayed neutrons;

λ_i = decay constant of i^{th} group of delayed-neutron emitters;

and

s = Laplace transform parameter.

Thus, only the frequency of oscillation must be known in order to determine the required reactivity amplitude, since $G_0(s)$ is a known function of frequency. Figure 71 is a plot of the calculated zero-power transfer function $|G_0(s)|$ vs frequency for a generalized BORAX-V boiling core.



ID-103-A3367

Fig. 71. Calculated Gain of Zero-power Transfer Function

Combining the information from the curve of differential flooding-reactivity worth, and noting that the observed frequency was always about 0.1 cps, resulted in the following relationship:

$$\frac{\rho_0 \Delta Z}{\Delta n/n_0} = F(Z), \quad (6)$$

where

$Z \equiv$ superheater water level, ft;

$\Delta Z \equiv$ change in superheater water level, ft;

and

$\rho_0 \equiv$ total superheater flooding reactivity worth, %.

If the above function is plotted against superheater water level, then the change in superheater water level required for a given power amplitude can be determined. (This plot is not shown.) The results of this analysis for the three observed cases in which power oscillations occurred are summarized in Table XV.

Table XV
OSCILLATIONS WITH PARTIALLY FLOODED SUPERHEATER,
CORE CSH-1A

| Date | Time, hr | Fig. Ref. | Superheater Flooding Reactivity Worth, % | Control Rod Positions, in. | Super- heater Water Level, ft | Peak-to-peak Oscillation, % of Power | ΔZ^a , in. | $\Delta Z'^b$, in. |
|--------|-------------|--------------|--|-------------------------------------|---|--|-----------------------|------------------------|
| 8/2/63 | 2058 | 70 A | 1.18 | All rods at 14.60 | 3.56 | 7.5 | 0.51 | 6.0 |
| 8/6/63 | 2025 | 70 C | 1.4 | No. 1 at 25.00 Nos. 2-9 at 13.39 | 4.06 | 3.8 | 0.30 | 2.2 |
| 8/6/63 | 2105 | 70 D | 1.4 | No. 1 at 25.00 Nos. 2-9 at 13.00 | 4.89 | 7.0 | 1.64 | 6.2 |

^a ΔZ = Peak-to-peak oscillation of superheater water level required for power-level oscillation observed, assuming that the level varies identically in all 12 assemblies.

^b $\Delta Z'$ = Peak-to-peak oscillation of superheater water level required for power-level oscillation observed, assuming that the level in each pass oscillates 180° out of phase.

Because of the large differential reactivity worth of flooding the CSH-1 superheater core, only small changes in superheater water level would have been required if the level oscillated "as a whole."

However, if the superheater level oscillated with each pass being 180° out of phase, then much greater level variations would have been required.

Although superheater water-level oscillations appear to be the most probable reactivity oscillator, the reasons for an oscillatory driving force are poorly understood. It is clear, however, that while the power fluctuations did not trace perfect sine waves, on the other hand, neither did they appear to be the result of a random driving phenomenon. Figure 70 D indicates the possibility of both passes of the superheater oscillating 180° out of phase with each other, since the peaks are alternately large and small. Note that the period of oscillation then becomes 20 instead of 10 sec.

A case in which power oscillations did not occur with a partially flooded superheater is shown in Fig. 70 B, which was recorded 5 min before Fig. 70 C where oscillations are evident. It is possible that some time is required for oscillations to build up after the necessary unstable conditions are reached.

A limited qualitative analysis was made to determine the probable mechanism causing superheater water-level oscillations in the hot reactor. Leakage of water from the water moderator to the superheater region would cause flashing of some water to steam in the superheater. Since small leaks were present between the two regions via the superheater assembly seals, water leaked into the superheater by virtue of the net head difference between the reactor water level (10-11 ft) and the superheater level (3-5 ft). Calculations show that a leak of reasonable size would allow the measured flow of 1.0-2.3 gal/hr. Approximately 0.1% (by mass) of this saturated water would flash to steam, causing a maximum void fraction of 4 v/o to exist in the water of the partially flooded superheater. Thus, an oscillation in superheater water level and effective density of this water could develop due to changes in the pressure difference across the leakage area, which in turn would cause variations in the water leakage rate and void content of the superheater water. Void volume changes in the superheater would thus cause superheater water-level changes.

The above reasoning indicates that oscillations in which each pass is 180° out of phase are more probable. If the superheater level oscillates so that each pass is 180° out of phase, then much greater variations in superheater water level would be required than for the 12-assembly in-phase mode, to give the same power oscillations, since the reactivity effects in the two passes would be at least somewhat cancelling. However, exact cancellation would be unlikely because of the rapid changes and differences in differential flooding worth vs level for positive and negative changes in the two passes.

The above observations indicate that an inherent instability exists somewhere in the system at zero-power operating temperature and

pressure conditions with the superheater partially flooded. It should be recognized, however, that the superheater level may oscillate for other reactor conditions as well, but apparently is effective only for the specific set of conditions described herein.

2. Short-period Scram

During the control rod calibration experiments that were being conducted at 600 psig, 489°F, zero-power conditions with the superheater drained, an automatic short-period scram occurred in both period circuits on the third decade of a period measurement. The positive period measured for the second decade was 30 sec; the period circuits scram on a 5-sec period. At the start of the period, the superheater water-level indicator suddenly rose from 9 in. to 4 ft-6 in., where it remained until the superheater draining operation was performed about 4 min later.

The cause of this short-period scram was investigated and the following items considered:

Malfunction of the nuclear instruments was ruled out as a possible cause, since both duplicate period scrams operated simultaneously. The possibility of maloperation of control rods was ruled out because both the log and the linear flux instruments recorded the fact that the reactor was on a stable period, and no control rod movement was initiated or observed. The possibility of the superheater water-level indicator giving false information (that is, the water level in the superheater steam-coolant channels actually being somewhere in the core, rather than at the indicated level of 9 in.) was not considered probable because the control rod positions required to produce critical on the two criticality measurements preceding the period scram were the same. A rapid temperature change was not a probable cause, since the pressure and temperature recorders reported slowly decreasing pressure (1 psi in 10 min) and near-constant temperature, respectively. The reactor water level was rising slowly during the experiment. The reactor water-level recorder (LR-1) was at 9 ft-9 in. indicated value and about 9 ft-11 $\frac{1}{2}$ in. corrected value. The boric acid concentration was changed 3 hr before the scram, but a rapid decrease in concentration was considered unlikely because samples taken a half-hour before the scram and 8 hr after the scram gave concentrations of 5.14 and 5.25 g(H_3BO_3)/gal(H_2O), respectively.

Water suddenly entering the superheater coolant channels was the most likely cause of the fast period. The superheater flood valves had not been opened. It was believed that condensate collecting in the steam lines close to the reactor vessel somehow flowed into the second-pass superheater fuel assemblies via the exit superheated steam manifolds (see Fig. 7). Steam traps normally in service to dispose of this condensate were valved off. This was necessary to reduce heat losses to a point where the

electric preheaters could maintain the system at temperature. The delay in indication on the superheater water-level indicator was believed to be due to the time required for water to flow from the superheater to the lower superheated steam main, through the flow-restriction orifice present to limit the superheater flooding rate.

At a later date, an experiment was run simulating the same reactor and system conditions, but with the reactor shut down. Even though the reactor pressure was cycled above and below 600 psig for 10 hr, the condensate that collected in the steam lines could not be caused to flow into the superheater.

No proven explanation for the cause of the short-period scram is known at present. However, the period was long enough not to be hazardous. The procedure of placing all steam-line traps in operation before draining the superheater was strictly adhered to thereafter.

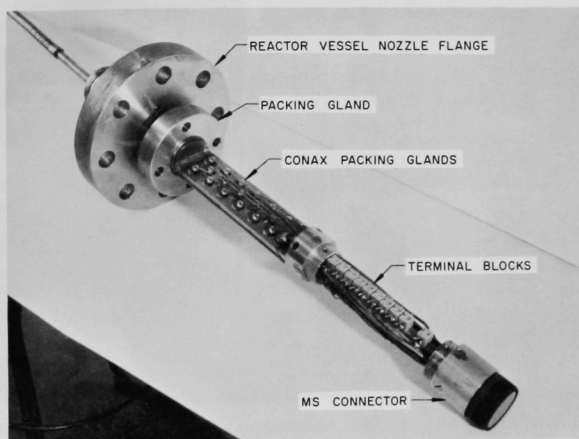
3. Effects of Moisture on High-impedance Thermocouple Extension Leads

During the power operation of core CSH-1B, it was discovered that moisture on thermocouple conductors in high-impedance circuits can produce large inaccuracies in temperature readings.

a. Description

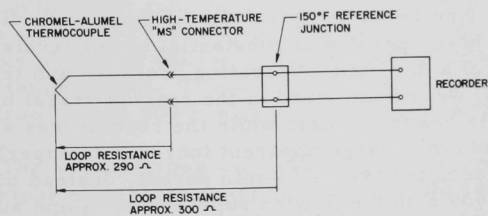
Many thermocouples and other instruments were installed in the reactor to monitor the performance of core CSH-1B. Most of these devices were connected to external equipment through penetrations in the top head of the reactor vessel. Electrical termination and pressure sealing of extension leads from thermocouples in instrumented fuel assemblies were accomplished in the terminal box and packing gland arrangement shown in Fig. 72. The removable terminal-box covers are not shown. The thermocouples in the superheater fuel were Type K, with a sheath of Type 304 stainless steel, a nominal OD of 0.040 in., and insulated with Al_2O_3 . Conductor size was No. 34 AWG. Thermocouple wires were soldered to heavier wires at the ends of the sheaths, made mechanically rigid by cementing and use of clamping blocks, and waterproofed with two coats of baked silicone varnish. The larger conductors were soldered to a high-temperature, "MS"-type connector at the top of the terminal box. A diagram of external connections to potentiometer-type equipment or high-gain amplifiers is shown in Fig. 73.

An exterior view of the reactor vessel top head, arranged for operation with the central superheater core loading, is shown in Fig. 74. The area above the head was covered during power operation by portable, high-density, concrete shielding slabs. The region around the reactor vessel head below the shielding slabs was normally ventilated by a forced-air exhaust system.



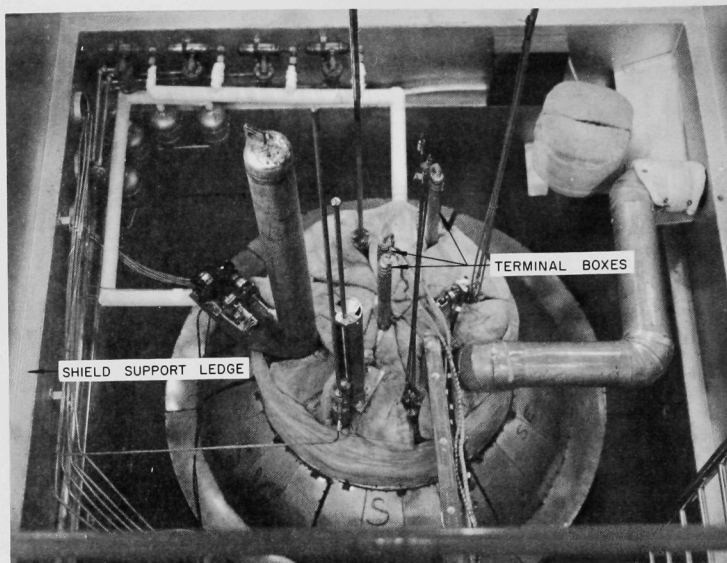
ID-103-3579

Fig. 72. Terminal Box for Instrumented Superheater Fuel Assembly



ID-103-A3289

Fig. 73. Thermocouple Measuring Circuit Schematic Diagram for Superheater Fuel and Steam Temperatures



ID-103-3572

Fig. 74. Reactor Head and Pit Installation,
Core CSH-1B

b. Experience

Erroneous temperature readings were discovered after the reactor had been operated at substantial power levels and was shut down at the end of a day shift. Operating pressure and temperature (600 psig, 489°F) were maintained in the reactor vessel by means of an auxiliary electric heating system while the reactor was shut down. About 1½ hr after shutdown, a large apparent increase in superheater fuel temperatures was noted over a 15-min period. Instead of the saturation temperature of 489°F in the flooded superheater, some superheater fuel and steam thermocouples indicated temperatures as high as 960°F. All nuclear instruments showed the reactor to be shut down, and the steam plant instruments gave no evidence of abnormal reactor conditions. Indicated temperatures then slowly decreased and returned to normal values after about 2 hr, coincident with the beginning of a plant cool-down which was ordered because of excessive steam leaks through seals and packing glands on the reactor vessel head penetrations.

It was later found that the indication of increased temperature was also related to the inadvertent loss of ventilating air flow which allowed steam leaking from head nozzle seals to condense on the terminal

boxes. An inspection of the mated "MS" connectors showed moisture present in quantities sufficient to bridge most contacts. It was determined that moisture entered the connector bodies by way of the external threads on the shell and not by way of the cable, which was potted to the connector in silicone rubber.

c. Tests

To investigate the possibility that water on the "MS" connector had caused the false temperature indications, laboratory tests were conducted based on the assumption that the connector pins and conductors would function as electrochemical cells whose net effect would depend mainly on circuit load and pH of the electrolyte. Two groups of tests were run:

(1) One thermocouple circuit of the reactor installation was simulated using a thermocouple with a dummy load resistance of 288 ohms (loop), an "MS" connector pair, a furnace for the heat source, and a potentiometer for reading voltage. The connector was subjected to various conditions of moisture while the voltage was monitored.

(2) The output of a Chromel-Alumel electrochemical cell was measured as a function of conductor spacing, conductor area in solution, pH of electrolyte, and external load resistance.

The first group of tests on the simulated installation (1) proved to be most valuable in duplicating the conditions experienced. Three runs were made, and in all cases the thermocouple hot junction was maintained at 500°F. In the first run, the connector was left at room temperature, which resulted in a true 500°F reading. In the second and third runs, the connector pair was placed in boiling water and steam, with the connectors initially at room temperature. These last two runs produced equivalent outputs ranging from 120 to 900°F with no predictable pattern of behavior.

The second group of tests (2) gave some indication of the outputs of various electrochemical cells formed by using Chromel and Alumel conductors. Voltages were monitored by a Keithley Model 151R microvoltmeter (10 megohms input resistance). Electrolyte pH and resistivity were determined by Leeds & Northrup Model 7664 pH indicator and a Leeds & Northrup Model 4866-60 conductivity bridge, respectively. Table XVI indicates some typical values of cell potentials measured. Note that cell potentials and polarities are related to solution pH. These values are representative only for the samples used, since it was found that work-hardening of the conductors, produced by bending or scraping, could drastically influence the results. It is evident from both groups of tests that the presence of electrolytes can cause serious errors in temperature measurement.

Table XVI
ELECTROCHEMICAL CELL POTENTIAL FOR CHROMEL-P* VS
ALUMEL* AS A FUNCTION OF CONDUCTOR SPACING, LOAD,
AND ELECTROLYTE pH

| Electrolyte | | | Output, mV | |
|-------------|---------------------|-------------------|------------------------|-------------------------|
| pH | Resistivity, ohm-cm | Load, ohms | For 2.5-in. Spacing | For 0.25-in. Spacing |
| 8.5 | 0.345×10^4 | 10^7 | -65.0 | -36.0 |
| | | 9.1×10^5 | -51.0 | -26.0 |
| | | 9000 | -2.4 | -0.62 |
| | | 1000 | -0.24 | -0.06 |
| | | 10 | -0.003 | -0.003 |
| 8.0 | 0.334×10^4 | 10^7 | -40.0 | |
| | | 9.1×10^5 | -39.0 | |
| | | 9000 | -5.6 | |
| | | 1000 | -0.66 | |
| | | 300 | -0.17 | |
| 6.95 | 0.348×10^4 | 10 | -0.004 | |
| | | 10^7 | 30.0 | |
| | | 9.1×10^5 | 24.0 | |
| | | 9000 | 0.90 | |
| | | 1000 | 0.10 | |
| 6.9 | 0.338×10^4 | 300 | 0.026 | |
| | | 10 | 0.0 | |
| | | 10^7 | | 9.8 |
| | | 9.1×10^5 | | 9.6 |
| | | 9000 | | 0.28 |
| 6.0 | 0.305×10^4 | 1000 | | 0.035 |
| | | 10 | | 0.0 |
| | | 10^7 | 42.0 | 50.0 |
| | | 9.1×10^5 | 38.0 | 38.0 |
| | | 9000 | 1.5 | 1.2 |
| 4.0 | 0.259×10^4 | 1000 | 0.17 | 0.12 |
| | | 300 | 0.05 | - |
| | | 10 | 0.004 | 0.001 |
| | | 10^7 | 84.0 | 125.0 |
| | | 9.1×10^5 | 79.0 | 100.0 |
| 3.0 | 0.155×10^4 | 9000 | 18.0 | 12.0 |
| | | 1000 | 3.4 | 3.0 |
| | | 300 | 1.1 | - |
| | | 10 | 0.04 | 0.048 |
| | | 10^7 | 51.0 | 44.0 |
| 2.5 | 0.7×10^3 | 9.1×10^5 | 47.0 | 41.0 |
| | | 9000 | 39.0 | 38.0 |
| | | 1000 | 23.0 | 23.0 |
| | | 300 | 11.0 | 12.5 |
| | | 10 | 0.5 | 0.55 |
| | | 10^7 | 62.0 | 46.0 |
| | | 9.1×10^5 | 62.0 | 44.0 |
| | | 9000 | 56.0 | 42.0 |
| | | 1000 | 38.0 | 31.0 |
| | | 300 | 20.0 | 18.5 |
| | | 10 | 1.1 | 1.1 |

*Hoskins Manufacturing Co. trade names.

Conductors of No. 16 AWG (0.053-in.-diam) were immersed 2 in. into tap water at 25°C (room temperature). Immersed area per conductor was 0.335 sq in. Two runs were made, varying solution pH by addition of H_2SO_4 , with 0.25- and 2.5-in. conductor spacing in the electrolyte. The Chromel-P conductor was connected to the (+) instrument terminal throughout all tests.

d. Conclusions

From the tests and on-site observations, it was concluded that the problem in the reactor installation was due to the presence of condensate on the connectors of the terminal boxes. The initial indicated temperature rise was probably due to formation of condensate on the conductors, and the later indicated temperature decrease could have been caused either by condensate dilution of the electrolytic solution or by completion of the local chemical reaction based on the available cell materials (conductor metals and free ions in the electrolyte). The effects were exaggerated by traces of brazing flux which were found at the soldered connections on the "MS" connectors. (A silver-cadmium hard solder was used along with fluoride-based flux to join conductors to the pins of the "MS" connector.) A series of cleaning operations on all the solder joints apparently was not adequate.

To correct the problem, each "MS" connector was boiled, with wires attached, in several demineralized water baths. Conductivity of the solution, with the connector immersed, was monitored during the cleaning operation. When the solution no longer showed an increase in conductivity, the connector was considered clean. The connectors and cables were thoroughly dried under heat lamps, and the original silicone rubber potting compound was retouched to insure against moisture entry along the cables. More self-curing silicone rubber was used to cover the ends of the thermocouple sheaths and their junction points, and was then applied to seal the cover plates to the terminal box. The two portions of the "MS" connector were assembled and potted in silicone gel. Each terminal-box cover plate was equipped with an air inlet fitting near the top and a small purge hole at the bottom. The terminal box was then maintained at 5 psig, using clean, dry instrument air. The positive pressure and silicone gel kept moisture from the vulnerable parts of the assembly. The gel could be easily cut to allow "breaking" of the connectors.

C. Reactor Vessel

1. Radiation Effects

Iron, nickel, and titanium neutron flux wires were installed in a thimble next to the reactor vessel wall at the start of core CSH-1B power operation to serve as irradiation monitors for the reactor vessel shell. Because of the limited power production from this core, the wires were left in place and not counted.

2. Temperature Distribution in Reactor Vessel Wall

The satisfactory reactor vessel wall-temperature distribution, a maximum differential of 35°F, which was attained during the operation of core B-2,⁽⁴⁾ continued through the operation of core CSH-1.

3. Reactor Vessel Water-level Measurement

The use of a cold, rather than heated, reference water-level leg for reactor water-level measurement continued to give the most reliable performance obtained.

The use of external steam-heated tracers on the reactor-water-level gauge glasses was uniformly unsatisfactory. The gauge glasses could not be brought up to reactor temperature, and so full temperature compensation was not achieved. Also, the temperature distribution over the length of the glasses was nonuniform, so level correction factors could not be applied. Finally, the external (and nonuniform) heating of the gauges led to frequent glass and gasket failure. Gauge glass heating was discontinued.

In-vessel water-level measurements were made by means of both an acoustic probe and a steam probe. The details of these experiments are presented in Section V.A.8. above.

4. Belleville Spring

The Belleville spring, between the reactor vessel head gussets and the core structure hold-down grid, performed its function of supplying the central superheater core structure hold-down load in a satisfactory manner.⁽²⁾ An average room-temperature spring deflection of 0.128 in. gave a hold-down load of 10,500 lb. An additional average deflection of 0.046 in. was measured at operating-temperature conditions due to differential thermal expansions between vessel and core structure. This resulted in a total hot deflection of 0.174 in. and 14,300 lb of core structure hold-down load.

Following power operation and removal of the reactor vessel head, the deflection of the Belleville spring was found to be uneven around the periphery. It is believed that the feedwater sparger hold-down bracket prevented the core structure struts on the north side from compressing normally, thereby causing added deflection to the Belleville spring on that side. This condition was rectified on the next installation.

D. Water and Steam Systems

1. Steam Systems

The steam systems and associated equipment were routinely operated and in general performed satisfactorily. The steam desuperheating equipment performed its function properly while in manual control, but the short operating period did not permit final adjustment of the automatic controls.

Excessive steam leakage through the double-seated, main-steam, back-pressure control valve during warming-up operations necessitated the installation of a new steam vent valve in the low-pressure, main steam line in the turbine building. This valve was kept open until the steam line reached operating temperature and turbine-generator operation was to be started. It thereby kept the main steam-line pressure to the turbine system below 50 psig during the warming-up period.

An interlock was added to prevent opening of the superheater vent valve if the superheater flood valves were open and there was water in the superheater. This interlock was added to prevent the loss of an excessive amount of reactor water or damage to the outlet steam piping. With the reactor at pressure, water could have been forced from the reactor vessel through the flood valves and superheater fuel assemblies to the steam piping system.

2. Boron Addition and Batch Feed Systems

The boron addition system was revised to provide a 10-min time delay between the opening of the storage-tank steam-admission valve and the tank-to-reactor discharge valves. The boron tank could then be held at a temperature of about 200°F instead of 489°F. In the event of a need to add the boric acid solution to the reactor, the delay permitted the tank to be brought to reactor pressure before the dump phase was started. Since this change, the system has performed satisfactorily. The delay can be manually bypassed by the control room operator should the need arise.

The batch emergency feedwater system was not operated during the operation of core CSH-1.

3. Turbogenerator System

The antiquated turbogenerator plant (37 yr old) performed in a satisfactory manner. The maximum vacuum attainable on the turbogenerator unit during CSH-1 core power operation was about 18 in. Hg.

The air ejector exhaust system, modified to pass full-dilution air flow through both absolute and charcoal filters, performed in a satisfactory manner.

4. Feedwater System

The feedwater system and associated equipment performed satisfactorily. The newly installed continuous bypass orifices at each feed pump worked well, as did the feedwater storage tank cooling system.⁽⁴⁾

5. Auxiliary Water System

Performance of the auxiliary water system was good, with one exception. The newly installed carbon-ring mechanical seal on the auxiliary water circulating pump failed early in service at 600 psig, 489°F as did a replacement unit. The reason for failure was not established, although the problem was investigated with the manufacturer. The seal system was removed and the packed stuffing box was reinstalled. Packing performance was more satisfactory.

6. Superheater Flood-and-drain System

Two modifications to the superheater flood system were made before the power runs with the central superheater core. First, a low-rate flood system was installed, in parallel with the high-rate system, which permitted a superheater flooding time of 9-10 min. The purpose of this system was to reduce thermal shock to high-temperature fuel plates on normal shutdown under high-decay heat conditions. Second, an orifice was installed on the superheater external flood-and-drain line which increased the high-rate flooding time for the superheater coolant channels to 33 sec. In practice, operation of the flood-and-drain systems was satisfactory. Because of limited power operation, little decay heat was noted on superheater shutdown, and cooling and flooding were thus simplified. The high-rate flood system was used exclusively.

During removal of the central superheater core structure from the reactor vessel, the shielded remote-disconnect procedure for the in-vessel connector in the flood-and-drain extension pipe was performed satisfactorily.

7. Superheater Steam Outlet Manifolds and Couplings

Postoperative inspection of the superheater steam outlet manifolds and attached DSD temperature-compensated couplings* showed them to be in excellent condition. Due to the extremely low radiation levels at the tops of the superheater fuel assemblies, the capability for remote disconnect

*DSD Manufacturing Co., Hamden, Conn.

of manifold couplings to the superheater fuel assemblies was not utilized. The remote-disconnect procedure was used satisfactorily to remove the three manifolds from the reactor vessel to storage.

E. Reactor Control, Electrical

Before power operation with the nuclear superheater, interlock circuitry and performance of the control systems were reviewed. As a result of this review, two additional reactor scram interlocks were added. The first was a duplicate high-reactor-water-level scram, which was a back-up for the original high-water-level scram. The second was a duplicate low-steam-flow scram, also a back-up for the original low-steam-flow scram.

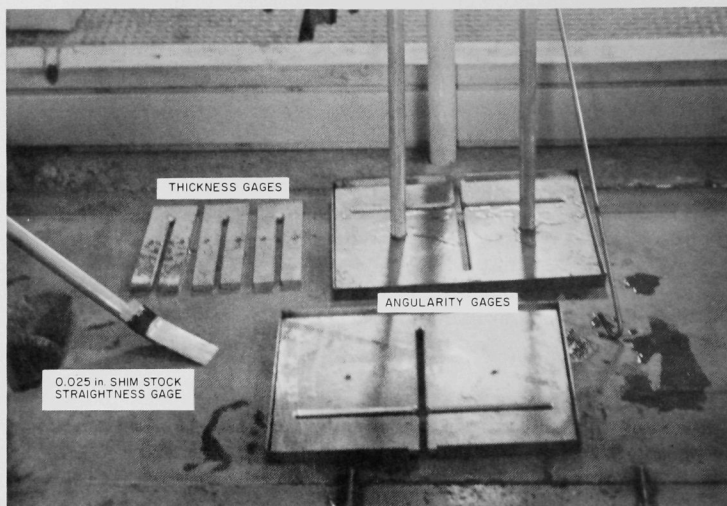
The intermediate control-rod-drive two-speed motors that had failed during boiling core operation⁽⁸⁾ performed satisfactorily after rewinding. All of the motors were rewound with high-temperature-insulation wire, but two of them had to be rewound a second time due to insulation breakdown in the windings. When a good-quality winding job had been accomplished, the motors performed satisfactorily.

The control rod operating speeds were changed so that any individual rod traveled at a maximum speed of 6 in./min when being withdrawn. The intermediate control rods, when withdrawn as a group, traveled at one-fourth that speed. These changes in speed were possible because of the reduction in relative reactivity worth of the central control rod located in the superheater.

F. Control Rods

The fourth inspection of BORAX-V control rods numbered 1, 2, 8, 3, 11, 5, 7, 6, and 10, from core positions 1 through 9, respectively, took place after completion of operation on the central superheater core during the changeover to the peripheral superheater core. The control rods, which were radioactive (up to 35-55 R/hr on contact), were stored in the water storage pit, where the inspection was carried out under water. Figure 75 shows the inspection gauges used. Subsequent repair operations were done on the operating floor, with the control rods behind concrete shield slabs which were placed to reduce radiation to personnel.

The stainless-steel-clad Boral poison section of the control rods passed the 0.330-in. thickness gauge with the exception of one blade each from control rods Nos. 3 and 5. These blades from rods Nos. 3 and 5 did pass the 0.365-in. thickness gauge and were considered to be in good condition. No rub marks or bulges were visible.



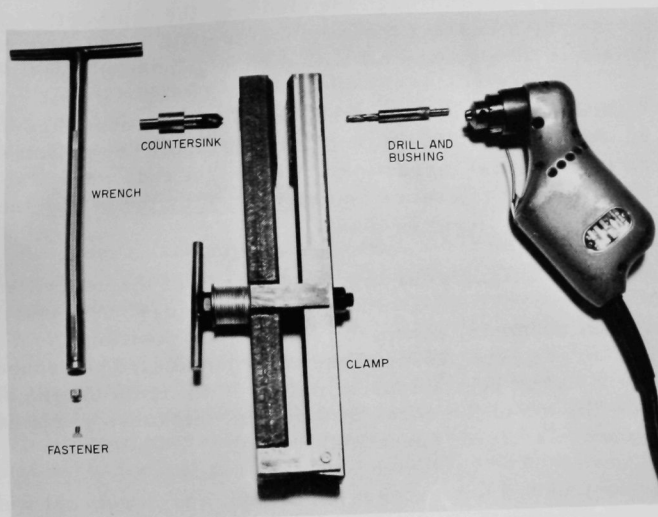
ID-103-3713

Fig. 75. Control Rod Inspection Tools

The laminated X-8001 aluminum followers of the T-shaped control rods would not pass the 0.438-in. thickness gauge or the 0.438-in. angularity gauge. The 0.438-in. angularity gauge did pass all the followers on the cruciform control rods, and the 0.365-in. thickness gauge would pass about half the followers. Closer inspection revealed that some of the spot welds holding the 1/16-in.-thick follower cladding to the 3/16-in.-thick core plate had broken, causing minor bulges in the followers. Rub marks were clearly visible, but the bulges could be depressed by hand. The cladding at the spot welds was not torn, and so far as could be determined, no metal was pulled from the core of the follower.

A repair procedure was devised by which the bulged high spots on the control rod followers were brought back into dimensional tolerance and greater venting capability given to each blade. A control rod was mounted horizontally on a fixture between four concrete shield slabs, two slabs on a side. A working slot 18 in. wide was left between the two slabs so that a man could work from each side. A special stainless-steel mechanical fastener, the same as that used to join the poison section and extension shaft to the follower, was used to squeeze the cladding on both sides of the blade to the core of the follower. A combination clamp-and-drill fixture was made to drill a through hole, and a special countersink, with a stop against the fixture to control the depth, was used to countersink both sides of the hole. These items are shown in Fig. 76. The screw was inserted, the nut turned up tight, and the wrench head of the nut broken off. The nut

was then tack-welded to the screw and the surface ground smooth. This was repeated until each follower blade would pass the 0.365-in. thickness gauge.



ID-103-A3059

Fig. 76. Control Rod Follower Repair Tools

The number of fasteners added to each control rod follower is as follows:

| <u>Control Rod No.</u> | <u>Core Position</u> | <u>Number of Fasteners</u> |
|------------------------|----------------------|----------------------------|
| 1 | 1 | 10 |
| 2 | 2 | 10 |
| 8 | 3 | 22 |
| 3 | 4 | 9 |
| 11 | 5 | 16 |
| 5 | 6 | 12 |
| 7 | 7 | 10 |
| 6 | 8 | 9 |
| 10 | 9 | 16 |

Although the original design of the follower incorporated vents at top and bottom to allow water or steam between cladding and core to escape, this may not have been adequate. Therefore, each blade was given

an additional seven vent holes of 1/8-in. diam on each side, for a total of 14 vent holes per blade. The vent holes went through the cladding only. Venting was accomplished by taping a locating fixture to the blade to be drilled and drilling a hole through the cladding, the depth of the hole (3/32 in.) being determined by a bushing mounted on the drill. The small burr on each vent hole was then ground off with a hand grinder.

At final inspection, all control rod followers passed the 0.365-in. thickness gauge and the 0.390-in. angularity gauge. The poison sections remained as in the initial inspection. All control rods were also within the straightness-and-twist tolerance as determined by the straightness-and-twist fixture.

The shroud channels for the control rods of the central superheater core structure were inspected with a thickness gauge. A 0.467-in. thickness gauge passed all channels, except for control rod positions Nos. 3 and 5. A 0.441-in. thickness gauge passed these two channels. The reduced thickness of the channels was at points approximately 30 in. from the top of the shroud or 2 in. below the top of the core. A 0.485-in. thickness gauge had passed through all channels before operation.

The control rod drives were inspected, and in general were in excellent shape. The linear floating ring labyrinth seals were cleaned of some rust and fine particles. The Teflon wipers were replaced, and a scratch on one extension shaft was stoned smooth and the shaft reinstalled.

G. Fuel

1. Boiling Fuel Rods

Brief visual inspections of several boiling fuel rods after the unloading of core CSH-1 revealed no evidence of failure or deformation. The fission product monitoring system gave no indication of boiling fuel failure. During boiling assembly loading changes, it was noted that the Inconel-X latch springs on a few of the fuel rods appeared to have inadequate strength. It is believed this latching difficulty was due to crud buildup between the rods and fuel assembly guide grid, causing greater friction. Pulling on the rod-handling tool was required to insure proper latching of these fuel rods.

2. Boiling Fuel Assembly Boxes

Based upon underwater observations and the noted ease of fuel rod removal and installation, the boiling fuel assemblies and the A-nickel grid-holding rivets appeared to be performing satisfactorily.⁽⁴⁾

3. Fuel Handling and Storage

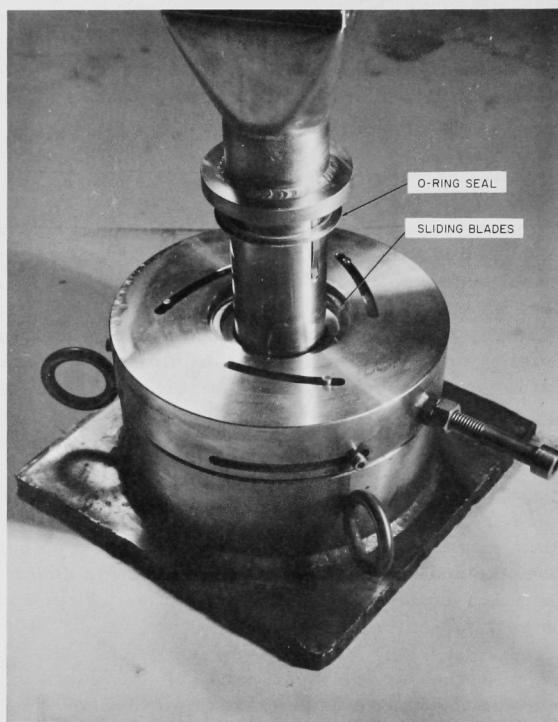
Fuel handling and storage created no problems during either the loading or unloading of core CSH-1. At the end of operations with core CSH-1, the control rods and core structure were removed from the reactor vessel and then moved, unshielded, to the storage points, using the same temporary crane-operator shielding and crane-indexing system as for core B-2.⁽⁴⁾ The radioactivity of both control rods and core structure was low, and the removal was uneventful.

4. Superheater Fuel Seals

In general, the superheater fuel assembly hollow metal O-ring seals performed as designed.⁽²⁾ The total leakage rate of moderator water into the 12 central superheater fuel assemblies averaged 1 to $1\frac{1}{2}$ gal/hr during core CSH-1B operation, before the transition weld failure discussed in Section VIII below. Care was taken to insure clean seal-mating surfaces during seal installation. New, clean seals would seldom remain on the nozzle leaf springs on removal of fuel assemblies. As a result of crud buildup during power operation, however, the seals were satisfactorily retained on the nozzle leaf springs during superheater fuel removal.

During room-temperature critical experiments, hold-down loads on the seals were cycled several times with no adverse effect on seal leakage rates. New seals were installed, however, before power operation. After power operation, the seal-removal jig was utilized for underwater replacement of radioactive used seals with new seal rings. This operation was performed in a satisfactory manner.

The superheater fuel seal-removal jig, shown in Fig. 77, is a sliding-blade device to remove used seals from the superheater fuel assembly nozzles and to replace them with new seals. The operation is performed under water for shielding purposes. The blades are opened, the fuel assembly nozzle with seal attached is inserted into the jig, the blades are closed, and the fuel assembly is then withdrawn, leaving the O-ring behind. New O-ring seals are installed by reversing the above procedure.



ID-103-A3065

Fig. 77. Superheater Seal-removal Jig

VIII. SUPERHEATER FUEL EXPERIENCE

A. Superheater Fuel Assembly Leak Repairs

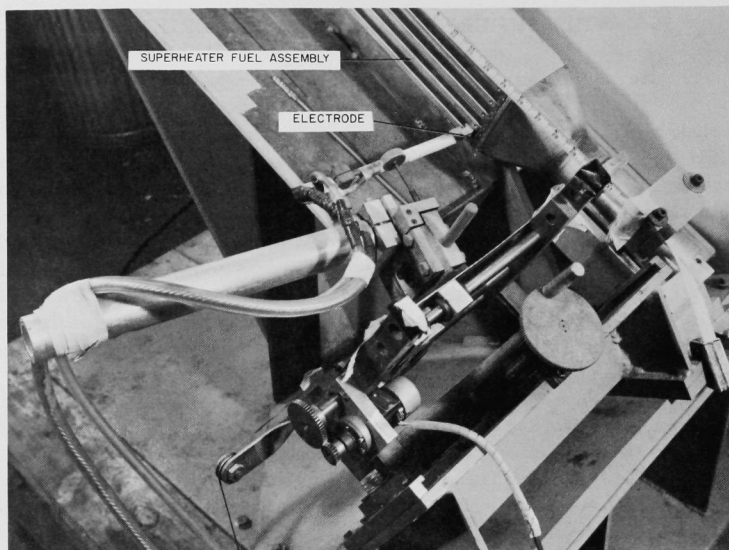
During the early zero-power, room-temperature experiments on core CSH-1, superheater leak tests indicated an excessive leakage of moderator water into the superheater coolant channels. Investigation revealed that six superheater assemblies out of the 12 in the core were leaking through welds at the joints between the fuel subassembly and the top riser and bottom nozzle. These welds were repaired, and each fuel assembly passed a 3-psi pneumatic leak test. After the fuel assemblies were reinstalled, a satisfactory superheater leak rate of 1 gal/hr was measured. During this measurement, three of the 12 assemblies had taped detachable nozzles.

In preparation for zero-power tests at operating temperature, the detachable bottom nozzles of four superheater fuel assemblies were welded on, and all assemblies in the reactor were leak-tested by filling the steam passages of each assembly with water. Five fuel assemblies were found to have leaks through faulty welds between insulating tubes and flow vanes. These welds were repaired by manual T.I.G. welding.

While the zero-power, operating-temperature experiments were being run, further leak problems at high temperature were discovered in the following manner: The hole where the interpass steam thermocouples penetrated an upper flow vane on the three instrumented superheater fuel assemblies was inadvertently left unbrazed during fabrication. This omission was corrected at the reactor site by sealing the holes with a special corrosion-resistant silver braze. After no leaks were detected by an air-leak test, instrumented superheater assembly C-16 was placed in an autoclave, seals were leak-tested, and all thermocouples were intercalibrated at temperatures up to 490°F.

Upon removal from the autoclave, after approximately 10 hr at temperatures between 200 and 490°F, the assembly was filled with water and all metal joints were checked for leaks. Several weld joints, as well as the thermocouple braze, were found to leak. A similar autoclave test on a standard superheater assembly also showed faulty welds.

The leaks were in weld seams where the five individual fuel elements in an assembly are joined to top and bottom flow vanes. The flow vane maintains the moderator gap spacing between elements at this joining point. To improve the integrity of this joint, a fillet weld was made on every joint in every assembly. This required 16 seam welds per assembly, in slots 0.365 in. wide and 3.875 in. long. A special welding machine, shown in Fig. 78, which shielded the radioactive fuel assemblies (1/2 to 2 R/hr on contact) and allowed viewing and remote manipulation of the inert-gas-shielded tungsten electrode within the slot, was developed for this purpose.



210-943

Fig. 78. Repair Welding Machine for Superheater Fuel Assemblies (Shielding Removed)

The possibility of excessive weld penetration burning through the insulating tube into the bottom of fuel plates was realized. Considerable time was spent in obtaining proper weld penetration by machine-welding samples and mock-ups. Final inspection for weld burn-through could be achieved only by cutting off the bottom nozzle of each assembly. This was not done.

While two of the instrumented superheater fuel assemblies were being repaired, the bottom steam thermocouples were damaged and required replacement. New thermocouples were placed in the lower nozzle of each assembly, and the extension leads were brought through stainless-steel tubing mounted external to the assembly.

Measurements made on the superheater fuel assemblies before and after welding indicated only a slight shrinkage in width and breadth, so the dimensions of the moderator water gaps were essentially unchanged. Shrinkage in overall assembly length averaged about 0.050 in., which resulted in a downward superheater fuel displacement of half that amount. All the assemblies required straightening after welding. All assemblies were finally leak-tested by filling them with water, and any leaks that still existed were repaired.

B. Fission Product Experiments

Because of the fission product and leakage problems, discussed in Section VII.A. above, power operation was interrupted and the reactor vessel head was removed to permit examination of the superheater fuel. To determine which superheater fuel assemblies were yielding fission products, equipment was installed to obtain water samples from all 12 assemblies at a point about 4 in. above the top of the fuel plates. Water was sampled at zero power, and then the reactor was operated at 100 kW for 55 min. Another water sample was then taken immediately after the run. The samples before and after the power run were counted and compared. Two tests were made with essentially the same results.

The results of the second test, showing the gross gamma count on 4-ml aliquots of each sample and counts on radiochemical iodine separations, are tabulated in Table XVII. The superheater fuel locations are shown in Fig. 67.

Table XVII
FISSION-PRODUCT EXPERIMENT, CORE CSH-1B

| Superheater Fuel Assembly No. | Core Position | Gross Gamma Count, counts/min | Iodine Separations Count, counts/min |
|-------------------------------------|------------------|----------------------------------|---|
| First Pass | | | |
| C-1 | 35 | 45,500 | 2,450 |
| C-14-I | 45 | 4,000 | 170 ^a |
| C-10 | 46 | 30,400 | 95 ^a |
| C-9 | 55 | 30,500 | 150 ^a |
| C-11 | 56 | 38,800 | 53 ^b |
| C-13 | 65 | 33,200 | 310 ^a |
| Second Pass | | | |
| C-2 | 34 | 28,500 | 150 ^a |
| C-12 | 43 | 28,800 | - |
| C-16-I | 44 | 20,100 | - |
| C-3 | 53 | 80,000 | 3,860 |
| C-4 | 54 | 32,900 | 1,530 |
| C-6 | 64 | 28,000 | 140 ^a |
| Superheater Drain Line | | 2,250 | 295 ^a |
| Bottom of Reactor Vessel | | 40 | - |
| Average Low Count | | | 190 |

^aUsed for average low count.

^bPossible iodine separation error.

The gross gamma count was made from 1 to 2 hr after shutdown, and the values have been corrected for decay. The iodine separation count reported here was run 3 days after shutdown and was not corrected for decay. A gamma-ray spectrometer analysis indicated that the iodine at this time was mostly I^{131} .

Some fission product iodine was found in each superheater fuel assembly, but assembly C-3 had the largest amount, followed by C-1 and C-4. The ratio of the iodine separation count to the average low count for these assemblies is as follows:

| Assembly No. | Count |
|--------------|----------------|
| | Avg. Low Count |
| C-3 | 22.7 |
| C-1 | 9.0 |
| C-4 | 6.7 |

C. Examination of Defective Superheater Fuel

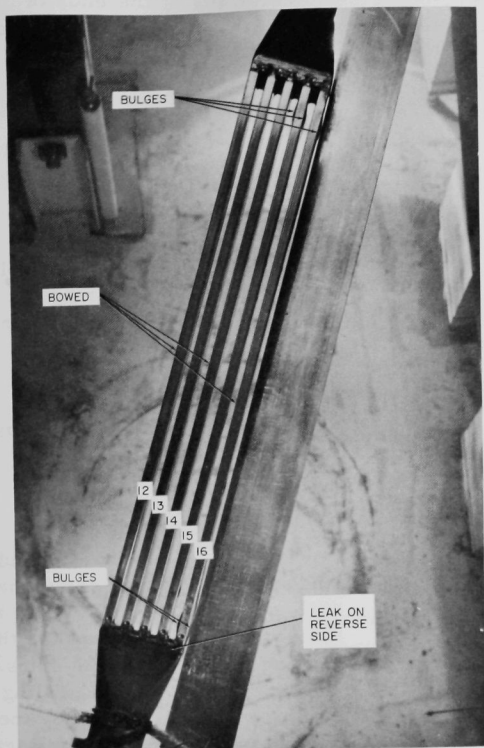
1. On-site Superheater Fuel Inspection

A pneumatic leak test was run on all the superheater fuel assemblies while still in place in the reactor. Bubbles rose from between two assemblies only. Removal and individual leak testing of all three fuel assemblies in the west quadrant of the superheater indicated a leak only in fuel assembly C-3 from core position 53. The leak was caused by a crack about 1/2 in. long in the weld between the bottom nozzle and the five-element fuel subassembly. Underwater visual inspection of this assembly revealed two localized bulges near the end of each of two fuel-element insulating tubes adjacent to the repair fillet welds, as shown in Fig. 79. In addition, two outside and one inside fuel elements of the same assembly appeared to have a slight longitudinal bow. The internal contact points of the spacer wires on the outer insulating tube are visible in Fig. 80, but no undulations could be felt with a probe moved over the surface.

The other two fuel assemblies inspected did not leak and had no visible damage.

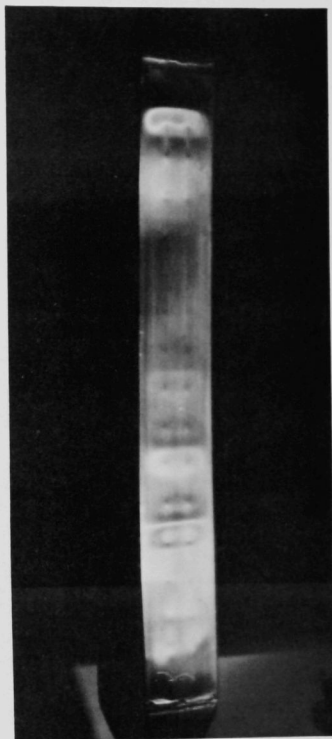
Superheater fuel assembly C-3 was replaced with spare assembly, C-7, and the reactor reloaded. Another leak test at room-temperature conditions indicated a 1.2-gal/hr leakage of moderator water to the superheater. The fission products detection experiment was repeated. The ratios of iodine separation counts on samples from superheater fuel assemblies C-1 and C-4 to the average low count were about the same as in the previous experiment summarized in Table XVII. The count on the sample from the fresh fuel assembly, C-7, was about the same as the average low count. Probably

this trace of iodine in a fresh assembly came from either fuel surface contamination of that assembly, or from other fuel assemblies by diffusion through the water in the interpass plenum chambers.



ID-103-3951

Fig. 79. Southeast Side of Superheater Fuel Assembly C-3, Core CSH-1



ID-103-3952

Fig. 80. Northeast Side of Superheater Fuel Assembly C-3, Core CSH-1

An underwater inspection was made of all irradiated central superheater fuel assemblies, except assembly C-3. This inspection included periscopic observation of: (1) light passed through the length of the central portion of the fuel-assembly coolant channels, enabling viewing of a $1\frac{1}{2}$ -in.-diam circle which comprised about 15% of the coolant channel volume; and (2) the fuel-plate bottom ends. All assemblies inspected showed some weld penetration through insulating tubes to the bottom of adjacent fuel-plate dead ends. None showed cooling-channel distortion or reduction of coolant-channel dimensions in the central light-test area, or apparent

bowing of the insulating tubes. Eight assemblies showed minor distortion of the bottoms of fuel plates, and three showed moderate distortion. Of the three moderately distorted assemblies, assembly C-1, which was found to leak fission products, had several small outward bulges at the ends of the insulating tubes, one assembly had a similar single bulge, and the third had none. The other fuel assembly found to be leaking fission products, C-4, showed only minor fuel-plate distortion.

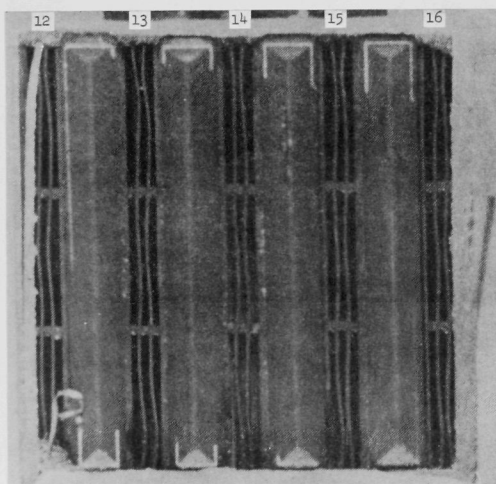
2. Examination of Superheater Fuel Assembly C-3

To determine the cause of the fission product release and the insulating tube bulges, superheater fuel assembly C-3 was dissected and examined in a hot laboratory. Orientation during the disassembly and ex-

amination of the fuel assembly is indicated by referring to the "top" and "bottom" of the assembly as it was located in the reactor. The five four-plate fuel elements are numbered 12 through 16 from left to right in Fig. 79.

a. Disassembly

All the hot-cell cutting operations were performed with a power hacksaw, using a fine-tooth blade, except for the slitting of the insulating cans. These were cut with a milling machine. Burrs caused by the cutting operations may be seen in several figures.

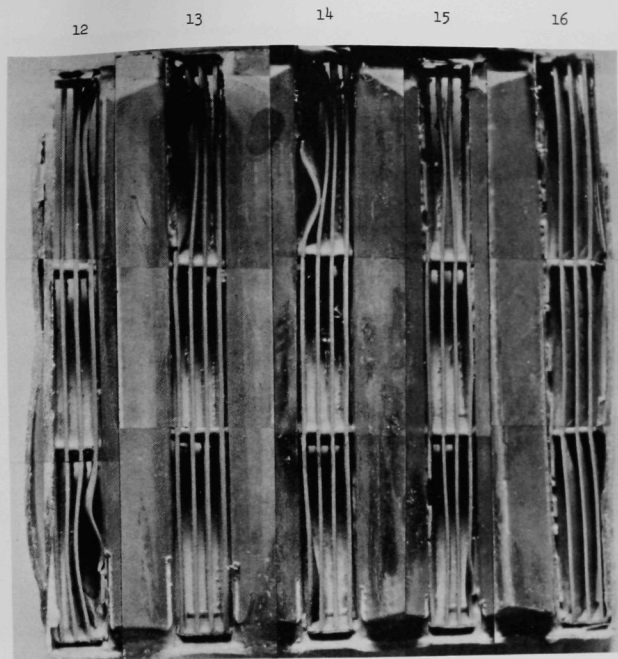


141-2010

Fig. 81. Upper End of Superheater Fuel Assembly C-3, Core CSH-1

The fuel assembly top riser and bottom nozzle were cut off above and below the flow vanes. Cuts were

then made which entered the flow vanes (spacers that separate the five fuel elements) but were just clear of the fuel plates. Figure 81 is a top view and Fig. 82 a bottom view of the fuel subassembly. Figure 82 is a composite of 15 separate, enlarged photographs in which the angle of view in each picture is not the same. For example, some of the plates are seen edge-on and others are tilted so that the plate numbers on the face can be seen. Areas of fusion of the outer fuel plates in each element to the insulating tube are evident. This fusion was caused by burn-through of insulating-tube leak-repair welds. Next, the flow-vane assemblies were removed from both ends by cutting just inboard of the vanes and through the unfueled ends of the fuel plates. This separated the five elements from each other.



106-7611

Fig. 82. Lower End of Superheater Fuel
Assembly C-3, Core CSH-1

b. Crack in Lower-nozzle Weld

The crack in the weld between the lower nozzle and the fuel element subassembly mentioned in Section VIII.C.1. was examined. A closeup of this crack is shown in Fig. 83. This crack lies just below element 15 and extends to element 16. Microscopic examination of the crack showed that either there had not been complete weld fusion, or, if there had originally been good welding, most of this had been ground off during fabrication.

c. Examination of Individual Elements

By shining light through the steam channels and by probing with a steel tape, it was found that elements 12, 13, and 14 were essentially open. Element 15 was blocked about 8 in. from the top end, and element 16 was blocked 1 in. from the bottom. The blockages were only partial, since at least 144 ml of water per minute could be poured through any of the nine individual coolant channels in each element.



141-2011

Fig. 83. Cracked Weld below Element 15, Superheater
Fuel Assembly C-3, Core CSH-1

(1) Element 12

Element 12 showed the least damage. At the bottom, one of the outer fuel plates was tack-welded to the insulating tube at two places, as shown in Fig. 82. The weld adjacent to the slightly buckled plate had torn loose. The other weld was intact, and this probably had caused the plate to buckle.

Plate distortion at the top is shown in Fig. 81. This amount of distortion was also present in the other elements and appears not to be related to the fusion-caused damage at the bottom. To determine how far this distortion extended into the element, seven cuts were made at 1/2-in. intervals, starting 3/8 in. from the top of the fuel plates. Two of these sections are shown in Fig. 84. The distortion essentially disappeared 15/16 in. below the top of the element.

3/8 in. from Top
of Fuel Plates



15/16 in. from Top
of Fuel Plates

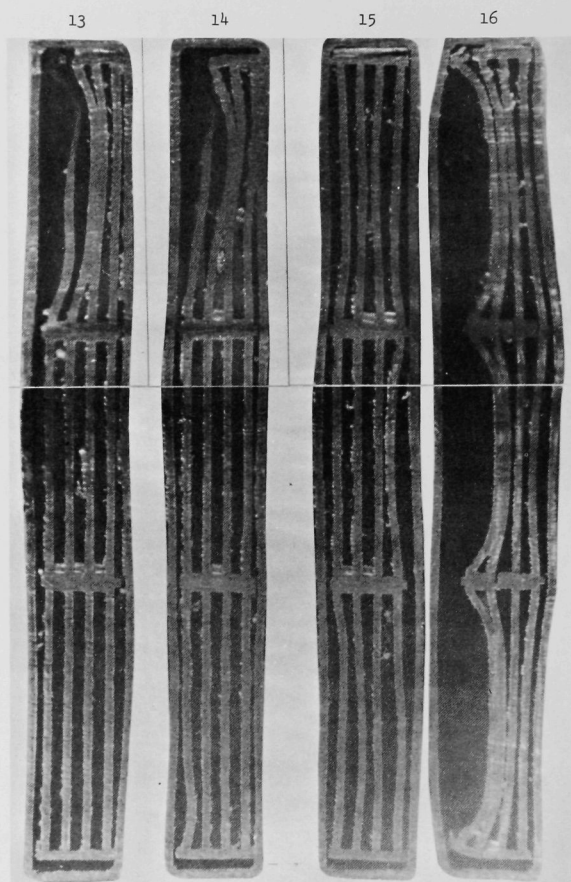


141-2007

Fig. 84. Sections through Element 12, Superheater
Fuel Assembly C-3, Core CSH-1

(2) Element 13

At the bottom of element 13, one of the outer plates was welded for 1 in., as shown in Fig. 82. The buckling associated with this weld extended upward for about 1 in. This may be seen in Fig. 85, which is a photograph of the section made immediately above the flow vanes or about 3/8 in. above the bottom end of the fuel plates. It can also be seen that the plate has been torn at one end.



141-2006

Fig. 85. Section $3/8$ in. above Bottom of Fuel Plates,
Superheater Fuel Assembly C-3, Core CSH-1

(3) Element 14

Damage to this element was almost identical to that in element 13, including a tear in a plate.

(4) Element 15

At the bottom of element 15, both outer plates were firmly welded to the insulating tube over most of the width of the plate, as can be seen in Fig. 82. Notches can be observed in the plate ends. These appear to be the result of complete weld melting at these points.



141-2009

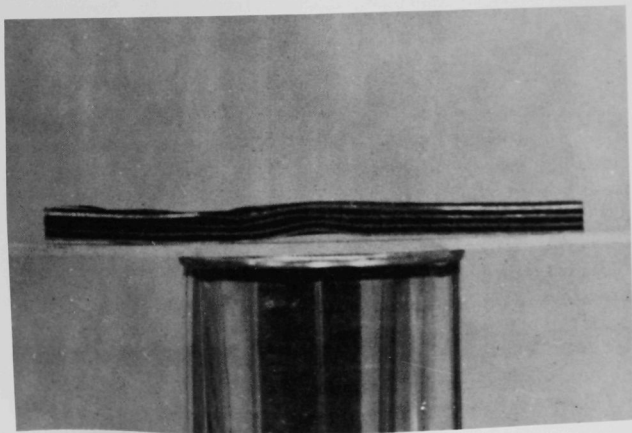
Fig. 86. Buckling in Element 15, Superheater Fuel Assembly C-3, Core CSH-1

Only minor distortion of the fuel plates occurred at the bottom of this element and at the cut $3/8$ in. above the bottom. Removal of the insulating tube revealed buckling of the whole fuel element about 8 in. up from the bottom, as shown in Fig. 86. Two dark spots occurred where the ripples in the fuel subassembly caused it to touch the insulating tube. Similar spots occurred on the reverse side. Closer examination and scratching of the surface showed that these were not burned spots but deposits of a reddish material. Matching spots were found on the inside of the insulating tubes.

Longitudinal sections through this area, shown in Fig. 87, indicated that the fuel assembly buckled as a unit.

(5) Element 16

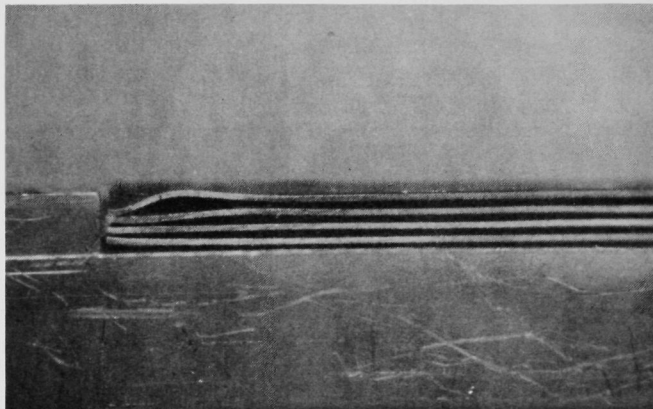
In Fig. 82, the bottom of one of the outer fuel plates in this element can be seen almost completely welded to the insulating tube. At the cut made



141-2012

Fig. 87. Buckling in Element 15, Longitudinal Section, Superheater Fuel Assembly C-3, Core CSH-1

$3/8$ in. above the bottom of the fuel plates, shown in Fig. 85, this plate had buckled over against its neighbors and forced them out of normal position. A longitudinal section of the element shown in Fig. 88 revealed that the bulge extended only $1/2$ in. above this point. Figure 85 also shows that the plate spacers have separated from the plates in the region of the bulge. There was no indication that the plate cladding was torn off the plate, thus exposing the fuel. A closer view of this area, looking downward (not shown), indicated that there were two cracks in the bulged plate where it joined the spacers.



141-2013

Fig. 88. Longitudinal Section of Element 16, Superheater Fuel Assembly C-3, Core CSH-1

d. Source of Fission Products

In an effort to find the source of leaking fission products, several likely spots were smeared and counted for alpha activity. Seven other smears were analyzed with a gamma radiation spectrometer. The results were not conclusive, since similar amounts of alpha-activity fission products and activated cladding were found at all points.

The tears in the plates in elements 13, 14, and 16 pointed out above were in each case about $3/8$ in. above the lower end of the fuel plates. These individual plates were examined and compared with corresponding radiographs made during manufacture. By measurement, the torn plate in element 14 was the only one in which the tear could extend up as far as the fuel. For confirmation, metallography samples were taken from elements 13 and 14. It can be seen in Fig. 89 that the fuel did extend down to the tear in element 14. The area in which fuel was exposed is estimated to be $1/2$ in. long by $1/100$ in. thick. Any porosity would, of course, increase the effective area.

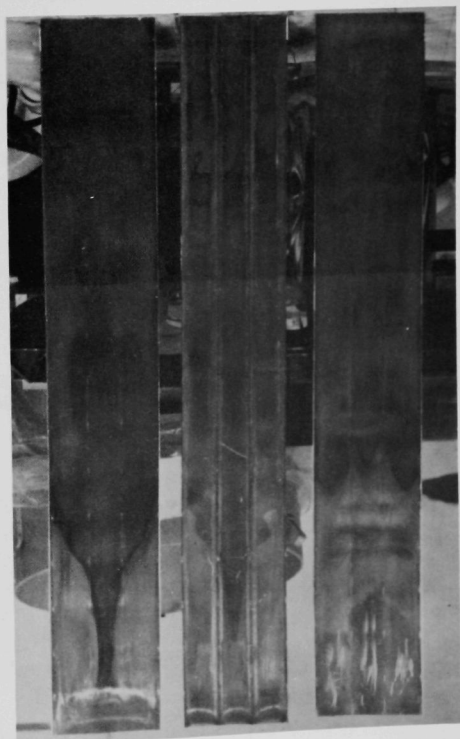
e. Deposits in the Insulating Gap

The amount of reddish deposits between the insulating tube and the fuel element was heavier in element 15 than in the other elements. A distinct pattern could also be observed on the inside of the tube, as seen in Fig. 90. These deposits may be related in some way to the fact that this insulating space was nearly sealed off from the reactor by fusion of the fuel plates to the tube at the bottom of the element.



106-7646

Fig. 89. Metallographic Section of Torn Lower End of Fuel Plate from Element 14, Superheater Fuel Assembly C-3, Core CSH-1



141-2008

Fig. 90. Deposits on Fuel Plate and Inside of Insulating Tube, Element 16, Superheater Fuel Assembly C-3, Core CSH-1

3. Conclusions

In each case, the distortion at the bottom of some of the fuel plates in assembly C-3 may be attributed to the inadvertent burn-through of insulating-tube leak-repair welds into the bottom dead end of the fuel plates. The lower end of the fuel element was designed to be free to expand both transversely and longitudinally in relation to the insulating tube. The weld burn-through restrained this expansion.

Where only a small amount of weld fusion to the insulating tube existed, as in elements 12, 13, and 14, the individual fuel plate was buckled, stretched, and in some cases torn by differential thermal expansion during power operation. Where the entire width of the plate was welded, as in element 16, the plate buckled sharply for its entire width. Where both outer plates were fused to the tube, as in element 15, a large and balanced compressive (and tensile) force would have been generated in the fuel element and tube. The fuel element failed in compression by buckling. The location of the fuel element buckling was in the area of highest neutron flux and high temperature where the material would be the weakest.

The hypothesis that the bulge at the bottom of element 16 was caused by vaporization of water trapped in the insulating space does not appear to be valid. This conclusion is based on the fact that the long axis of the bulges in both tube and fuel plate ran laterally. Hydrostatic pressure would be expected to produce bulges with the axis longitudinal to the element.

The crack in the weld between the fuel subassembly and the lower nozzle was adjacent to, and the bulged insulating tubes were in, elements 15 and 16. This crack in a weak weld may have been caused by the high differential expansion forces set up in these two elements.

The slight fuel plate warpage at the top of the fuel assembly was caused by a design defect. The welding of the tops of the outer fuel and side plates to the insulating tube at this level restrained the transverse expansion of the fuel plate. It is thought that the tops of the fuel plates were stressed beyond the elastic limit and that they buckled because of fabrication and repair-weld shrinkage, in combination with an operating temperature difference of as much as 400°F between the tops of the fuel plates and the restraining, cooler insulating tube and adjacent, relatively massive, flow vanes.

No evidence of coolant channel blockage or melting was found on superheater fuel assembly C-3. The only evidence of exposed fuel was the small tear into the stainless steel- UO_2 matrix at the bottom corner of one plate in element 14.

The fission product release from the fuel defects in core CSH-1B was on a very low level.

ACKNOWLEDGMENTS

The authors of this report wish to express their appreciation to the following people whose diligent efforts and interest made the publication of this report possible:

D. H. Shaftman, Reactor Physics Division, consultant on reactor physics; M. Novick and F. W. Thalgott for advice and consultation; B. M. Beardsley, J. A. Koerner, and L. McKell for mathematical and computer services; R. N. Curran and R. D. DeForest for design and consultation on nuclear instrumentation; R. E. Macherey, C. H. Bean, and W. C. Kramer, Metallurgy Division, and C. S. Kipfer, A. A. Denst, C. T. Szymko, and O. E. Layton, Central Shops, for development and fabrication work on the superheater fuel; J. H. Kittel, Metallurgy Division, for coordination of examination of the defective superheater fuel; R. Carlander and W. C. Kettman, Metallurgy Division, for metallographic work, and W. D. Jackson, C. J. Abrams, and B. J. Kestel, Remote Control Division, for the hot-cell work that was part of this examination.

R. S. Harding, L. R. Monson, E. W. O'Neal, E. Atkin, L. F. Karan, J. F. Kerr, B. J. Nelson, J. P. Newman, C. T. Payne, R. L. Rogers, D. B. Sarutzki, V. E. Wixom, R. S. Woolf, and R. J. Yeager of the BORAX Operating Crew; D. L. Birdsall, instrument technician; J. F. Sommers, P. R. Arnsberger, K. K. Mansfield, and A. E. Wilhelm, health physics technicians; R. Villarreal, chemistry technician; Jo Ann Detroit for numerical calculations, curve plotting, etc.; D. R. Greenwood, C. M. Ekelund, D. Whitney, and R. D. Harris for detailed design work; D. T. Wall, G. F. Twitchell, W. F. Strackeljahn, and H. J. Myers for fabrication and modifications of plant and experimental equipment; J. L. Durney, temporary summer employee; G. L. Egan, W. R. Heineman, and J. D. Ramshaw, Student Aides.

REFERENCES

1. BORAX-V Project Staff, Experiments with Peripheral Superheater Core PSH-1, BORAX-V, ANL-6962 (to be published).
2. BORAX-V Project Staff, Design and Hazards Summary Report, BORAX-V, ANL-6302 (June 1961).
3. BORAX-V Project Staff, Zero-power Experiments on Boiling Core B-1, BORAX-V, ANL-6689 (June 1963).
4. BORAX-V Project Staff, Experiments on Boiling Core B-2, BORAX-V, ANL-6849 (Nov. 1964).
5. Wallin, W. R., et al., Operating Instructions, BORAX-V (April 1964).
6. Plumlee, K. E., Q. L. Baird, G. S. Stanford, and P. I. Amundson, Critical Experiment with BORAX-V Internal Superheater, ANL-6691 (Nov. 1963).
7. Hagen, J. I., and F. S. Kirn, BORAX-V Exponential Experiment, ANL-6707 (April 1963).
8. Reactor Development Program Progress Report, March 1963, ANL-6705.

ARGONNE NATIONAL LAB WEST



3 4444 00008812 0

X